

María Teresa Seco Salvador

Robot Localization in Tunnel-like Environments.

Director/es

Villarroel Salcedo, José Luis
Espelosín Ortega, Jesús Javier

<http://zaguan.unizar.es/collection/Tesis>



Universidad
Zaragoza

Tesis Doctoral

ROBOT LOCALIZATION IN TUNNEL-LIKE
ENVIRONMENTS.

Autor

María Teresa Seco Salvador

Director/es

Villarroel Salcedo, José Luis
Espelosín Ortega, Jesús Javier

UNIVERSIDAD DE ZARAGOZA
Escuela de Doctorado

2021



Universidad
Zaragoza



Instituto Universitario de Investigación
en Ingeniería de Aragón
Universidad Zaragoza

PH.D. THESIS

Robot Localization in Tunnel-like Environments

TERESA SECO SALVADOR

Supervised by
José Luis Villarroel Salcedo
Jesús Espelosín Ortega

Robotics, Perception and Real Time Group (RoPeRT)
Instituto de Investigación en Ingeniería de Aragón (I3A)
Escuela de Ingeniería y Arquitectura (EINA)
Universidad de Zaragoza (UZ)

December 2020

To Samuel, Leo and Olivia.

Agradecimientos

En primer lugar me gustaría darle las gracias a mi director José Luis Villarroel por su apoyo y guía a lo largo de toda la tesis. Junto a él, he tenido la oportunidad de conocer de primera mano las dificultades y retos que entrañan este tipo de entornos subterráneos.

También me gustaría darle las gracias en especial a mi co-director y amigo Jesús Espelosín por su apoyo personal tanto en los buenos como en los malos momentos. Su confianza y fe en mí, su optimismo y su carácter motivador y entusiasta me han hecho sentir siempre acompañada en este camino.

Muchas gracias a Carlos Rizzo por sus valiosas aportaciones y por su implicación y apoyo durante la elaboración de los artículos. Esta tesis no habría tenido sentido sin toda su investigación anterior.

Me gustaría darle también las gracias a Carlos Millán por motivarme y animarme a empezar la tesis. A José Manuel Rodríguez, siempre dispuesto a echarme una mano y a compartir conmigo sus conocimientos. Muchísimas gracias a Mayte Lázaro que me introdujo en el mundo del graph-slam y cuyo apoyo desinteresado ha sido fundamental para que esta tesis llegase a buen puerto.

Gracias al grupo de robótica de la Universidad de Zaragoza, Luis Montano, Luis Riazuelo y Danilo Tardioli, por las interesantes conversaciones durante los experimentos, no sólo de robótica sino también gastronómicas. En especial, me gustaría darle las gracias a Francisco Lera por hacerme entendible el mundo de la propagación de señal en estos entornos.

También agradecer a Martin Magnusson, Tomasz Kucner y Achim J. Lilienthal de la Universidad de Örebro en Suecia, su cálida acogida y su interés en mi trabajo.

Muchísimas gracias a mi grupo de amigas, Pilar, Laura, Silvia, Esther, Paloma, Jessica, Nuria, Gusa, Merche, Ana y Patricia, por estar siempre a mi lado durante todo este tiempo. En especial a Pam, por hacer que mi "spanglish" sea un poco mejor y por su enorme esfuerzo a la hora de corregir los fallos de la memoria.

Por último, mi más profundo agradecimiento a mis hermanas, Nunchi y Olga por su apoyo y comprensión durante todos estos años, y sobre todo a mis padres Juan y Mari, por estar siempre ahí y por haberme inculcado los valores de esfuerzo, sacrificio y perseverancia sin los cuales no hubiese sido posible desarrollar esta tesis.

Acknowledgements

First, I would like to thank my supervisor José Luis Villarroel for his support and guidance throughout the thesis. With him, I had the opportunity to learn first-hand about the difficulties and challenges involved in these types of underground environments.

I am particularly grateful to my co-supervisor and friend Jesús Espelosín for his personal support in both good and bad times. His trust and faith in me, his optimism, enthusiasm and encouragement have made me feel accompanied at every step of this journey.

Many thanks to Carlos Rizzo for his invaluable contribution, and for his dedication and support during the preparation of the papers. This thesis would not have made sense without his previous research.

My sincere thanks to Carlos Millán for encouraging me to start the thesis. To José Manuel Rodríguez, always willing to give me a hand and share his knowledge with me. Special thanks to Mayte Lázaro who introduced me to the world of graph-slam and whose selfless support has been essential for the success of this thesis.

Thanks to the robotics group of the University of Zaragoza, Luis Montano, Luis Riazuelo and Danilo Tardioli, for the interesting conversations during the experiments, not only about robotics but also all things foodie. In particular, I would like to thank Francisco Lera for making intelligible the world of signal propagation in these environments.

I am also grateful to Martin Magnusson, Tomasz Kucner and Achim J. Lilienthal from the AASS centre at Örebro University in Sweden for the insightful feedback and warm welcome.

Many thanks to my group of friends, Pilar, Laura, Esther, Silvia, Paloma, Jessica, Nuria, Gusa, Merche, Ana and Patricia, for being by my side during all this time, in particular to Pam, for making my "spanglish" a little bit better and for her enormous effort helping to proofread this manuscript.

Finally, my deepest gratitude goes to my sisters, Nunchi and Olga for their support and understanding during all these years, and especially to my parents Juan and Mari, for always being there and for instilling in me the values of effort, sacrifice and perseverance without which it would not have been possible to develop this thesis.

Funding

This thesis has been supported by the Spanish Ministry of Science, Innovation and Universities Project “Robot navigation and deployment in challenging environments - Robochallenge” (ref.DPI2016-76676-R-AEI/FEDER-UE) and the project "AUTO-DUMP: AUTOMation of the tunnel debris removal by means of robotized conventional DUMPers" (RTC-2015-4099-4) funded by Spanish Economy and Competitiveness Ministry and European ERDF.

Resumen

Los entornos confinados como tuberías, túneles o minas constituyen infraestructuras clave para el desarrollo de las economías de los diferentes países. La existencia de estas infraestructuras conlleva la necesidad de llevar a cabo una serie de tareas de mantenimiento mediante inspecciones regulares para asegurar la integridad estructural de las mismas. Así mismo, existen otras tareas que se tienen que realizar en estos entornos como pueden ser misiones de rescate en caso de accidentes e incluso las propias tareas derivadas de la construcción de los mismos. La duras condiciones de este tipo de entornos, ausencia de luz, polvo, presencia de fluidos e incluso de sustancias tóxicas, hace que la ejecución de las mismas suponga un trabajo tedioso e incluso peligroso para las personas. Todo esto, unido a los continuos avances en las tecnologías robóticas, hacen que los robots sean los dispositivos más adecuados para la realización de estas tareas.

Para que un robot pueda desempeñar su cometido de manera autónoma, es fundamental que pueda localizarse de manera precisa, no sólo para poder decidir las acciones a llevar a cabo sino también para poder ubicar de manera inequívoca los posibles daños que se puedan detectar durante las labores de inspección. El problema de la localización ha sido ampliamente estudiado en el mundo de la robótica, existiendo multitud de soluciones tanto para interiores como para exteriores mediante el uso de diferentes sensores y tecnologías. Sin embargo, los entornos tipo túnel presentan una serie de características específicas que hacen que la tarea de localización se convierta en todo un reto. La ausencia de iluminación y de características distinguibles tanto visuales como estructurales, hacen que los métodos tradicionales de localización basados en sensores láser y cámaras no funcionen correctamente. Además, al tratarse de entornos confinados, no es posible utilizar sensores típicos de exteriores como es el caso del GPS. La presencia de fluidos e incluso de superficies irregulares hacen poco fiables los métodos basados en odometría utilizando encoders en las ruedas del robot.

Por otra parte, estos estornos presentan un comportamiento peculiar en lo que a la propagación de la señal de radiofrecuencia se refiere. Por un lado, a determinadas frecuencias, se comportan como guías de onda extendiendo el alcance de la comunicación, pero por otro, la señal radio sufre fuertes desvanecimientos o *fadings*. Trabajos previos han demostrado que es posible obtener *fadings* periódicos bajo una configuración

determinada.

Partiendo de estos estudios, en esta tesis se aborda el problema de la localización en tuberías y túneles reaprovechando esta naturaleza periódica de la señal radio. Inicialmente, se propone un método de localización para tuberías metálicas basado en técnicas probabilísticas, utilizando el modelo de propagación de la señal como un mapa de radiofrecuencia. Posteriormente, se aborda la localización en túneles siguiendo una estrategia similar de reaprovechar la naturaleza periódica de la señal y se presenta un método de localización discreta. Yendo un paso más allá, y con el objetivo de mejorar la localización a lo largo del túnel incluyendo otras fuentes de información, se desarrolla un método inspirado en el paradigma del graph-SLAM donde se incorporan los resultados obtenidos de la detección de características discretas proporcionadas por el propio túnel. Para ello, se implementa un sistema de detección que proporciona la posición absoluta de características relevantes de la señal periódica radio. Del mismo modo, se desarrolla un método de detección de características estructurales del túnel (galerías) que devuelve la posición conocida de las mismas. Todos estos resultados se incorporan al grafo como fuentes de información.

Los métodos de localización desarrollados a lo largo de la tesis han sido validados con datos recolectados durante experimentos llevados a cabo con plataformas robóticas en escenarios reales: la tubería de Santa Ana en Castillonroy y el túnel ferroviario de Somport.

Abstract

Confined environments such as pipes, tunnels or mines, are key infrastructures for the economic development of the different countries. The existence of these infrastructures demands a series of maintenance tasks through regular inspections to ensure their structural integrity. Additionally, there are other tasks that have to be accomplished in these environments, like rescue missions in case of accidents, or the ones derived from the construction itself. The hard conditions of these types of scenarios, darkness, dust, presence of fluids or even toxic substances, make these tasks unfriendly and even risky for humans. All of the aforementioned situations, together with the continuous advances in robotic technologies, make robots the most suitable devices for executing these tasks.

For the robot to autonomously perform the tasks, it is essential to obtain an accurate localization, not only for the decision making process, but also to unequivocally locate possible defects detected during the inspection works. The localization problem has been widely studied in the robotics community, with multiple indoor and outdoor solutions using different sensors and technologies. However, tunnel-like environments present a variety of specific characteristics that make the localization a challenging task. The absence of light and the lack of distinguishable visual and structural features, make standard localization methods based on laser sensors and cameras not work properly. Moreover, outdoor techniques using GPS are not feasible in confined scenarios. The presence of fluids and irregular surfaces make the odometry-based methods using wheel encoders even more unreliable.

From the point of view of radio frequency signal propagation, tunnel-like environments present a particular behavior. On the one hand, these environments behave as waveguides above certain frequencies extending the communication range, but on the other hand, the signal suffers from strong attenuations (fadings). Intensive previous works have shown that periodic spatial fadings can be obtained under certain configurations.

Building on these works, this thesis addresses the localization problem in pipes and tunnels taking advantage of the periodic nature of the RF signal. First, a localization method based on probabilistic techniques is proposed for metallic pipes, using the radio signal propagation model as an RF map. Subsequently, the localization in tunnels

is faced with a similar strategy of using the RF periodic signal. As a result, a discrete localization method is presented. Taking a step further, aiming the improvement of the localization along the tunnel involving other sources of information, a method inspired by the graph-SLAM paradigm is developed, where the results obtained from the detection of discrete features provided by the tunnel itself are incorporated. For this purpose, a detection system is implemented to detect relevant features of the RF signal providing the absolute known position of those features. In the same way, a method to detect some mandatory structural features present in tunnels (galleries) is developed. The results of both methods are introduced to the graph as sources of information.

All the localization approaches developed during the thesis have been validated with data collected during experimental campaigns conducted with robotic platforms in real scenarios: the Santa Ana dam pipe in Castillonroy and the Somport railway tunnel.

List of Figures

1.1	Challenging underground environments: (a) Smooth and monotonic inner surface of a pipe (b) Lack of lighting and features in a tunnel (c) Presence of fluids and uneven grounds in a tunnel under construction.	3
1.2	The appearance of periodic fadings in pipes (a) and tunnels (b).	5
2.1	Santa Ana dam pipe. Symmetric and smooth inner surface without distinguishable features.	13
2.2	Different propagation scenarios in Castillonroy from [Rizzo et al., 2014a]. (a) below cutoff: $f = 40$ MHz. monomodal: $f = 51$ MHz. (b) bimodal: $f = 71$ MHz , trimodal: $f = 75$ MHz trimodal.	17
2.3	Periodic fadings caused by the interaction of two modes propagating in a 4-meter diameter pipe.	18
2.4	Pipe front view. Transmitter-receiver positions for different cross-section fadings analysis from [Rizzo et al., 2021].	19
2.5	Received signal power in the left and right half ((a) and (c)) vs upper and lower half((b) and (d)), together with the electric field distribution for: bimodal propagation ((a) and (b)) and trimodal propagation ((c) and (d)). The blue arrows represent constructive interference between the electric fields of the two modes interacting, while the red arrows the opposite (see [Rizzo et al., 2021]).	20
2.6	Pipe experimental setup.	21
2.7	Theoretical received signal corresponding to the upper half and lower half of the pipe for trimodal propagation.	23
2.8	MCL Steps.	24
2.9	Particle filter initialization along the first fading period.	25
2.10	Weighting step.	26
2.11	Measured received power (dotted) vs theoretical propagation model.	29

2.12	Algorithm evolution. Due to the uni-dimensional nature of particles position, odom position and ground truth, the y-axis values for them have been set only for visualization purposes.	30
2.13	Weighted particles distribution at two different timestamps.	31
2.14	Odometry and Particle Filter position estimation error as a function of the travelled distance (ground truth).	32
2.15	Comparison of the estimated position using different methods.	32
2.16	RF signal model (blue) and sensor measurement model variance (red) for $W_{up} = 5^2$, $W_{low} = 3^2$ and $W_{offset} = 3^2$	34
2.17	Cutoff frequency obtained by means of the FFT analysis and linear acceleration resultant after the Butterworth filter.	35
2.18	Odometry and particle filter position estimation error during the displacement of the robot along the pipe using the IMU sensor in the prediction step. Red line: pose error using only odometry. Blue and green line, pose error using the particle filter solution for different values of variance (blue: $L = 0.005$ and $V = 0.03^2$, mean error = 0.552 m, green: $L = 0.001$ and $V = 0.1^2$, mean error = 0.572 m).	36
2.19	Comparison between EKF and particle filter during the displacement of the robot along the pipe: (a) Position error and (b)-(c) comparison of position estimation with EKF, particle filter and odometry methods with respect to the ground truth.	39
2.20	Evolution of the covariance during the displacement of the vehicle using EKF and particle filter-based methods.	40
2.21	Steps of the EKF localization algorithm with two RF signals. After the prediction step, the position and covariance (\hat{X}_t, \hat{P}_t) are updated using the values resulting from the particle filter (x_{S1}, V_{S1}) that works with the first RF signal. In a second correction step, the position and covariance obtained in the previous step (X_{e1t}, P_{e1t}) are updated using x_{S2} and V_{S2} provided by the particle filter working with the delayed RF signal. The result of this step is the position and uncertainty of the vehicle at each time stamp (X_{e2t}, P_{e2t}).	41
2.22	Results from the variance tuning process: $L \in [0.001, 0.01]$, $V \in [0.01, 0.1]^2$. Color range represents the position error. Darker color corresponds to less position error. Best results enclosed by the white dotted circle.	44
2.23	Odometry and position estimation error as a function of the distance traveled (ground truth). Blue, green and purple curves represent the results of three iterations of the proposed algorithm using two RF signals. The same variance values have been chosen for all the iterations.	45

2.24	EKF localization method results using two RF signals during the displacement of the robot along the pipe: (a) Position error comparison using the proposed method and the particle filter-based method using one single RF signal. (b) Variance representing the uncertainty in the measurement for each virtual sensor. (c) and (d) Detail of both position errors and variances corresponding to the dotted enclosed area. The final position error is influenced by the best of both virtual sensors in terms of uncertainty.	46
2.25	Estimated position of the vehicle during its displacement along the pipe: (a) Comparison between the EKF method using both RF signals (black), particle filter using one signal (green and purple dashed line), odometry method (red) and ground truth (blue). (b) Detail of changes in the vehicle position over time corresponding to the enclosed area. The position provided by the EKF (black) is adapted to the best estimation of the two virtual sensors.	47
2.26	Particles distribution vs normal distribution after the resampling step. (a) Result using Signal 1. (b) Result using Signal 2 (180 degree phase difference). The two distributions are similar enough to conclude that the assumption of a Gaussian distribution is tenable.	48
3.1	(a) Measured Received Power at 2.4 GHz inside the Somport tunnel, from [Rizzo et al., 2013a]. The transmitter was kept fixed and the receiver was displaced along 4 km from the transmitter. In (b), the same experiment was repeated for three different receiver's cross-section positions: left half (sector 1), center and right half (sector 2). The solid lines represent the modal theory simulations, and the dotted lines the experimental results. In (c), the red line represent the modal theory simulations, and the blue the experimental results.	55
3.2	General stages of the localization algorithm.	57
3.3	Algorithm flow chart: (a) Map generation, (b) Prediction and Estimation steps.	59
3.4	Distance calculation between minimums of the actual signal.	61
3.5	The Somport tunnel. (a) general dimensions and shape (b) the interior of the tunnel (c) emergency shelters and galleries map.	62
3.6	Instrumented platform.	63
3.7	Experimental transmitter-receiver setup.	63
3.8	Received signal strength from antenna 12. The vertical dashed line denotes the limit between the fast fadings and the selected work zone.	64

3.9	Results of the propose algorithm based on RLS and Mahalanobis distance: (a) minimums map from fadings model used as known information, (b) filtered signal obtained by a first order filter, (c) results of the application of the RLS method to actual data, (d) final minimums detection result after the IC Test , (e) position correction during the displacement of the vehicle, (e) position error comparison between odometry method and the presented approach.	67
4.1	Involved reference frames in the robot localization problem.	76
4.2	RF minimum detection process. The green points represent the theoretical minimum model and the black points the real minimum model. . . .	77
4.3	RF signal minima detection steps: (a) Theoretical model (green points inside the dashed green square A) extracted from the RF signal model (red). (b) Real model generation during the displacement of the vehicle from the real RF signal. (c) Both models referenced to the same system coordinates. (d) Point classification depending on the Mahalanobis distance between the real data and the closest neighbors from the theoretical model (e) Minimum detection if the number and proportion of inliers satisfy the threshold. (f) Estimated position by the odometry x_m (blue point) and position reference from the RF map $x_{m_i}^A$ (green point) of the detected minimum.	78
4.4	Pattern extraction (gallery 17 of the Somport tunnel). The origin of the pattern reference system FEA_REF_i corresponds to the intersection of two lines: the axis of the tunnel and the axis of the gallery (in the present example).	82
4.5	Hough transform to obtain the line in polar coordinates which represents the tunnel right wall. The resultant parameters ρ and α are used to transform the laser points from ROB_REF to MOB_REF	83
4.6	RF transmitter-receivers setup during the experiments in the Somport tunnel.	85
4.7	Odometry conditions. (a) Comparison between the ground-truth, the odometry position in the Somport tunnel and the degraded odometry for the validation. (c) Detail of the positions.	86
4.8	Results of the mimima detection process. The RF signal model is represented with respect to the ground truth whereas the RF real values are represented with respect to the position estimated by the odometry. . . .	87

- 4.9 Gallery detection process. (a) First gallery detection timestamp. The detection uncertainty falls below the threshold (around the 90th iteration) (d) and the relative distance between the vehicle position and the gallery is provided by the detection algorithm (g). (b) The vehicle passes through the gallery position corresponding to the pattern reference. The uncertainty remains under the threshold (e) and the relative distance is provided during this time (h). (c) The vehicle (laser data) moves away from the gallery (pattern) and the uncertainty increases above the threshold (f). The condition of gallery detection is unsatisfied. (i) Relative distances between the vehicle position and the gallery during all the detection process. 88
- 4.10 Matching process results for several galleries represented by different patterns during the displacement of the vehicle. 89
- 4.11 Evolution of the gallery detection uncertainty during the displacement of the vehicle from gallery 17 to gallery 6. The starting position of the vehicle corresponds to gallery 17. 89
- 5.1 (a) Graphical representation of a portion of a pose graph where two nodes \mathbf{x}_i and \mathbf{x}_j are related by a binary edge (blue point) and where a unary edge is associated to node \mathbf{x}_i (green point). (b) Binary edge representing the relative position between \mathbf{x}_i and \mathbf{x}_j nodes. (c) Unary edge corresponding to an absolute position associated to \mathbf{x}_i node. 94
- 5.2 Pose-graph creation steps: (a) Minimum identification at time T . (b) Insertion of the node and the unary constraint corresponding to the detected minimum. (c) False positive case detail, deactivation (removal) of the previous unary edge. (d) Resulting pose-graph after three minimums. 96
- 5.3 Gallery pose-graph creation steps: (a) Initial situation. The vehicle starts moving (b) The gallery is detected for the first time and the gallery node is introduced. (c) Nodes addition each time the gallery is detected. (d) Graph nodes once the vehicle has traversed the gallery. Blue dots denote binary edges and green dots unary edges. 98
- 5.4 Node graph with RF minimums and galleries detection. (a) Complete node graph before (red) and after (blue) optimization. The y axis values have been set only for visualization purposes to avoid the overlapping of both graphs. (b) Area of the node graph showing the nodes incorporated during the gallery 17 detection join together with regular nodes before and after the gallery detection. (c) Detail corresponding to the nodes representing the vehicle position from which gallery 17 is detected (cyan). The node corresponding to the gallery position is represented in black. 103

5.5	Results of the online pose-graph localization approach. (a) Estimated position along the tunnel provided by the odometry (red) and our proposed approach (blue) in comparison with the ground truth (black). (b) Detail of the estimated positions corresponding to the time slot when a RF minimum (dashed blue lines) and two galleries (dashed green lines) are detected. The position is corrected with each detection. (c) Position error during the displacement of the vehicle.	105
5.6	Results of the pose-graph approach after the service routine of the vehicle.	106
A.1	Pioneer 3-AT Robot: (a) Santa Ana pipe experiment. (b) Detail of the instrumentalized robot. (c) RF Explorer receiver.	120
A.2	All-terrain vehicle: (a) wheel-encoders. (b) SICK laser sensor.	120
A.3	All-terrain vehicle: RF sensors layouts.	121
A.4	Robucar TT robotic platform.	122
A.5	The robotized dumper. Front part of the vehicle (a). Dumper hardware and communications architecture (b).	123
A.6	Santa Ana dam pipe.	124
A.7	Access to the Santa Ana dam pipe.	124
A.8	Experiments in the Santa Ana dam pipe.	125
A.9	Somport railway tunnel.	126
A.10	Experiments preparation and setup.	127
A.11	Experiments with the all-terrain vehicle.	127
A.12	Experiments with the robotized dumper.	128
A.13	Tunnel under construction Durango-Amorebieta.	128
A.14	Experiments with the robotized dumper in the tunnel under construction.	129
A.15	The team during the experiments.	130
A.16	Autodump project team.	130

List of Acronyms

EM	Electromagnetic
EKF	Extended Kalman Filter
GPS	Global Positioning System
IMU	Inertial Measurement Unit
INS	Inertial Navigation System
LIDAR	Light Detection And Ranging
MCL	Monte Carlo Localization
NNS	Nearest Neighbor Search
PIG	Pipeline Inspection Gauge
RF	Radio Frequency
ROS	Robotic Operating System
RSS	Received Signal Strength
RSSI	Received Signal Strength Indicator
SLAM	Simultaneous Localization and Mapping
UAV	Unmanned Aerial Vehicle
UWB	Ultra Wide-Band

Contents

Agradecimientos	v
Acknowledgements	vii
Funding	ix
Resumen	xi
Abstract	xiii
List of Figures	xv
List of Acronyms	xxi
1 Introduction	1
1.1 Introduction	1
1.1.1 Previous work: The appearance of periodic RF fadings	4
1.2 Thesis Framework	5
1.3 Thesis Structure and contributions	6
1.3.1 Publications	7
I Robot Localization based on RF Fadings in Tunnel-like Environments	9
2 Localization based on RF Fadings inside Pipes	11
2.1 Introduction	11
2.2 Fundamentals of Electromagnetic propagation in metallic pipes	15
2.2.1 Longitudinal fadings analysis	16
2.2.2 Transversal fadings analysis	18
2.3 Test Scenario and Experimental Setup	19

2.4	Robot Localization using one RF Signal Fadings	23
2.4.1	Continuous Localization system based on RF fadings using Particle Filters	23
2.4.2	Experimental results	27
2.4.3	Variable RF sensor measurement model variance	33
2.4.4	IMU for prediction purposes	34
2.4.5	Continuous Localization system based on RF fadings using Extended Kalman Filter	37
2.5	Robot Localization using two RF Signal Fadings	40
2.5.1	Algorithm formulation	40
2.5.2	Experimental results	43
2.6	Concluding remarks	45
2.7	Summary	49
3	Localization based on RF Fadings inside Tunnels	51
3.1	Introduction	51
3.2	Fundamentals of electromagnetic propagation in tunnels	53
3.3	Discrete localization algorithm based on RF minimum detection	56
3.3.1	Minimums map generation	57
3.3.2	Prediction and estimation using RLS and Mahalanobis Distance	60
3.4	Test scenario and Experimental setup	61
3.4.1	Real scenario: the Somport Tunnel	61
3.4.2	Experimental setup	62
3.5	Results	64
3.5.1	Localization algorithm implementation	64
3.5.2	Experimental results	65
3.6	Concluding remarks	66
3.7	Summary	68
II	Graph-based Robot Localization in Tunnel-like environments	71
4	Tunnel Features detection for Localization purposes	73
4.1	Introduction	73
4.2	Reference systems definition	75
4.3	RF Minima Detection	76
4.4	Emergency galleries detection	80
4.5	Experimental results	85
4.5.1	Scenario and Experimental setup	85
4.5.2	Minima detection results	86

4.5.3	Gallery detection results	87
4.6	Summary	90
5	Multi sensor graph-based robot localization in Tunnels	91
5.1	Introduction	91
5.2	Pose Graph formulation	93
5.3	Graph-based robot localization using fadings and galleries	95
5.3.1	Management of RF fadings minima detection in the pose-graph	95
5.3.2	Management of the galleries detection in the pose-graph	97
5.4	Experimental results	99
5.4.1	Scenario and Experimental setup	99
5.4.2	Algorithm implementation	100
5.4.3	Graph-based localization results	102
5.4.4	Graph-based localization performance evaluation	104
5.5	Concluding remarks	107
5.6	Summary	108
6	Conclusions	111
6.1	Conclusions	111
6.2	Future Work	113
7	Conclusiones	115
7.1	Conclusiones	115
7.2	Trabajo futuro	117
A	Experiments	119
A.1	Robotic Platforms	119
A.1.1	Pioneer 3-AT	119
A.1.2	All-terrain Vehicle	119
A.1.3	Robucar TT	121
A.1.4	Robotized Dumper	121
A.2	Scenarios	122
A.2.1	The Santa Ana Dam pipe	122
A.2.2	The Somport Railway Tunnel	126
A.2.3	The under construction Tunnel Durango-Amorebieta	128
A.3	Experiments	129
A.4	The team	130
	Bibliography	131

Chapter 1

Introduction

1.1 Introduction

Underground infrastructures are largely spread all around the world and are crucial for the social and economic development. Tunnel like environments, including pipes, road and railway tunnels and sewers, have increased in both total length and number, and will continue to do so on a global scale.

The structural performance of these infrastructures is affected by deterioration processes induced by natural and human impacts or the simple effect of ageing. Furthermore, some of them were constructed over 50 years ago, and many have exceeded their intended design service life.

Therefore, periodic inspection, assessment and maintenance are required to ensure that these constructions remain in safe condition and continue to provide reliable levels of service not only for humans but also for the infrastructure itself. Additionally, some other tasks need to be developed in those scenarios, like rescue missions in case of accidents, or the processes involved during the construction of the infrastructures. Tunnel-like environments are characterized by dust, humidity, the absence of natural light, presence of fluids and the existence of toxic substances among others. These harsh conditions convert these tasks into arduous, unfriendly and even risky for human operators.

The growth in the field of robotics and the recent advancements in perception technologies have significantly increased the usage of robots in such applications. Compared with traditional human-based approaches, robots are more robust and efficient and are able to access places that are dangerous for humans. In this context, accurate robot localization is essential not only for identifying the position of any damage during the inspection task, but also for autonomous navigation.

Localization is the process of determining the pose of a robot with respect to its environment. It is one of the most fundamental competencies required of an autonomous

robot as the knowledge of the robot's own location is essential to make decisions about future actions. In a typical robot scenario, a map of the environment is previously available. The localization problem then consists of estimating the robot position and orientation within the map using information gathered from the sensors. Robot localization techniques must handle noisy observations and generate not only an estimation of the robot's location but also a measure of the uncertainty of the location estimation. Usually, the robot can estimate its location relative to where it started integrating data from sensors, which monitors its own movements (e.g. wheel encoders, Inertial Measurement Unit sensors IMUs) and using its motion model. This process is known as odometry or dead reckoning and tends to accumulate errors over time due to the uncertainty of the sensors and even of the motion model itself. Odometry errors can be corrected when the robot observes its environment using other sensors (laser range sensors, cameras) and it is able to match the information gathered by these sensors with the information contained in the map. Probabilistic approaches based on Bayesian filtering, e.g. Extended Kalman Filter (EKF) or particle filter, have been commonly addressed in the literature to solve the localization problem. The key idea of these methods is, instead of relying on a single "best guess", representing information by probability distributions over a whole space of possible hypotheses, modeling the uncertainty explicitly.

When a map of the environment is not available, the robot localization problem becomes significantly more challenging. In this case, both the position estimation and the construction of the map should be performed simultaneously, leading to the so-called Simultaneous Localization and Mapping (SLAM) problem. There are several approaches to solve this problem that can be classified in filtering and optimization (graph)-based approaches. The former is the classical approach and models the problem as an online state estimation where the state consists in the current robot position and the map. The estimate is updated with the new measurements as they become available. The most popular techniques are all the Kalman filter family and the particle filter. Optimization (Graph)-based approach usually uses an underlying graph structure to represent the robot measurements. The graph nodes represent the robot poses and the measurement acquired at this position and the edges represent a spatial constraint relating two robot poses. Once the graph is constructed, the optimization process starts to find the configuration of the robot poses that best satisfies the constraints, solving an error minimization problem.

A large number of techniques have been proposed and implemented to solve the localization in indoor and outdoor scenarios with or without a prebuilt map with amazing results. However, robot localization inside tunnel-like environments is a challenging task due to the hostile conditions of the scenario. Outdoor techniques based on GPS are discarded due to the absence of a satellite signal in confined environments. The lack of distinguishable features causes traditional methods based on scan-matching techniques using laser sensors to fail. Something similar occurs with techniques based on the use

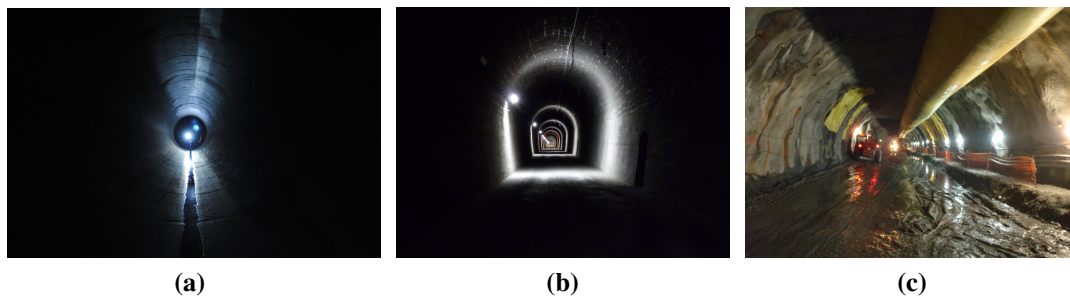


Figure 1.1: Challenging underground environments: (a) Smooth and monotonic inner surface of a pipe (b) Lack of lighting and features in a tunnel (c) Presence of fluids and uneven grounds in a tunnel under construction.

of cameras, e.g. Visual SLAM, where a proper illumination is needed to extract visual features. The absence of light and even the low-textured scenario make these methods also to perform erratically. Lastly, the presence of fluids and uneven surfaces make the wheel-odometry methods unreliable. Fig. 1.1 shows three typical scenarios that illustrate the localization challenges.

In recent years, promising technologies for indoor localization relying on the use of the Radio Frequency (RF) signal, have emerged as alternative methods. For instance, Ultra-Wideband (UWB) provides better accuracy than other RF technologies. However, these methods require placing with high precision several beacons in the infrastructure along with a previous commissioning step to obtain an RF map, being in most cases not feasible due to the nature of the environment. Moreover, infrastructure modifications are sometimes impracticable.

From the point of view of the RF signal propagation, tunnel-like environments, such as tunnels, mines, or pipes, differ from regular indoor and outdoor scenarios. On the one hand, depending on the wave frequency and the cross-section dimension, these environments can act as waveguides extending the communication in comparison to free space. On the other hand, the signal suffers from strong attenuations, known as fadings, due to the multipath nature of the propagation in these scenarios. In this context, [Rizzo, 2015] developed extensive and in-depth theoretical and experimental analysis of signal propagation in tunnel-like environments in order to address the issues related to the deployment of robots in confined environments with connectivity constraints. These studies showed that it is possible to obtain periodic spatial fadings under a certain transmitter-receiver configuration, being able to take advantage of this periodic signal structure for location purposes.

The results of this work constitute the starting point of this thesis. Our work aims to achieve an alternative robot location system for tunnel-like environments based on the use of the periodic RF signal. The goal is to overcome the main issues encountered in

these featureless scenarios which make traditional methods ineffective.

Firstly, filtering approaches were explored to solve the localization in metallic pipes and tunnels fusing the RF information with the odometry data. The results of these solutions and the challenges presented mainly in tunnels, led us to explore other approaches based on graphs, where different sources of information available in those scenarios are originally introduced to the localization process.

1.1.1 Previous work: The appearance of periodic RF fadings

Although the periodic RF fadings phenomena is described with more detail in the following chapters, in this section we summarize the foundations upon which this thesis was developed [Rizzo, 2015]:

- Tunnel-like environments behave as waveguides extending the communication range.
- The RF signal suffers from strong fadings due to multipath nature of the environments. The fadings are caused by the interaction between propagation modes.
- It is possible to obtain periodic fadings selecting the appropriate transmitter-receiver configuration.
- The period of the signal can be calculated in advance. In the case of metallic pipes, it only depends on the operating frequency and the pipe diameter. In tunnels, the period depends also on the operating frequency and the tunnel dimensions.
- In the case of tunnels, two regions can be distinguished in the signal: the *near sector* with fast fluctuation in the signal (*fast fadings*) and the *far sector* where the fading periodicity is observable (*slow fadings*).
- The fadings proved to be repeatable in the time domain and, in the case of pipes, the received signal is low in noise.
- In both cases, metallic pipes and dielectric tunnel, the propagation theory provides theoretical models that represent the behaviour of the RF signal along the environment.

In summary, a known-geometry periodic fading structure can be generated and its detection can be used during the localization process. Moreover, the fidelity of the theoretical model with the actual RF signal makes us consider the former as a position reference, playing the role of a known RF map (Fig 1.2).

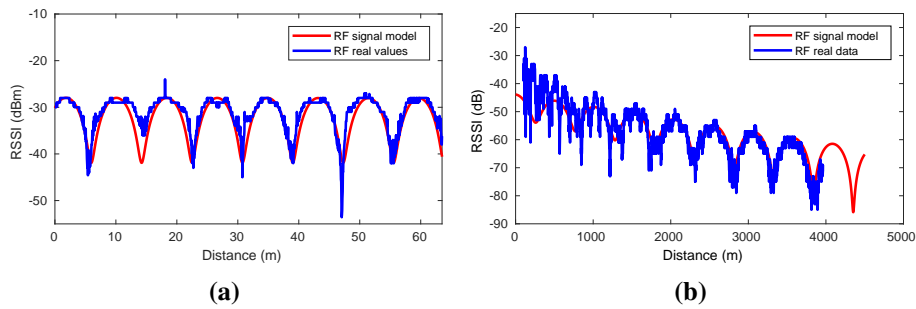


Figure 1.2: The appearance of periodic fadings in pipes (a) and tunnels (b).

1.2 Thesis Framework

This thesis was born from the common interest of the Robotics, Perception and Real-Time Group (RoPeRT) from Universidad de Zaragoza and the Instituto Tecnológico de Aragón (ITAINNOVA) in the development of technologies for robotic applications in hostile environments, such as tunnels and pipes. On the one hand, the RoPeRT group is a recognized group with great experience in the field of ground robotics in tunnel-like environments, being its recent activity in this field framed within a public funding project "Robot navigation and deployment in challenging environments - Robochallenge". On the other hand, the Robotics Group of ITAINNOVA is especially focused on robotic applications involving public works machinery in challenging environments, which resulted to the AUTODUMP project, "AUTOMation of the tunnel debris removal by means of robotized conventional DUMPers", in which both entities participated [Tardioli et al., 2018].

The thesis has been developed over 6 years in the period between 2014 and 2020. The motivation arises from the interest to continue with the research developed throughout the thesis *Propagation, Localization and Navigation in Tunnel-like Environments* [Rizzo, 2015] also performed in the RoPeRT group of the University of Zaragoza. Along this work and prior to the development of this thesis, several experiments to model and characterize the radio signal propagation in these type of environments were performed in two real scenarios: the Santa Ana dam drainpipe and the Somport tunnel. The obtained results concerning the spatial periodic structure of the RF signal, constitute the starting point of this thesis.

During the thesis, several experiments were carried out in the same real scenarios in order to collect data to validate all the proposed approaches. For the pipe experiments, an equipped Pioneer P3AT was used as the robotic platform. For the validation of the tunnel localization approaches, an equipped all-terrain vehicle was mainly used for the experiments, although other platforms were also used occasionally: the Robucar TT platform and a robotized dumper.

Although the whole thesis took place at the University of Zaragoza, a short research visit to the Centre for Applied Autonomous Sensor Systems (AASS) at Örebro University in Sweden was made from August 14 to September 8, 2017. During this visit, the work was primarily focused on novel approaches for applying Monte Carlo localization to radio frequency based localization in tunnels.

1.3 Thesis Structure and contributions

This thesis presents several contributions to the field of robot localization in tunnel-like environments, structured in two main parts: the use of the RF signal for localization purposes and a more generic graph-based approach. These contributions are organized as follows:

- First, in **Chapter 2**, we address the robot localization problem in metallic pipes exploiting the periodic structure of the RF signal in order to overcome the challenges presented in these scenarios. An adapted version of a particle filter using the RF signal and the theoretical propagation model as an RF map is developed and validated with experimental data collected in a real pipe. This contribution was presented in [Seco et al., 2016]. Subsequently, and taking into account the promising results of the proposed method, a comparison with EKF based solution is carried out as well as the development of an extended approach using the information of two RF receivers. With this configuration, which provides a 180 phase difference in the signal, the improvement in the accuracy and the reliability of the continuous localization is also demonstrated. The complete work regarding the localization in pipes was presented in [Rizzo et al., 2021].
- Following a similar strategy, in **Chapter 3**, we propose and implement an RF-based discrete localization system for tunnels, taking advantage of the periodic fadings also found in these scenarios under certain configurations. Each time a minimum of the RF signal is detected, the position of the robot in the tunnel is corrected using the position reference provided by the RF signal model. For the identification of the minima and the matching with the RF map, the use of the Recursive Least Square (RLS) algorithm and the individual compatibility test (IC) are proposed. The localization solution is validated with the data collected during the experiments carried out in a real tunnel. The empirical results show that it is possible to periodically reset the error accumulated by the odometry. This work was presented in [Seco et al., 2018].
- Taking into account the additional challenges regarding the RF signal in the case of tunnels, we went a step further with the aim of achieving a more robust localization in these scenarios. With that purpose in mind, we propose an alternative

graph-based localization system where we take advantage of the information provided by the relevant characteristics present in tunnel scenarios. In **Chapter 4** two detection methods of tunnel features are described. First, an alternative detection process based on geometrical matching between the real signal and the RF map to extract the information of the RF signal minima is developed. Secondly, a scan-pattern matching method is proposed to detect and identify structural features (galleries) present in tunnels. The valuable information resultant from both methods provides absolute measurements to be introduced in the graph.

- **Chapter 5** presents a multi-sensor graph-based approach to address the localization in tunnels which makes use of the information provided by the detectors presented in the previous chapter. The strategies to originally introduce into the graph the RF minima results and the data involved in the gallery detection as prior information are described. The method has been evaluated experimentally in a real tunnel scenario. The results confirm the feasibility of the detection approaches and the suitability of the graph localization approach to solve the localization in tunnels, showing the strength of the method for inspection tasks. Additionally, a performance analysis is deployed, which confirms the accuracy improvement depending on the sources of information involved in the localization process. The advantages of the proposed approach are also highlighted. This contribution was primarily presented in [Seco et al., 2020] using only the information regarding the RF minima and subsequently in the under-review article [Seco et al., 2021] with the incorporation of the galleries detection in the localization process.
- Finally, **Chapter 6** summarizes the conclusions and the directions for future work.

1.3.1 Publications

The novelty and originality of the approaches presented in this thesis are supported by the following peer-reviewed international robotics journals and conferences:

- Seco, T., Lázaro, M. T., Espelosín, J., Montano, L., and Villarroel, J. L. (2021). Robot Localization in Tunnels. Combining Discrete Features in a Pose-Graph Framework. *Under review*.
- Rizzo, C., Seco, T., Espelosín, J., Lera, F., and Villarroel, J. L. (2021). An alternative approach for robot localization inside pipes using RF spatial fadings. *Robotics and Autonomous Systems*, 136:103702.
- Seco, T., Lázaro, M. T., Rizzo, C., Espelosín, J., and Villarroel, J. L. (2020). Graph-based robot localization in tunnels using RF fadings. In Silva, M. F., Luís Lima, J., Reis, L. P., Sanfeliu, A., and Tardioli, D., editors, *ROBOT 2019*:

Fourth Iberian Robotics Conference, pages 580–592, Cham. Springer International Publishing.

- Seco, T., Rizzo, C., Espelosín, J., and Villarroel, J. L. (2018). Discrete robot localization in tunnels. In Ollero, A., Sanfeliu, A., Montano, L., Lau, N., and Cardeira, C., editors, *ROBOT 2017: Third Iberian Robotics Conference*, pages 823–834, Cham. Springer International Publishing.
- Tardioli, D., Riazuelo, L., Seco, T., Espelosín, J., Lalana, J., Villarroel, J. L., and Montano, L. (2018). A robotized dumper for debris removal in tunnels under construction. In Ollero, A., Sanfeliu, A., Montano, L., Lau, N., and Cardeira, C., editors, *ROBOT 2017: Third Iberian Robotics Conference*, pages 126–139, Cham. Springer International Publishing.
- Seco, T., Rizzo, C., Espelosín, J., and Villarroel, J. L. (2016). A Robot Localization System based on RF Fadings using Particle Filters inside Pipes. In *2016 International Conference on Autonomous Robot Systems and Competitions (ICARSC)*, pages 28–34.

Part I

Robot Localization based on RF Fadings in Tunnel-like Environments

Chapter 2

Localization based on RF Fadings inside Pipes

Accurate robot localization represents a challenge inside pipes due to the particular conditions that characterize this type of environment. Outdoor techniques (GPS in particular) do not work at all inside metal pipes, while traditional indoor localization methods based on camera or laser sensors do not perform well mainly due to a lack of external illumination and distinctive features along pipes. Moreover, humidity and slippery surfaces make wheel odometry unreliable. In this chapter, we present an alternative robot localization system using particle filter which takes advantage of the periodicity nature of spatial RF signal fadings that appears inside pipes under certain settings. The effectiveness of the method to solve the localization problem in the longitudinal dimension along the pipes is demonstrated experimentally in a real scenario. After studying the results some improvements are proposed and implemented. We also present a comparison of the previous method with respect to an EKF-based implementation following the same strategy. Finally, the accuracy and reliability of the RF-approach method is improved by taking advantage the 180-phase difference which appears when placing two RF receivers at specific positions in the robotic platform. All this work was reflected in [Seco et al., 2016, Rizzo et al., 2021].

2.1 Introduction

Pipe environments such as sewers, gas pipelines or dam drainpipes are exposed to structural damage over time. Inspection tasks are critical in order to detect and identify fissures, rusty areas, cracks or leakages that could have serious consequences for the safety of the infrastructure.

In recent years, robots have emerged as one of the best options for performing inspection tasks due to the harsh conditions of this type of environment: darkness, humi-

dity and even physical limitations [Siqueira et al., 2016]. In this context, accurate robot localization is essential not only for identifying the position of any damage, but also for autonomous navigation.

To do that, it is mandatory to generally establish a set of sensors for providing information about the surroundings of the robot. In order to solve global localization problem, that information is compared with an *a priori* knowledge, such as a map, database images, etc, which depends on the sensors used. To carry out this task it is usual to extract useful features from the sensor information in a way that makes possible a reliable matching process with previously mentioned attained information. To solve the local localization problem, it is possible to measure the orientation and position variations of the robot along time, and then, through different integration methods, obtain the localization relative to the initial point at each timestamp [Cox and Wilfong, 1990].

While identifying robot's position in the cross-section of pipes could be achieved using traditional techniques, localization along the longitudinal axis represents a challenge due to the fact that pipe's internal surfaces tend to be uniform (possibly without detectable features) and they are typically much longer than they are wide. Moreover, the aforementioned special nature of the environment makes the use of some common localization sensors unfeasible. This is the case of GPS sensor, for instance, that cannot be used in confined scenarios.

In [Guan et al., 2019] the authors present a review of localization methods for small-diameter pipelines using PIG (Pipeline Inspection Gauge) technology. The localization methods are mainly based on the fusion of the information provided by Inertial Navigation System (INS) and odometers. The accumulated error is corrected in two ways: using Above Ground Markers (AGMs), which detect the passage of the PIG and provides it with GPS coordinates, and by means of detecting the pipeline junction with information from the inertial sensor ([Sahli and El-Sheimy, 2016, Guan et al., 2017, Al-Masri et al., 2018]). However, although PIG-based solutions are adequate for a wide range of small-diameter pipes, the drive systems of these devices, either by pressure difference between ends or by the use of a tether cable, makes them unfeasible for large-scale pipes. In addition, they are not self-contained and require installation of infrastructure (e.g. AGMs). At last, communication from inside the pipe is not always feasible.

In several studies, visual odometry-based methods are proposed to solve these issues. Hansen et al. use monocular cameras [Hansen et al., 2011b], stereo cameras [Hansen et al., 2011a] or a monocular fisheye camera [Hansen et al., 2015] with visual odometry algorithms for navigation in small cylindrical pipes. The authors claimed that good results depend on the presence of small-scale features on the internal surface detected by cameras close to walls. In [Alejo et al., 2017], the authors present a localization system for sewers based on visual odometry combined with a manhole detection system using RGBD cameras and machine learning techniques working with a known



Figure 2.1: Santa Ana dam pipe. Symmetric and smooth inner surface without distinguishable features.

topological map. Visual-based algorithms only work properly if there are enough distinguishable surface features or irregularities. Nevertheless, these algorithms based on cameras or lasers tend to perform erratically in those cases of pipes that present symmetry and limited features (see Fig.2.1). The unsuitability of the use of a LIDAR-based systems in these type of environments to solve the longitudinal localization is also mentioned in [Tardioli et al., 2019] and [Zhao and Whittaker, 2020].

The problems of vision and laser-based approaches are outlined, for example, in [Ozaslan et al., 2015] and in [Ozaslan et al., 2017] for the inspection of penstocks using Unmanned Aerial Vehicles (UAVs). Penstocks are large cylindrical pipes with two long non-parallel straight sections joint with an elbow. Having ruled out the use of vision in these environments, the authors propose the use of an Inertial Measurement Unit (IMU) and laser rangefinder sensors for localization. Nevertheless, the absence of detectable features makes longitudinal localization impossible if the junction between sections is not in the range of the laser.

Other methods rely on wheel odometers for localization, but due to the high humidity and even the presence of fluids and mold, pipes tend to be slippery, making these methods inaccurate and unreliable for position estimation. In [Murtra and Tur, 2013], the position of the robot along the pipe is obtained fusing the information provided by an IMU and a cable encoder which measures the length from the starting point to the tethered robot. Most of the time, these methods are unfeasible because of the length of

the pipe or the type of robotic platform (e.g. drones).

Due to the aforementioned infeasibility of using sensors like GPS, cameras or lasers to determine the longitudinal localization of a robot inside a pipe, other technologies must be explored. Recently-developed indoor positioning technologies rely on the use of Radio Frequency (RF) signal ([Torres-Solis and Falk, 2017, Alarifi et al., 2016]). Ultra-Wideband (UWB), for example, is one of the most promising technologies for indoor localization, providing more accurate positioning and better performance than other RF technologies. Nevertheless, these RF-based indoor localization methods require prior collection of RF fingerprints of the scene to be compared afterwards with the online data (RF fingerprinting method) or at least three reference nodes placed with high precision in the infrastructure in the case of using trilateration algorithms to obtain the position [Daixian and Kechu, 2011]. Taking into account that inspection tasks are usually carried out during limited maintenance periods (e.g., a water pipe that needs to be emptied), the need for a commissioning step in order to place beacons or create an RF map makes these methods impractical. In [Wu et al., 2016], a robotic sensor network is proposed for localization in an underground plastic water pipeline. The system, tested in simulation, consists of a mobile sensor node carried by the robot and multiple relay nodes placed aboveground (in a line parallel to the water pipeline), covering limited sections of the pipe. The position is obtained by fusing the RF signal measurements from the relay nodes and the velocity provided by an onboard IMU with an Extended Kalman Filter (EKF) algorithm. This solution is not suitable, however, for metallic pipes where the Faraday cage effect hinders communication between the inside and outside. Another approach, using sound instead, is presented in [Ma et al., 2017]. The idea is to build a map of the vibration signals induced by a hydrophone in a metal pipe and use this map and a Kalman or particle filter for location purposes. Nevertheless, this approach has not been taken beyond a small lab experiment.

From the point of view of the RF signal propagation, tunnel-like environments, such as tunnels, mines, or pipes, differ from regular indoor and outdoor scenarios. On the one hand, these environments behave as waveguides above certain frequencies, extending the communication range in comparison to free space. On the other hand, the signal suffers from strong periodic spatial fading phenomena under certain transmitter-receiver configurations. In [Rizzo et al., 2014a], the authors present the results of an extensive analysis of RF propagation in the longitudinal dimension in a metallic pipe under different transmitter-receiver setups, demonstrating that it is possible to obtain strictly periodic spatial fadings, which are predictable and repeatable in both temporal and spatial domains. This work explores the use of the characteristic periodic fadings to design a discrete RF odometry-like localization method to localize a robot inside a pipe. A thorough analysis of the received RF power in the transverse (cross-section) dimension is also carried out in [Rizzo et al., 2021].

In this chapter, we design and implement a continuous robot localization system

using an adapted version of the well-known Monte Carlo Localization system (MCL). The main idea is to take advantage of the periodic nature of the RF waveform in this environment using the RF propagation model as an RF map. MCL is a probabilistic localization algorithm based on particle filters that has become one of the most popular algorithms in robotics. Its main strengths are that it is able to represent multi-modal distributions and thus can globally localize a robot. Moreover, it is easy to implement and it is better in terms of memory consumption compared to grid-based Markov localization [Dellaert et al., 1999, Thrun et al., 2001]. MCL has the great advantage of not being subject to linearity or Gaussian constraints on the robot motion and sensor measurement.

The same strategy is also implemented but based on the EKF algorithm in order to compare the results provided by both localization algorithms. Finally, the phase difference (spatial phase shift) obtained with multiple receivers resultant from the analysis of the received RF power in the transverse (cross-section) dimension, is used to improve the accuracy and reliability of the continuous localization approach.

One of the main advantages of this approach over other RF-based previously cited methods is that there is no need to previously adapt the infrastructure, being the only requirements the placement of a continuous wave transmitter at the starting point and a receiver (or two at most) on the robotic platform in order to generate and detect the periodic fading waveform respectively. Metallic pipes have a low attenuation rate, providing us with a maximum possible coverage length of several kilometers using this method. Moreover, there is no need for a previously known map of the environment.

The work presented in this chapter extends the methodology presented in [Rizzo et al., 2014a], from a discrete localization to a continuous solution to estimate the longitudinal position of a robot inside metallic pipes. The validation of the approach is demonstrated using real data collected during experiments carried out in a real scenario.

2.2 Fundamentals of Electromagnetic propagation in metallic pipes

This section summarizes the studies conducted at [Rizzo et al., 2014a] and [Rizzo et al., 2021] regarding the radio signal propagation in pipes and the appearance of periodic fading, which are relevant to the location method developed during this chapter.

2.2.1 Longitudinal fadings analysis

In free space, an RF source, such as an antenna, produces spherical waves that have a non-isotropic spatial distribution, corresponding to the radiation pattern of the antenna. Far enough from the emitter, the waves can be considered as locally plane Transverse Electromagnetic (TEM) propagating along the radial directions. If, however, an emitting antenna is inside an air filled pipe, the spherical wavefronts will be multiply scattered by the surrounding walls. The superposition of all these scattered waves is itself a wave that propagates in one dimension (along x , the pipe length) with a quasi-standing wave pattern in the transverse dimensions.

Applying the electromagnetic boundary conditions at the metallic wall, many different solutions for the field configurations can be obtained. These are customarily called *modes*, and are classified as *TE* or *TM* (Transverse Electric or Transverse Magnetic respectively). Each mode has its own wavelength, attenuation constant, and cutoff frequency (that depends on the pipe diameter), below which the mode does not propagate. The lower the order of the mode, the lower the cutoff frequency. The mode with the lowest cutoff frequency is called the dominant mode. Below the first mode cutoff frequency, the expected behaviour of the signal is a rapid attenuation, as the pipe does not act as a waveguide for these frequencies. For communication purposes, metallic waveguides are used mostly in the so called monomodal regime, choosing an operating frequency that allows only the dominant mode to propagate. Fig. 2.2a shows these two effects.

However, the results in [Rizzo et al., 2014a] showed that allowing propagation of two or three modes and by taking advantage of their geometry, strictly periodic fadings can be obtained, being exploited for localization in these featureless environments (Fig. 2.2b). In bimodal propagation, there is interference between the first two modes (TE_{11} and TM_{01}). The interaction between the first and third modes produces shorter period fadings compared to the bimodal case being more useful for localization purposes. This case is called trimodal propagation because a frequency above the cutoff is selected to excite the third mode. This frequency also involves propagating the second mode. The solution for eliminating the influence of the latter is, taking advantage of the geometry of the modes, to choose an emitter-receiver configuration with enhanced sensitivity for the first and third interference mode, while reducing the second mode. For practical purposes, aligning the antenna with the electric field lines, enhances the power coupling, while placing it perpendicular diminishes it.

The electric field for a given n^{th} mode can be represented as:

$$E_n(x, y, z) = E_0(y, z)e^{-\gamma_n x} \quad (2.1)$$

where $E_0(y, z)$ defines the electric field in the pipes cross-section – amplitude and direction – and the exponential part represents the propagation as a slightly attenuated wave along the pipe (x axis). γ_n is the so called propagation constant, given by:

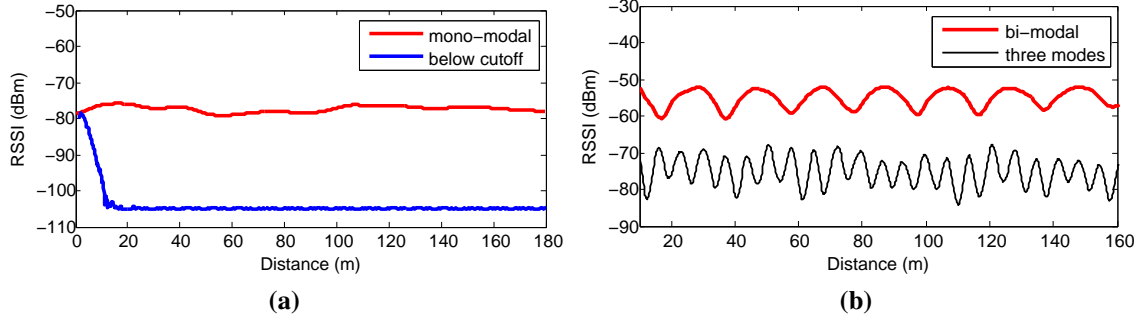


Figure 2.2: Different propagation scenarios in Castillonroy from [Rizzo et al., 2014a]. (a) below cutoff: $f = 40$ MHz. monomodal: $f = 51$ MHz. (b) bimodal: $f = 71$ MHz, trimodal: $f = 75$ MHz trimodal.

$$\gamma_n = \alpha_n + j\beta_n \quad (2.2)$$

Its real part, α , is the attenuation constant (Np/m) and its imaginary part, β , is the phase constant (rad/m).

Each mode has a different wavelength, given by:

$$\lambda_n = \frac{2\pi}{\beta_n} = \frac{c}{f \sqrt{1 - \left(\frac{f_{cn}}{f}\right)^2}} \quad (2.3)$$

where c is the free space speed of light, f the operating frequency and f_{cn} the n^{th} mode cutoff frequency, which is a function of the pipe's diameter and is calculated as in [Rizzo et al., 2014a].

The total field is the sum of the fields of the present modes. Hence, if two modes are interacting, the field can be calculated as:

$$E_{tot}(x) = K_1 e^{-\gamma_1 x} + K_2 e^{-\gamma_2 x} \quad (2.4)$$

where K_1 and K_2 are a function of the power coupled to each mode from the excitation source (determined by the antenna characteristics and position inside the pipe). To calculate them, a standard microwave procedure as described in Chapter 4 of [Poza, 2005] can be followed.

In the following, for localization purposes, we will adopt the Received Signal Strength Indicator (RSSI) in the receiving antenna as a practical RF signal model $h(x)$, calculated as:

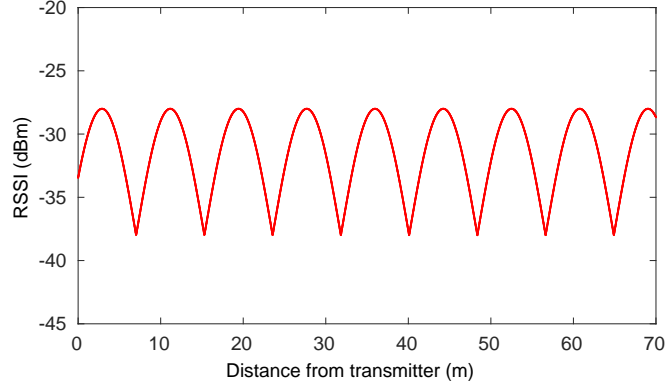


Figure 2.3: Periodic fadings caused by the interaction of two modes propagating in a 4-meter diameter pipe.

$$h(x) = 20 \log_{10} |E_{tot}(x)| \quad (2.5)$$

The period of this fading structure D is the distance that creates a relative phase of 2π among the two considered modes. If λ_1 and λ_2 are the two mode's wavelengths, then:

$$D = \frac{\lambda_1 \lambda_2}{|\lambda_1 - \lambda_2|} \quad (2.6)$$

Summarizing, the pipe diameter determines the different mode's cutoff frequencies. By selecting the operating frequency, one can choose the number of modes to propagate. If there are two modes propagating and interacting (e.g. by selecting a frequency above the second mode's cutoff frequency and below the third mode's) periodic fadings are obtained. The period of the fadings is a function of the operating frequency, and the pipe diameter (as it determines the cutoff frequencies). Moreover, it is possible to calculate the theoretical electromagnetic propagation (RF signal model) along the pipe using the presented equations. Fig. 2.3 illustrates an example of these periodic fadings, as a result of a simulation of two modes propagating inside a 4 m of diameter pipe.

2.2.2 Transversal fadings analysis

Having studied the fadings along the longitudinal dimension, in particular, the cases of bimodal and trimodal propagation, an analysis of the transversal structure of the fadings was carried out in [Rizzo et al., 2021]. The goal was to determine the influence of the cross-section position of the receiver on the RSSI and relative phase of the fadings.

By analyzing the electric field distribution of the first three modes, together with the practical placement of two receivers in a robot (Fig. 2.4), two cases emerge as relevant

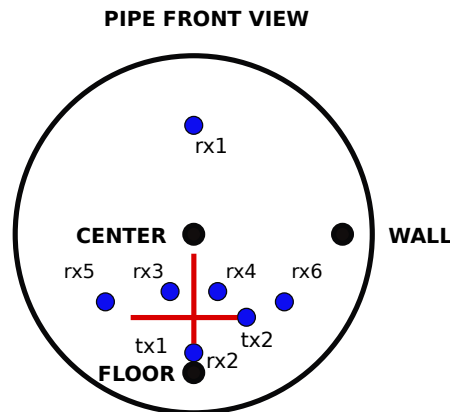


Figure 2.4: Pipe front view. Transmitter-receiver positions for different cross-section fadings analysis from [Rizzo et al., 2021].

for analysis: virtually dividing the pipe with respect to the center horizontally (upper vs lower half) and vertically (right vs left half). The work consisted of a complete analysis of the agreement or disagreement between the zones of interest (left vs right, up vs down) regarding to if the electric-field lines of the two modes interacting add positively (both lines go in the same direction), or the contrary case. Empirical results in a real pipe environment show that an agreement translates into the same spatial phase (both signals with matching maxima and minima), while a disagreement translates into a phase delay of 180 degrees (a maximum in one signal matching a minimum in the other). That is, depending on the chosen setup, the fadings corresponding to each sector are in phase or present a relative phase difference of about 180 degrees. The results of the transversal fadings analysis are summarized in Fig. 2.5.

The phase difference obtained using two receivers placed at certain positions, is exploited to improve the robustness and resolution of the fadings-based localization algorithm as will be shown in Section 2.5.

2.3 Test Scenario and Experimental Setup

As stated before, one of the goals of this thesis is to demonstrate the validity of the proposed localization methods in real scenarios. As the real environment and the experimental setup are common for the approaches presented in the next sections, we introduced them in advance to facilitate the reader's understanding and to avoid duplication of information.

The real scenario was a 4 m internal diameter and 300 m long carbon steel pipe, used as a drainpipe for the Santa Ana dam in Castillonroy, Spain. It consists of two

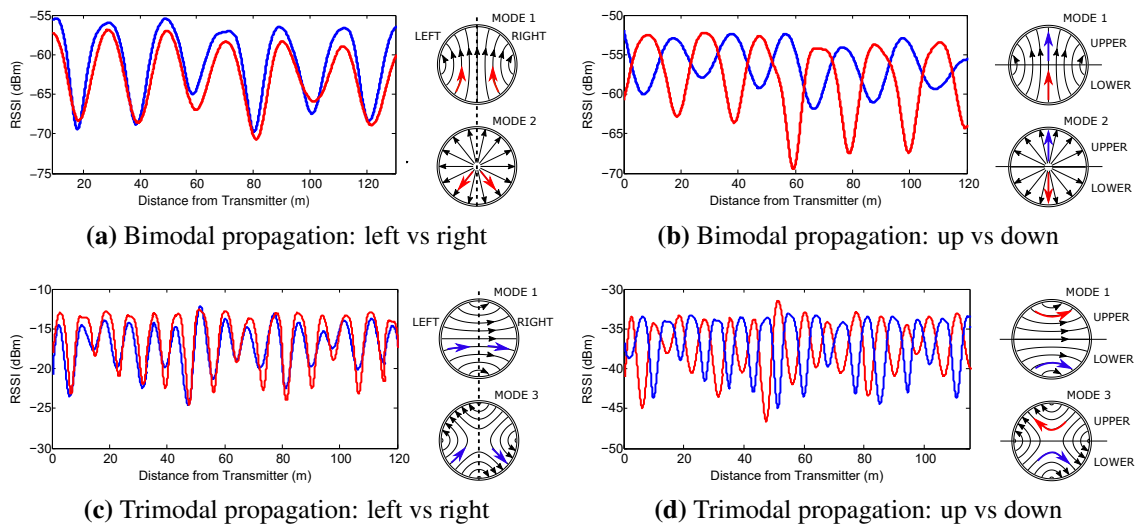


Figure 2.5: Received signal power in the left and right half ((a) and (c)) vs upper and lower half((b) and (d)), together with the electric field distribution for: bimodal propagation ((a) and (b)) and trimodal propagation ((c) and (d)). The blue arrows represent constructive interference between the electric fields of the two modes interacting, while the red arrows the opposite (see [Rizzo et al., 2021]).



(a) Straight and tilted parts of the pipe



(b) Instrumented Pioneer P3AT robot inside the pipe



(c) Structural landmarks (cardboard cylinders) at the laser field of view

Figure 2.6: Pipe experimental setup.

inclined parts (at the beginning and the end, tilted 23 and 30 degrees respectively), and a 120 m straight part (see Fig. 2.6a). A Pioneer P3AT wheeled robot was used as the mobile platform (Fig. 2.6b) simulating a service routine. The platform was equipped with two RF Explorer model 3G portable spectrum analyzers as RF receivers (in order to exploit the spatial diversity), two built-in wheel encoders, an Xsens MTI 100 IMU, and a SICK LMS200 laser range sensor. As the pipe has no structural features, a series of landmarks were added at the laser field-of-view level (separated 10 m one from each other, see Fig. 2.6c) in order to build a map of the pipe using the GMapping SLAM algorithm [Grisetti et al., 2007, Grisetti et al., 2005]. The real localization of the robot (ground truth) is obtained with the localization algorithm developed in [Lazaro and Castellanos, 2010], mixing the information from the odometry and the laser sensor over the previously built map of the pipe with the known position of the structural landmarks.

The instrumented robot was displaced inside the pipe up to 70 m from the transmitter, streaming and logging the data from the sensors to a computer running Robot Operating System (ROS) [Quigley et al., 2009] over Ubuntu. The robot travelled in a straight line with a mean speed of 0.5 m/s and hence, the heading variations are negligible. The distance travelled by the robot is lower than the total length of the pipe because of the inability of driving the robot along the two slopes of the extremes of the pipe.

To obtain shorter period fadings, trimodal propagation was chosen over the bimodal case. The frequency selected was $f=78.2$ MHz, producing fadings with a period of 8.26 m. The transmitter antenna was placed horizontally at 1 m from the floor, and the two receivers at 1.5 m and 2.5 m in height (0.5 m above and below the center of the pipe). With this configuration, a relative phase difference of about 180 degrees is expected between the receivers. As stated before, this feature will be exploited to improve the localization accuracy as will be explained in Section 2.5.

Given the operating frequency of 78.2 MHz, the inner pipe diameter of 4-m, and assuming an electrical conductivity of 4.5×10^6 S/m and a relative permeability of 100 (typical values for carbon steel), the propagation constants obtained are $\gamma_1 = \alpha_1 + j\beta_1 = 0.0001 + j1.356 \text{ m}^{-1}$ and $\gamma_2 = 0.0005 + j0.595 \text{ m}^{-1}$. The power wave amplitudes K_1 and K_2 can be determined offline or even adjusted online in a practical approach, once the first fading is traversed, given that the sum of the power amplitude of both modes is equal to the fading maximum, while the subtraction of both equals the fading minimum. The online adjustment of the power wave amplitudes would solve the potential disparity between the theoretical model and the actual signal in case of systematic errors (bias) in the RF sensors. The values obtained were $K_1 = 0.024$ and $K_2 = 0.016 \text{ mW}^{-1/2}$ (which actually adjust the total radiated power to -26 dBm, matching fairly good with our setup). Using all this data, it is possible to calculate the theoretical electromagnetic propagation along the pipe that will play the role of an RF map using Eq. (2.4). Fig. 2.7 shows the RF propagation models corresponding to the locations of both receivers.

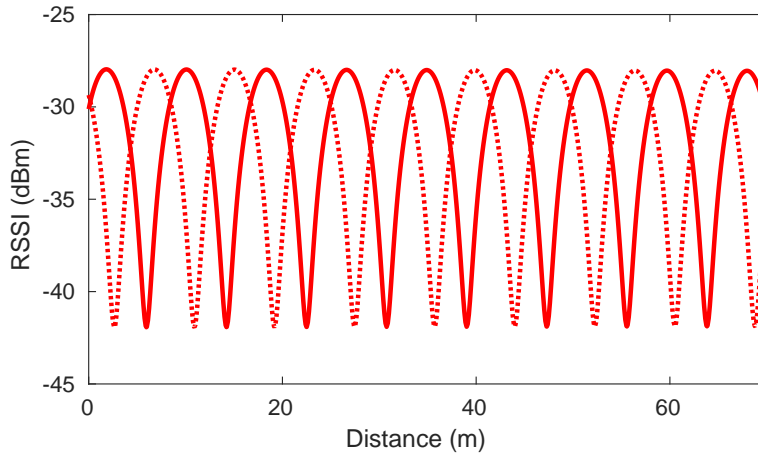


Figure 2.7: Theoretical received signal corresponding to the upper half and lower half of the pipe for trimodal propagation.

Recall that the period of the fading is never adjusted, it is easily theoretically calculated (given only the radius of the pipe and the operating frequency), and that the electrical conductivity and relative permeability only influence on the attenuation, which is relatively small in metallic pipes.

2.4 Robot Localization using one RF Signal Fadings

2.4.1 Continuous Localization system based on RF fadings using Particle Filters

As has been described in Section 2.2, the fadings waveform and its period can be calculated without the need for previous experimental measurements inside the pipe (see Eq. (2.4) and Eq.(2.6)). Each longitudinal position of the pipe has an associated RSSI value, meaning that this RF signal model serves as a unidimensional map (herein the RF map). RF sensor information will be compared with the fadings structure in a similar way that a laser sensor is used with a 2D occupancy grid.

Algorithm formulation

The goal is to obtain continuous robot localization along the pipe. For this purpose, let the state of the robot x_t at time t be calculated using its motion model f :

$$x_t = f(u_t, x_{t-1}) + \epsilon_t, \epsilon_t \sim \mathcal{N}(0, V) \quad (2.7)$$

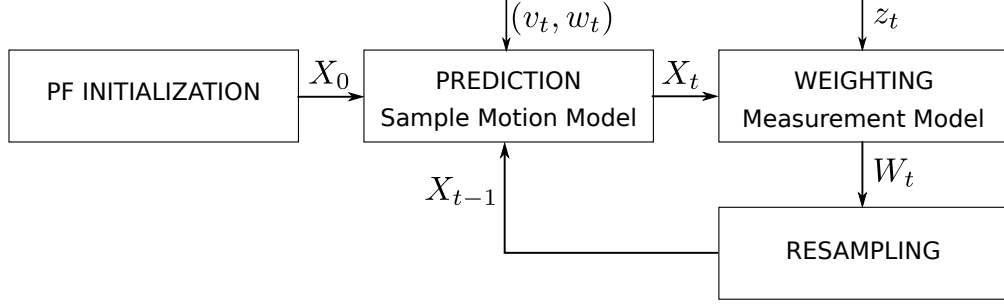


Figure 2.8: MCL Steps.

where u_t are the control inputs at time t and ε_t is a random variable that models the uncertainty introduced by the state transition based on variance V . Due to the cylindrical shape of the pipe, the robot travels in a straight line and only slight heading variations are observed. Therefore and from now on, the state x_t will refer to position x along the pipe.

During the displacement of the robot, the observations z_t at time t are provided by the sensors. The non-linear measurement model h relates the observations to the state of the robot x_t :

$$z_t = h(x_t) + \delta_t, \delta_t \sim \mathcal{N}(0, W) \quad (2.8)$$

where δ_t corresponds to the uncertainty of the measurement represented by a random noise based on variance W .

In our RF approach, the RF signal model (Eq. (2.5)) is used as the measurement model:

$$h(x_t) = 20 \log_{10} |(K_1 e^{-\gamma_1 x_t} + K_2 e^{-\gamma_2 x_t})| \quad (2.9)$$

where we have converted to RSSI in dBm units with K_p in $mW^{-1/2}$ units.

Following this general formulation, the proposed strategy relies on an adapted version of the Monte Carlo Localization (MCL) system using the RF signal model as an RF map.

As previously mentioned, MCL is based on the well known particle filter, a non-parametric filter which represents the posterior belief $bel(x_t)$ by a set of random weighted samples called particles $\mathbf{X}_t = \{x_t^1, x_t^2, \dots, x_t^M\}$ where M is the number of particles and x_t^m is the position of each particle, in this case, its longitudinal position along the pipe [Thrun et al., 2005]. Fig. 2.8 shows the basic steps of the MCL system.

In the first step, once the filter has been initialized, the predicted state of each particle x_t^m is calculated by means of its motion model taking into account the inputs of the system, linear and angular speed (v_t, w_t) , and the set of particles computed in the previous

iteration (\mathbf{X}_{t-1}). Then, a weight w_t^m is assigned to each particle according to the error between the expected observation by the predicted position of the particle and the real one z_t . Finally, during the resampling step, a new set of particles with different distribution is generated based on the weight associated to each particle ($\mathbf{W}_t = \{w_t^1, w_t^2, \dots, w_t^M\}$). The final pose estimation x_t is obtained as the mean of the positions represented by the new particle distribution resultant from the resampling step. These steps are repeated iteratively.

Particle filter initialization

To initialize the filter, an initial uniform distribution of particles \mathbf{X}_0 over a specific length of the pipe is created. In order to avoid ambiguity problems derived from the periodic nature of the fadings waveform, as well as the random initial phase of the fadings, the selected length will correspond to the length of the known period of the signal. The particles will be then distributed along the first fadings period:

$$X_0 = rand(M) * D \quad (2.10)$$

where M corresponds to the number of particles, $rand(M)$ returns normalized M random values (between 0 and 1) that are drawn from a uniform distribution, and the range of the distribution is the fadings period D (Fig. 2.9).

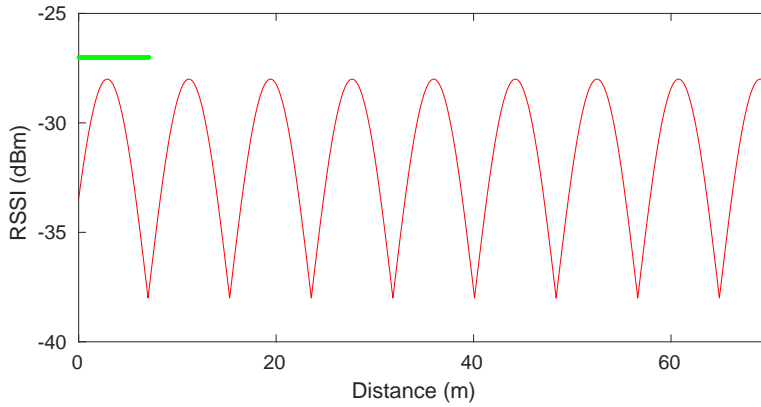


Figure 2.9: Particle filter initialization along the first fading period.

Prediction Phase: Motion Update

Once the filter is initialized with a set of particles, during the prediction step, the state of each particle x_t^m is updated based on its sample motion model f :

$$x_t^m = f(u_t, x_{t-1}^m) + \epsilon_t \quad (2.11)$$

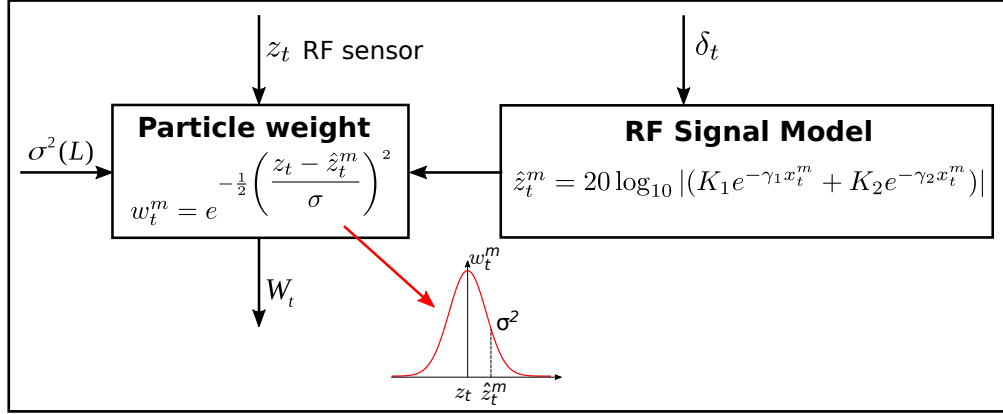


Figure 2.10: Weighting step.

where u_t corresponds to the inputs of the system, linear and angular speed (v_t, w_t) . The displacement applied to each particle corresponds to the distance travelled by the robot in the last timestamp taking into account the motion model and uncertainty of the vehicle odometry modeled by means of a random noise ε_t based on variance V .

Weighting

Once the predicted state for each particle is obtained, we weight them taking into account the actual observation and the expected observation predicted by the measurement model. Similarly to the typical matching process between laser scan measurements and a previously known grid map, the measurements provided by the RF sensor (actual observation) are compared with the RF map (expected observation).

The lower difference between the actual and the expected observation, the more probability that the particle will be a good hypothesis of the actual position. To calculate the weight that represents this probability any probabilistic density function can be used. The Gaussian function has been proven to be a good distribution to represent the divergence between the actual value and the measurement model when working with RSSI signals [Zàruba et al., 2007, Chiang et al., 2009]. The algorithm presented in this chapter makes use of it:

$$w_t^m = e^{-\frac{1}{2} \left(\frac{z_t - \hat{z}_t^m}{\sigma} \right)^2} \quad (2.12)$$

where $\sigma^2(L)$ is the variance of the likelihood function applied to the innovation process, z_t is the actual observation and \hat{z}_t^m is the expected observation for the m -th particle calculated using the RF signal model as the measurement model similarly to Eq. (2.9):

$$\begin{aligned}\hat{z}_t^m &= h(x_t^m) + \delta_t \\ &= 20 \log_{10} |(K_1 e^{-\gamma_1 x_t^m} + K_2 e^{-\gamma_2 x_t^m})| + \delta_t, \delta_t \sim \mathcal{N}(0, W)\end{aligned}\quad (2.13)$$

where the uncertainty of the measurement model δ_t is represented by a random noise base on variance W added to the predicted measurement value. Fig. 2.10 represents the weighting process.

Resampling

In the resampling step, the particles in the first-stage sample that are associated with small normalized importance weights are most likely to be discarded, whereas the best particles in the sample are replicated in proportion to their importance weights.

Various resampling approaches have been proposed in the literature on particle filtering (see [Douc, 2005, Li et al., 2015]). As a first approach we selected multinomial resampling method.

The core idea of this method is to generate independently N random numbers, U_t^n from the uniform distribution on $(0, 1]$ and use them to select particles from X_t . In the n -th selection, the particle x_t^m is chosen when the following condition is satisfied:

$$Q_t^{(m-1)} < U_t^n < Q_t^m \quad (2.14)$$

where:

$$Q_t^m = \sum_{k=1}^m w_t^k \quad (2.15)$$

Thus, the probability of selecting x_t^m is the same as that of U_t^n being in the interval bounded by the cumulative sum of the normalized weights as shown in Eq. (2.14).

In our proposed resampling implementation the number of random uniformly distributed particles is the same as the first-stage sample for each iteration (M).

Once a new set of particles are obtained from the resampling step, the estimated position of the robot x_t at time t is calculated as the mean of the positions represented by the particles:

$$x_t = \frac{1}{M} \sum_{m=1}^M x_t^m \quad (2.16)$$

2.4.2 Experimental results

Algorithm implementation

In order to check the validity of the continuous localization method in a real situation, the algorithm described in the previous section was implemented using the Robotics

Toolbox for MATLAB [Corke, 2011] and tested with real data collected during the experiments carried out in the real scenario described in Section 2.3. New classes were created to implement the differential vehicle model, the RF sensor and its measurement model, and the particle filter algorithm based on fadings.

As stated before, during the experiment, the robot moved up 70 meters from the transmitter position along the pipe collecting the data provided by the sensors mounted on the robot:

- Linear and angular speed (v, w) : These values are provided by the odometry sensors and correspond to the linear and angular speed of the robotic platform, used in the prediction step of the continuous localization methods.
- Linear acceleration and angular speed (a, w) : Data provided by the IMU corresponding to the linear acceleration and angular speed. The state of the vehicle is predicted with these values when the IMU is used instead of the odometry sensors.
- RSSI values (z_1, z_2) : These sensor measurements are provided by the RF receivers placed at different heights and are used in the update step of the different proposed methods.
- Ground truth: The real localization of the robot corresponding to the distance from the transmitter, obtained as previously explained. This value is used to compare the estimated pose of the robot provided by the localization algorithms with the robot real position. From now on, pose estimation error refers to the absolute value of the difference between the estimated position and the ground truth.

For the results described in this section, only one RF signal is used in the implemented algorithms (i.e., z_1 and its corresponding RF signal model from Eq. (2.5)).

During the filter initialization, M number of particles are randomly distributed over one spatial period of the fadings (8.26 m). Besides the initial distribution of the particles along the pipe, the variances values previously mentioned must be chosen in order to model the uncertainty of the elements involved in the system:

- V : variance associated with the uncertainty of the vehicle odometry.
- L : variance of the likelihood function used during the particle filter weighting process.
- W : variance to model the uncertainty of the measurement model.

To test the proposed localization algorithm, the number of particles (M) is set to 1000 and the number of iterations of the algorithm corresponds to the samples collected during the real experiment at a frequency of 10 Hz (which is the sampling rate of the

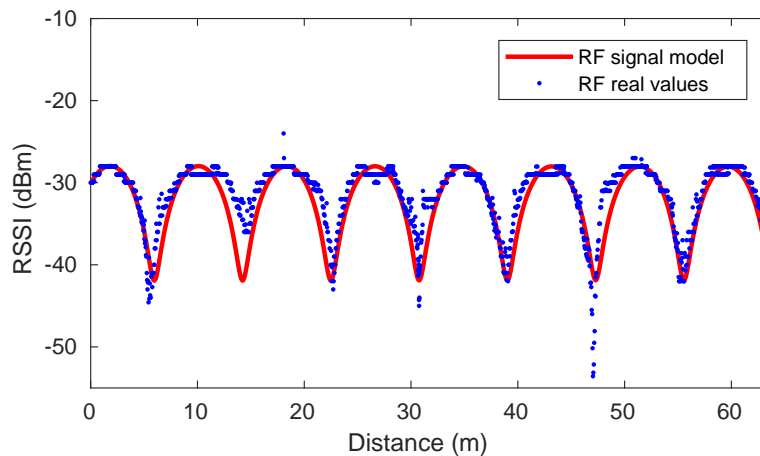


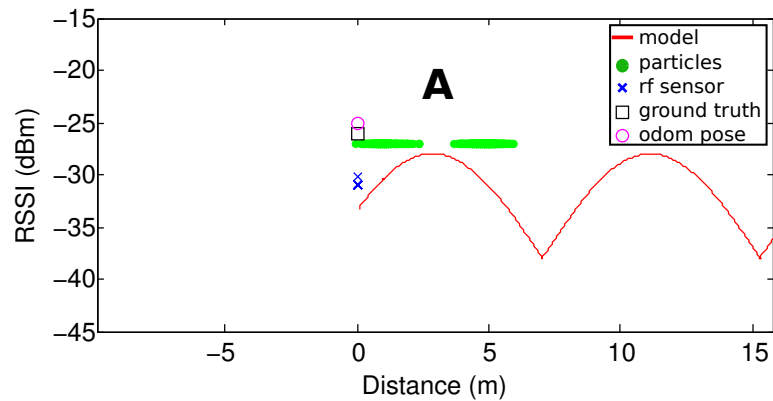
Figure 2.11: Measured received power (dotted) vs theoretical propagation model.

RF receiver). The variance values are selected based on the data sheets of the sensors: $V = 0.1^2 m^2$, $W = 2^2 dB^2$. The variance of the Gaussian likelihood function L is set to $0.5 dB^2$.

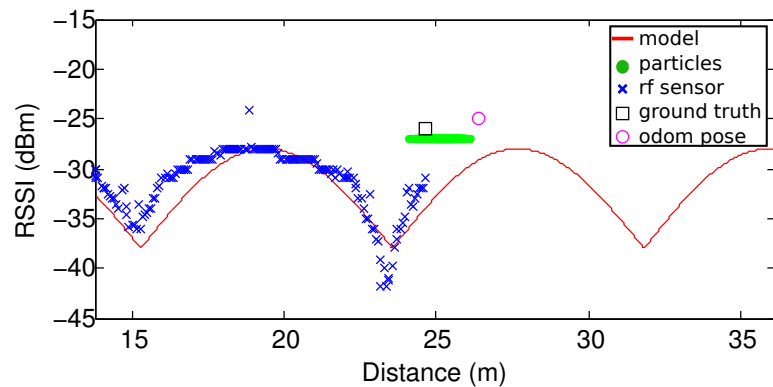
Results

The first stage of the validation process is to verify the periodicity of the received RF signal and then to prove the suitability of the proposed algorithm. Fig. 2.11 shows the RF signal model together with the measured RSSI values provided by the RF sensor, associated to the position with the ground truth. It can be seen that, despite these two signals being slightly different, the similarities between them are enough to make us believe that accurate localization can be achieved with the approach proposed in this thesis.

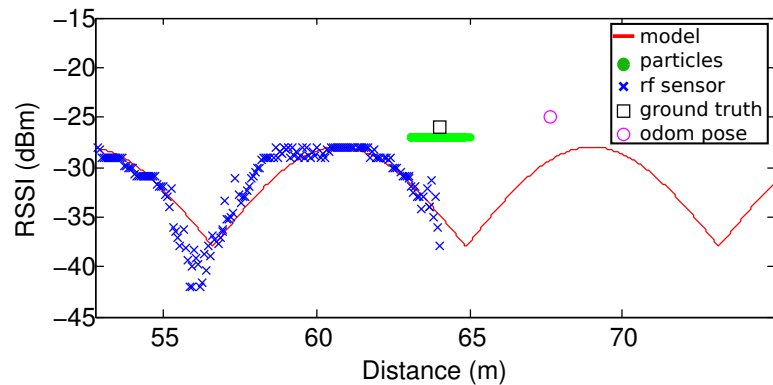
Fig. 2.12 shows the evolution of the particles during the longitudinal displacement of the robot along the pipe. The y-axis value of the particles, ground truth and odom pose has been set at these values only for visualization purposes (due to their uni-dimensional nature). The estimated position is the mean position of the particles for each iteration. The real position corresponds to the ground truth. Fig. 2.12a represents the initial stages of the particle filter. As expected from the initial distribution of the particles along the first period, after some steps of the algorithm, the particles are concentrated in two regions. This phenomena is due to the symmetrical shape of the signal, where two different longitudinal positions have the same RSSI value. The initial ambiguity will remain until a unique point will be reached, in this particular case the longitudinal position that corresponds with a change in the slope of the signal. As a consequence of this, during the first meters of the movement, the error value will not decrease, as it can be seen in Fig. 2.14 denoted by A. In Fig. 2.12b and Fig. 2.12c we can see



(a) Particle distribution ambiguity due to the periodic structure of the fading signal



(b) PF evolution after a robot displacement of 24 m. Ambiguity solved



(c) PF evolution after a robot displacement of 64 m. PF estimated position converges towards the ground truth whereas odometric estimation diverges from it

Figure 2.12: Algorithm evolution. Due to the uni-dimensional nature of particles position, odom position and ground truth, the y-axis values for them have been set only for visualization purposes.

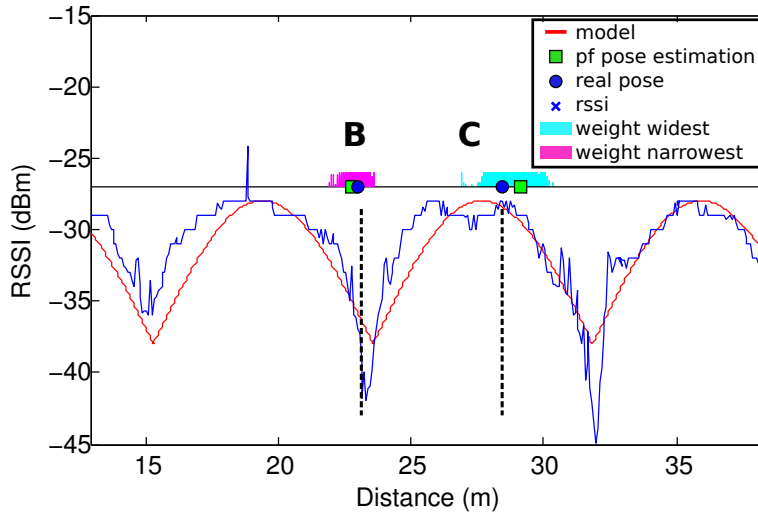


Figure 2.13: Weighted particles distribution at two different timestamps.

different points of the robot trajectory and how the uncertainty in the pose estimated by the proposed algorithm remains constant whereas the error between the real position and the position estimated with odometry increases along time. As shown, a good estimated position is obtained even working with a noisy RSSI signal. Fig. 2.13 represents the weight assigned to each particle at two different timestamps. As expected, narrower particles distribution arises in those zones where there are less possible positions for the same value of RSSI (**B**). In contrast, wider particle distribution is observed in those zones where low differences in the RSSI signal can match with a large range of positions (**C**). As a consequence, the uncertainty of the systems increases. The effect of these two behaviours over the position error is shown in Fig. 2.14. This figure also shows how the position error of the proposed method remains bounded around acceptable values whereas the position error resulting with the odometry estimation increases along the time.

The cumulative error of the odometry pose estimation can be observed in Fig. 2.15. In contrast, the estimated position obtained through our proposed method follows closely the real position of the robot.

First conclusions

The empirical results show that the mathematical model of the RSSI signal along the pipe is similar enough to the RF sensor measurements in the real scenario to be used as position reference. Fusing the information provided by two different sources, one based on the odometry system of the vehicle and the other one based on the periodic fadings signal inside the pipe, the position error remains within acceptable limits in contrast to

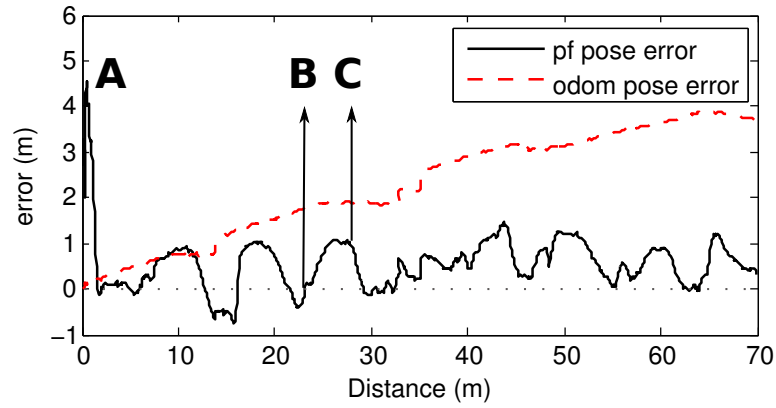


Figure 2.14: Odometry and Particle Filter position estimation error as a function of the travelled distance (ground truth).

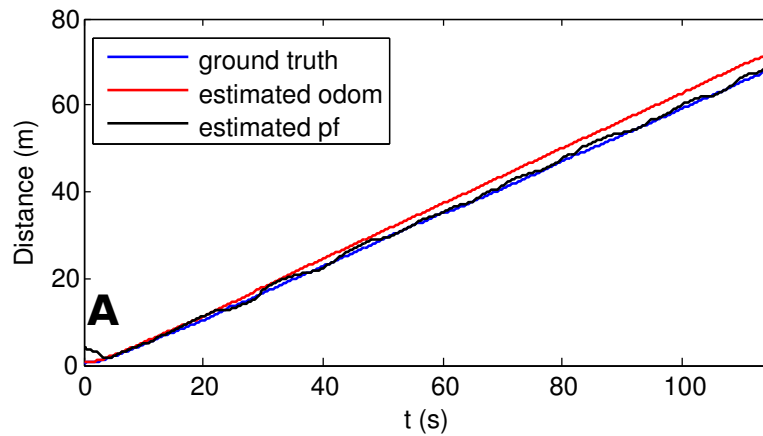


Figure 2.15: Comparison of the estimated position using different methods.

system purely based on odometry where the error increases along time.

The proposed localization method is able to provide good results in terms of the vehicle localization even in those areas where the longitudinal displacement of the vehicle corresponds to slight variations in the RSSI signal.

The analysis of these promising results leads us to propose improvements in the algorithm, as well as to evaluate other options based on the same radio signal exploitation strategy. The following sections describe the subsequent work aimed at improving the method.

2.4.3 Variable RF sensor measurement model variance

During the validation of the previously described method, the uncertainties involved in the algorithm were modeled using constant variance values provided by data sheets. After studying the experimental results, it is clearly seen how the uncertainty of the system increases in areas close to the highest values of the RF signal where the signal is flattened. The greater the number of possible positions corresponding to similar RF values, the wider the particle distribution and the greater uncertainty (**C**). On the contrary, the uncertainty decreases in areas close to the valleys of the signal (fadings), where the particle distribution becomes significantly narrower (**B**). Figs. 2.11 and 2.13 illustrates the aforementioned characteristics of the RF signal model and the actual RF measurements. The signal is more flattened close to the maxima, resulting in larger uncertainties. By contrast, the sharp form of the signal in the valleys results in smaller uncertainties. To take into account this behavior, we propose an improvement involving the use of a variable function for the variance related to the measurement model of the RF signal (W) instead of a constant value.

The goal is to obtain a transfer function which provides variance values with the same shape as the RF signal model. In this way, the applied variance will increase or decrease replicating the observed behaviour. The variance value at each timestamp W_t^m for particle m will depend on the RSSI value of the RF signal model as shown in Eq. (2.17).

$$\begin{aligned}
 W_t^m &= (RSSI_{fm}^m - \min(RSSI_{fm})) * f_{scale} \\
 &\quad + W_{offset} \\
 f_{scale} &= \delta_W / \delta_{RSSI_{fm}} \\
 \delta_W &= W_{up} - W_{low} \\
 \delta_{RSSI_{fm}} &= \max(RSSI_{fm}) - \min(RSSI_{fm})
 \end{aligned} \tag{2.17}$$

where $RSSI_{fm}^m$ is the RSSI value corresponding to the position of particle m provided by the RF signal model (Eq.(2.9)) and f_{scale} is a scale factor to convert the RSSI value to a variance value (dB^2) between an upper and lower limit (W_{up}, W_{low}) taking into account

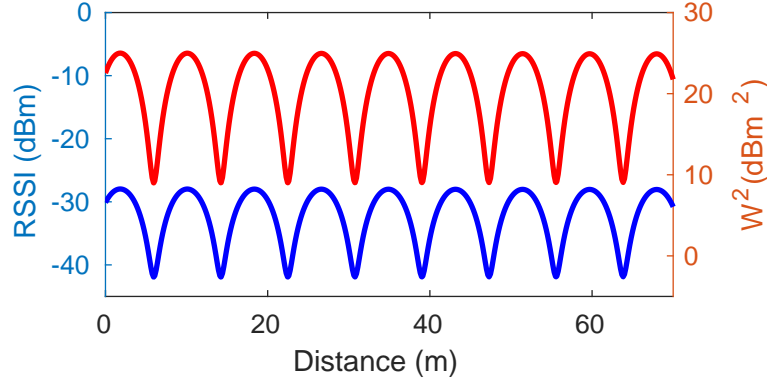


Figure 2.16: RF signal model (blue) and sensor measurement model variance (red) for $W_{up} = 5^2$, $W_{low} = 3^2$ and $W_{offset} = 3^2$.

the fadings model waveform amplitude ($\delta_{RSSI_{fm}}$). Finally, W_{offset} is the offset for the variance function. Fig. 2.16 provides an example of the resultant variance function together with the RF signal model.

As can be noticed from Fig. 2.11, the RF signal model along the pipe is similar enough to the RF sensor measurements in the real scenario to consider the bias error negligible.

From now on, the uncertainty of the measurement model applied during the weighting of each particle will be represented by the variance function W_t^m .

2.4.4 IMU for prediction purposes

The robotic platform used during the experimental validation of our approach belongs to the ground robots category. In the case of ground platforms, the odometry data, i.e. the linear and angular speed of the robot (v_t, w_t) for our differential vehicle, is provided by encoders placed on the wheels. These values correspond to the inputs of the system used during the prediction step of the algorithm (see Section 2.4.1).

There are other robotic platforms where the use of encoders is not feasible (e.g., aerial robots). In order to check the feasibility of the proposed method in these types of platforms, we propose the use of the values provided by an IMU. The information given by this sensor is the linear acceleration and the angular speed. In order to obtain the linear and angular displacement of the vehicle using the new inputs (a_t, w_t), it is necessary to add a new state in the motion model of the vehicle:

$$v_t = v_{t-1} + a_{t-1}dt \quad (2.18)$$

The new state allows to compute the linear speed by means of integration of linear acceleration over time. The integration process quickly accumulates errors due to the

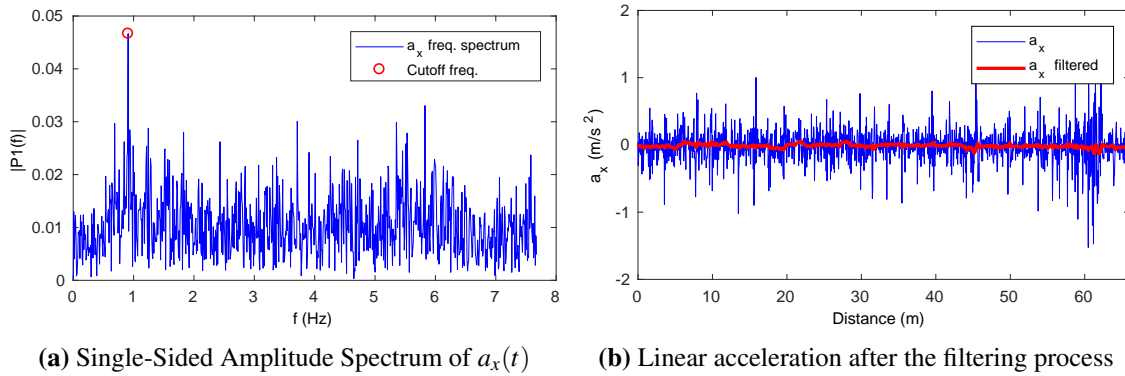


Figure 2.17: Cutoff frequency obtained by means of the FFT analysis and linear acceleration resultant after the Butterworth filter.

noisy nature of IMU sensors (the noise of the sensor is integrated at each iteration). In order to mitigate this effect, a first order Butterworth filter is applied to both the linear acceleration and angular speed during the displacement of the robot. This filter is selected to avoid as much as possible the delay added during the filtering of the signal. Each time a sample $(a_{raw}(t), w_{raw}(t))$ provided by the IMU sensor is received, the filter is applied. The expression corresponding to the transfer function is:

$$\begin{aligned}
 A_a(1)a(t) &= B_a(1)a_{raw}(t) \\
 &\quad + B_a(2)a_{raw}(t-1) \\
 &\quad - A_a(2)a(t-1) \\
 A_w(1)w(t) &= B_w(1)w_{raw}(t) \\
 &\quad + B_w(2)w_{raw}(t-1) \\
 &\quad - A_w(2)w(t-1)
 \end{aligned} \tag{2.19}$$

where (A, B) are the denominator and numerator coefficients of the rational transfer function corresponding to a first order Butterworth filter with normalized cutoff frequency:

$$H(z) = \frac{B(z)}{A(z)} = \frac{B(1) + B(2)z^{-1}}{A(1) + A(2)z^{-1}} \tag{2.20}$$

The cutoff frequencies were obtained applying the FFT (Fast Fourier Transform algorithm) to both signals. Fig. 2.17 shows the results of the filtering process for the linear acceleration. The angular variations are negligible and therefore the angular velocity is close to zero.

Table 2.1: Variance values and position error results

TEST	L (dB^2)	V (m^2)	mean error (m)
test 1	0.005	0.03^2	0.552
test 2	0.001	0.1^2	0.572

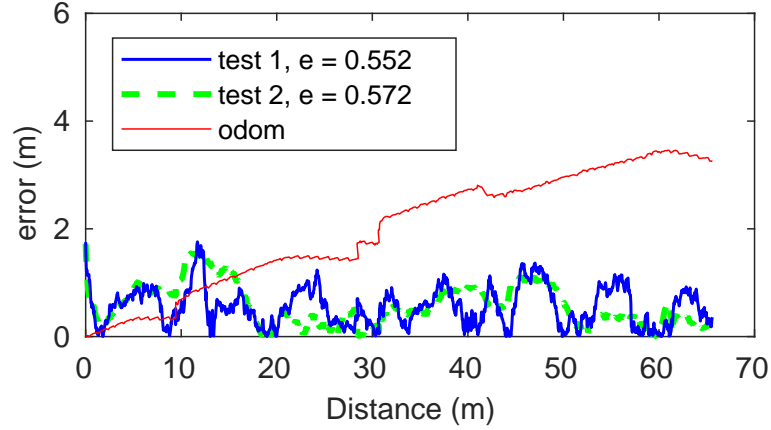


Figure 2.18: Odometry and particle filter position estimation error during the displacement of the robot along the pipe using the IMU sensor in the prediction step. Red line: pose error using only odometry. Blue and green line, pose error using the particle filter solution for different values of variance (blue: $L = 0.005$ and $V = 0.03^2$, mean error = 0.552 m, green: $L = 0.001$ and $V = 0.1^2$, mean error = 0.572 m).

Results

Several tests of the implemented localization method using the values provided by the IMU sensor were run to assess the stability and robustness of the solution. Fig. 2.18 shows the pose estimation error for different variance values: V , which models the uncertainty of the vehicle odometry, and L , variance of the Gaussian function used to weight the particles (see Table 2.1). The W variance is not selected as a constant value but obtained using the function of Eq. (2.17).

The cumulative error in the pose estimation when using only the odometry is clearly evident, whereas the position error remains limited around acceptable values when using the method based on particle filters. The results using the IMU as the main sensor for the prediction step are similar enough to the ones shown in Section 2.4.2 to suggest the feasibility of the proposed localization method using different robotic platforms.

As it is well-known, although the use of the IMU sensor overcomes the errors derived from the slipping of the wheels in these types of environments, the pose estimated by integrating the IMU sensor readings easily drifts due to the sensor noise and time-varying biases as we mentioned before. Although we tried to mitigate these effects by

means of the filtering of the signal, they could be even worse in the case of drones due mainly to vibrations. Usually in these systems, a combination of visual odometry with inertial systems is proposed to get a robust odometry [Hong and Lim, 2018]. Although it is beyond of scope of the thesis, our proposed method is expected to improve the odometry error of visual-inertial systems during the update phase by using the RF measurements, as the preliminary results of the experiments using the IMU during the prediction phase seem to indicate. Therefore, the proposed alternative method can be effective and should be evaluated when using different robotic platforms.

2.4.5 Continuous Localization system based on RF fadings using Extended Kalman Filter

The EKF [Thrun et al., 2005] is one of the most popular algorithms for state estimation in robotics applied to non-linear systems. The posterior distribution at time t is represented by the system state X_t and the covariance P_t . The EKF overcomes the Kalman Filter assumption of linear state transitions and linear measurements by means of a linearization process. Its strength lies in its simplicity and in its computational efficiency. In order to evaluate its feasibility for the localization of the robot inside pipes, an EKF algorithm was implemented using the RF signal.

During the EKF prediction step, the state of the robot \hat{X}_t is propagated according to the motion model (Eq. (2.7)):

$$\begin{aligned}\hat{X}_t &= f(u_t, X_{t-1}) \\ \hat{P}_t &= F_t P_{t-1} F_t^T + G_t V G_t^T \\ F_t &= \partial f / \partial X \\ G_t &= \partial f / \partial u\end{aligned}\tag{2.21}$$

where \hat{P}_t is the predicted covariance, f refers to the motion model of the vehicle, u_t are the inputs of the system (v_t, w_t) and (F_t, G_t) are the Jacobians calculated as the partial derivatives of the function f with respect to the state variable x and with respect to the inputs of the system u respectively. V is the variance associated with the vehicle odometry uncertainty.

The update step provides correction of the predictions by incorporating the measurements z_t :

$$\begin{aligned}X_t &= \hat{X}_t + K_t(z_t - h(\hat{X}_t)) \\ K_t &= \hat{P}_t H_t^T (H_t \hat{P}_t H_t^T + W_t)^{-1} \\ P_t &= (I - K_t H_t) \hat{P}_t \\ H_t &= \partial h / \partial X\end{aligned}\tag{2.22}$$

In this particular case, the observation z_t is the RSSI value provided by the RF receiver sensor and the measurement model h corresponds to the RF signal model used to predict the expected observation \hat{z}_t (similarly to Eq. (2.13)). W_t is related to the measurement model variance of the RF sensor.

The Jacobian H_t needed to calculate the Kalman gain of the filter is obtained through the derivative of the RF signal model equation with respect to the state variables.

Results

An EKF implementation of the localization algorithm was developed following the same strategy of using the RF signal during the estimation process. The validation of the method was carried out using the data collected during the experimental tests. A small uncertainty value in the vehicle's odometry was needed for the EKF method to provide good results in the position estimation. For higher variance values related to odometry, the EKF method was unable to solve the localization problem during the displacement of the vehicle along the pipe.

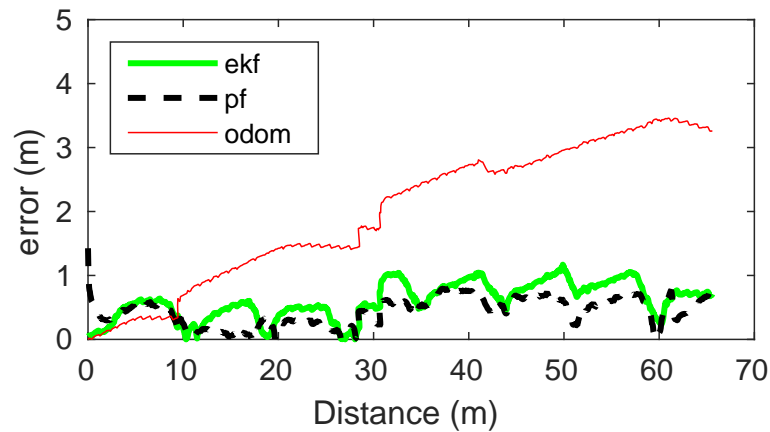
In order to compare both particle filter and EKF solutions, the same variance values were selected for both methods:

- EKF: $V = 0.01^2 \text{ m}^2$, W_{var} , and $P_0 = 0.01^2 \text{ m}^2$, where P_0 is the initial system variance.
- PF: $V = 0.01^2 \text{ m}^2$, W_{var} and $L = 4 \text{ dB}^2$

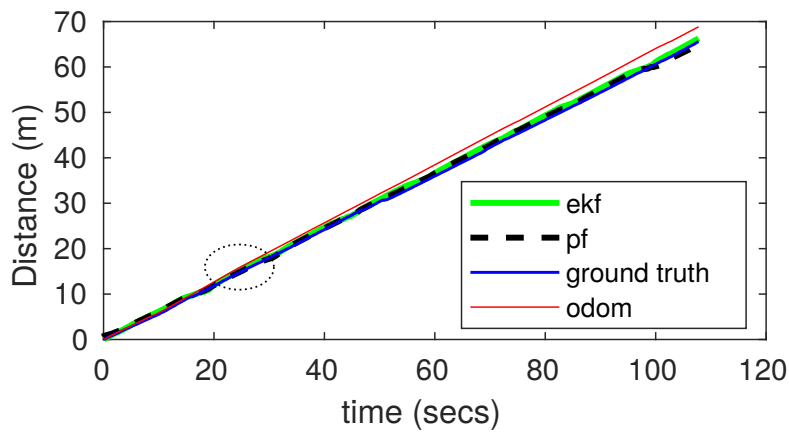
Fig 2.19a shows the position error obtained with the EKF and particle filter methods compared to the odometry method. The estimated position calculated using the three different solutions is represented in Figs. 2.19b and 2.19c. As can be deduced from the results, the EKF method does not perform as well as the particle filter method in terms of position estimation along the pipe. Nevertheless, the results are good enough to consider that the EKF method based on RF fadings may be suitable for localization inside pipes. For this reason, deeper analysis is required to evaluate the applicability of the EKF solution to solve this particular case.

A covariance analysis has been conducted in order to check the coherence of the application of the EKF algorithm to solve the localization problem using the RF signal. The evolution of the covariance during the displacement of the vehicle using both methods is shown in Fig. 2.20. As can be seen, the particle filter provides better results in terms of uncertainty than the EKF-based method.

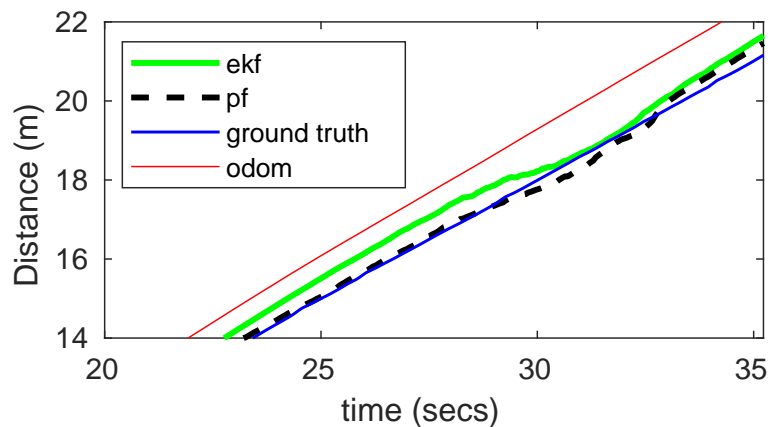
In brief, although both methods provide good results in terms of vehicle localization inside the pipe, the use of the particle filter is more adequate due to the high non-linearity of the RF sensor. Moreover, the position error is slightly better and the estimated position is closer to the real position of the robot when using the particle filter localization method. Apart from that, in order for the EKF method to provide a good solution, a



(a) Odometry, EKF and particle filter position estimation error



(b) Estimated position using odometry, EKF and particle filter



(c) Detail of estimated position within the dotted oval

Figure 2.19: Comparison between EKF and particle filter during the displacement of the robot along the pipe: (a) Position error and (b)-(c) comparison of position estimation with EKF, particle filter and odometry methods with respect to the ground truth.

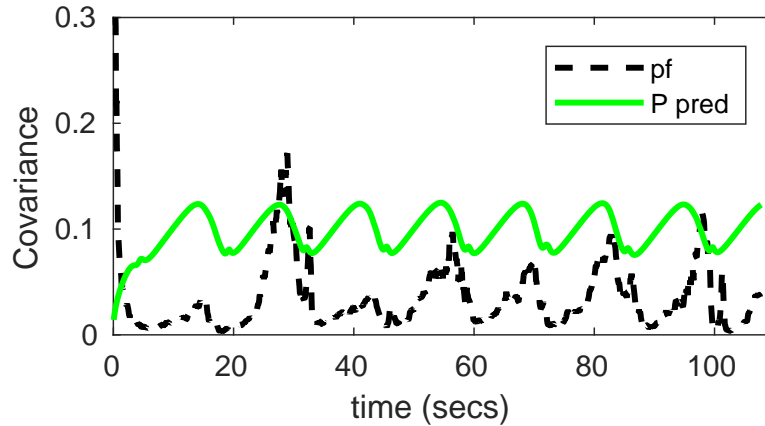


Figure 2.20: Evolution of the covariance during the displacement of the vehicle using EKF and particle filter-based methods.

small uncertainty of the state estimate is needed but in some cases, the assumption of a good odometry system is far from the real system. Therefore, we conclude that the EKF solution is less reliable compared to the particle filter.

2.5 Robot Localization using two RF Signal Fadings

The above localization results are provided being used only one RF receiver on the platform. As mentioned before in the transversal fadings analysis section, when using two RF receivers, with a specific setup of the transmitter and receivers antennas in the pipe cross-section, a 180 degree relative phase difference appears between the fadings corresponding to each receiver. Fig. 2.7 represents the RF signal model of each transmitter-receiver configuration.

The phase difference between the two RF signals can be exploited in order to improve the accuracy and reliability of the localization algorithm presented in the previous section that uses one single signal. Using the data provided by two RF receivers placed at different heights, twice as much information is available and it is possible to work with each signal with its own RF map.

2.5.1 Algorithm formulation

We could formulate the problem as a regular robot localization issue where two sensors (e.g., LiDAR sensors) placed at different positions on the robot give information about the perceived environment. The positions provided by both scan-matching processes working with a known map are fused using the EKF algorithm. The approach presented consists of applying two independent particle filters, each of them working with an RF

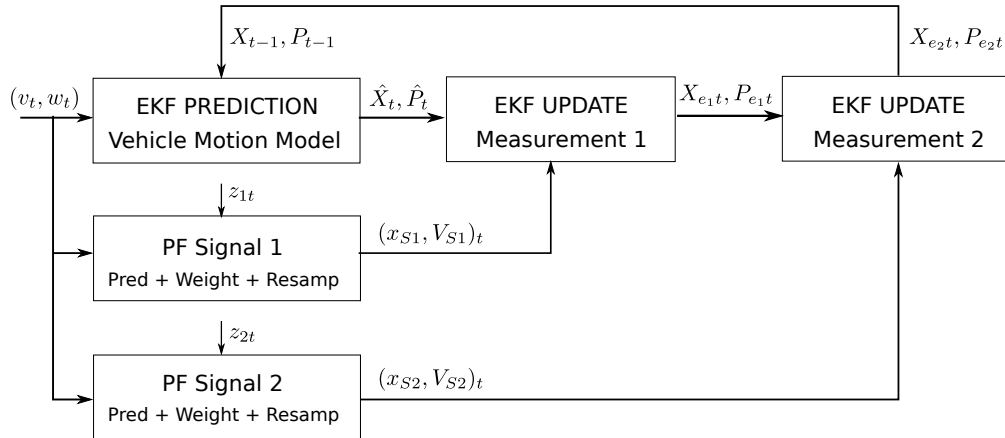


Figure 2.21: Steps of the EKF localization algorithm with two RF signals. After the prediction step, the position and covariance (\hat{X}_t, \hat{P}_t) are updated using the values resulting from the particle filter $(x_{S1}, V_{S1})_t$ that works with the first RF signal. In a second correction step, the position and covariance obtained in the previous step (X_{e1t}, P_{e1t}) are updated using x_{S2} and V_{S2} provided by the particle filter working with the delayed RF signal. The result of this step is the position and uncertainty of the vehicle at each time stamp (X_{e2t}, P_{e2t}) .

receiver, in a way that the resulting pose of each particle filter with its uncertainty is considered a virtual sensor. The information that comes from these virtual sensors is fused using the EKF algorithm in order to obtain the position of the robot along the pipe.

The goal of this method is to take advantage of the results of each particle filter in the areas where each of them works best, that is, where the particle distribution is the narrowest and therefore the uncertainty is the smallest. The less uncertainty in the pose estimation of the virtual sensor, the more influence this sensor will have in the EKF update step.

In summary, the proposed method is based on the application of an EKF algorithm as the localization method using the pose estimations obtained through two particle filters working with both RF signals as measurements during the EKF update step (Fig. 2.21).

The main stages of the proposed method are:

EKF prediction

During this step, the state \hat{X}_t and covariance \hat{P}_t are predicted using the inputs of the system (v_t, w_t) and the odometry motion model (Eq. (2.21)).

Particle filter for each signal

As mentioned before, the steps of the particle filter are followed in order to obtain the estimated position. The RSSI value provided by the first radio frequency sensor (z_{1t}) (rx2 in Fig. 2.4) along with its corresponding measurement model (Eq. (2.9)) are used in the weighting process to assign weights to each particle:

$$\begin{aligned} w_{1t}^m &= e^{-\frac{1}{2} \left(\frac{z_{1t} - \hat{z}_{1t}^m}{\sigma} \right)^2} \\ \hat{z}_{1t}^m &= h(x_{1t}^m) + \delta_t, \delta_t \sim \mathcal{N}(0, W_{var}) \\ h(x_{1t}^m) &= 20 \log_{10} |(K_1 e^{-\gamma_1 x_{1t}^m} + K_2 e^{-\gamma_2 x_{1t}^m})| + \delta_t \end{aligned} \quad (2.23)$$

The result of the resampling step of each particle filter is a new particle distribution. The estimated position is obtained by calculating the mean position of the particles for each iteration. In the same way, the variance of the particle distribution is computed. Eq. (2.24) represents the pose estimate and its variance for each iteration:

$$\begin{aligned} x_{S1} = \mu &= \frac{1}{M} \sum_{m=1}^M x_1^m \\ V_{S1} &= \frac{1}{M-1} \sum_{m=1}^M |x_1^m - \mu|^2 \end{aligned} \quad (2.24)$$

where M is the number of particles and x_1^m is the position of particle m .

Similarly, a second pose estimate is obtained using the RSSI value provided by the second receiver (z_{2t}) and its RF signal model. For symmetry reasons, the measurement model for this receiver placed at the upper half of the pipe (rx1 in Fig. 2.4) is represented by Eq. (2.25):

$$h(x_{2t}^m) = 20 \log_{10} |(K_1 e^{-\gamma_1 x_{2t}^m} - K_2 e^{-\gamma_2 x_{2t}^m})| \quad (2.25)$$

To summarize, two pose estimates with variances are available acting as virtual sensors to be used in the EKF update step: $(x_{S1}, V_{S1}), (x_{S2}, V_{S2})$.

EKF update using the results of the particle filters as estimators

With the different virtual sensor measurements, which are characterized by an uncertainty level, a double correction step takes place using Eq. (2.22).

Firstly, using $(x_{S1}, V_{S1})_t$ as the measurement and variance of the first virtual sensor respectively, the state and covariance predictions of the system (\hat{X}_t and \hat{P}_t) are updated. Secondly, in a subsequent step, the results of the previous step X_{e1t} and P_{e1t} are again updated using the measurement and variance values corresponding to the second virtual sensor $((x_{S2}, V_{S2})_t)$ obtaining X_{e2t} and P_{e2t} .

Therefore, the results of the EKF algorithm using a double correction step are:

$$\begin{aligned} X_t &= X_{e_{2t}} \\ P_t &= P_{e_{2t}} \end{aligned} \quad (2.26)$$

where X_t represents the estimated position of the robot along the pipe and P_t is the system covariance that represents the uncertainty of the calculated position.

It should be noted that, as the values provided by the virtual sensors are direct measures of the state, the Jacobian matrix H_t -that relates the state to the measurement needed for the Kalman gain calculation- is equal to the identity matrix.

2.5.2 Experimental results

Similarly to the validation of the above approaches, the real data collected during the experiments described in Section 2.3 was used to verify the improvement in the localization pose achieved by using two signals.

In order to do that, the variance values must be chosen. The EKF method is more sensitive to covariance parameters than the particle filter, so a tuning process is proposed to select the most adequate values.

A batch of experiments were carried out with L values range from 0.001 to 0.01 (dB^2) and V values range from 0.01^2 to $0.1^2(m^2)$. W was provided by Eq. (2.17). The results of the iterations are represented in Fig. 2.22. The colour range from blue to red represents the average position error obtained at each experiment, where colours close to blue correspond to less error and colours close to red represent higher error values. A low percentage of tests provided position errors above 1, so for the complete colour range to be uniform distributed among the results, those errors were limited to 1. As shown in the colour graph, the darker blue zone corresponds to L values close to 0.007 and V values close to 0.04^2 (dotted circle). The centroid of the best area in terms of position error is calculated and selected as the value for the proposed algorithm ($L_1 = L_2 = 0.007, V = 0.038^2$). The same variance values are selected for both particle filters.

The uncertainty in the measurement model W is obtained with Eq. (2.17) during the execution of the algorithm and the initial system variance P_0 is set to $0.038^2(m^2)$.

The number of particles for each particle filter is set to $M = 1000$. The particles are initially distributed along the first period of the fading of each RF signal in order to avoid the ambiguity problems derived from the periodic nature of the fadings waveform.

Once again, several tests were performed using the variance values selected in order to check the stability of the solution regardless of the probabilistic nature of the algorithm. Fig. 2.23 shows, for example, the position error obtained using the proposed localization method for three different tests with the same parameter configuration. As can be clearly seen, the mean error remains below 0.5 m, whereas the odometry error

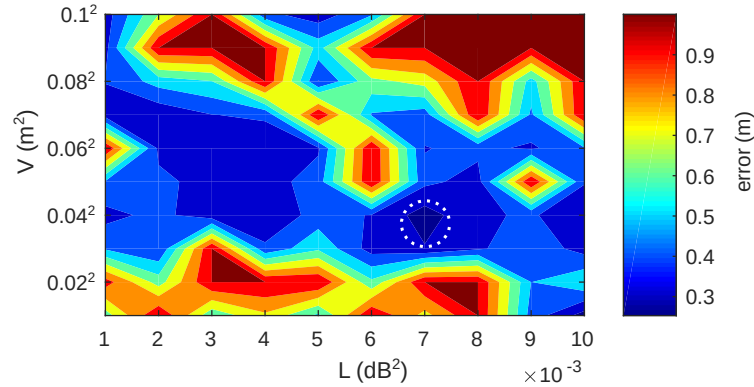


Figure 2.22: Results from the variance tuning process: $L \in [0.001, 0.01]$, $V \in [0.01, 0.1]^2$. Color range represents the position error. Darker color corresponds to less position error. Best results enclosed by the white dotted circle.

increases with time. These results demonstrate the adequacy of the variance values selected.

Moreover, the estimated position error using both signals improves on that obtained using one single signal as shown in Fig. 2.24a. The uncertainty of the position calculated at each timestamp for both virtual sensors is represented in Fig. 2.24b. As expected, the virtual sensor with the least variance has the most influence on the EKF algorithm and the position predicted is corrected with the position estimated by the “best” virtual sensor. This behavior can be observed in Figs. 2.24c and 2.24d which show a detail of the area delimited by the dotted vertical lines. The uncertainty of virtual sensor 2 (green) is lower than the uncertainty of virtual sensor 1 (blue), and hence, the estimated position is corrected based on the position estimated by the former. Therefore, the error remains bounded around the smallest error at each timestamp. Fig. 2.25a shows a comparison of the estimated position over time using the different methods. The localization method based on the particle filter using only one RF signal (green and purple) closely follows the real position (blue). Similarly, the proposed algorithm based on the EKF using two RF signals (black) provides a reliable estimated position. But the latter, as can be seen in the detail shown in Fig. 2.25b, corrects the position of the vehicle with the best solution of the two position estimators, in this case, the purple one. By contrast, the estimated position calculated using only the odometry (red) progressively moves away from the real position.

Coherence analysis

One of the assumptions of the EKF is the Gaussian distribution of the observations. As mentioned in the proposed method, the observations used in the update step correspond

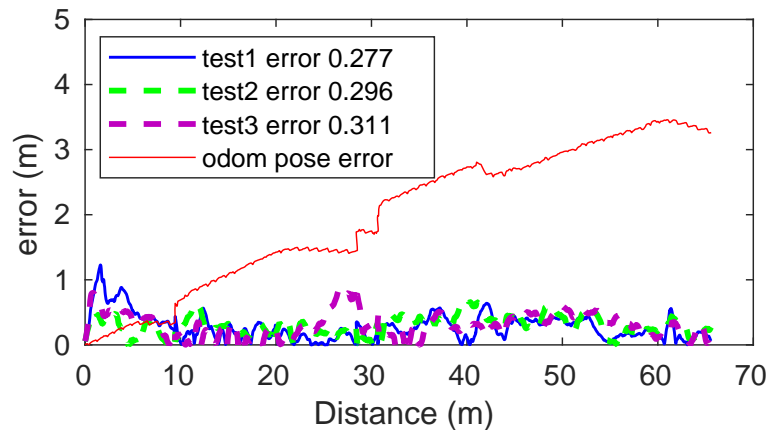


Figure 2.23: Odometry and position estimation error as a function of the distance traveled (ground truth). Blue, green and purple curves represent the results of three iterations of the proposed algorithm using two RF signals. The same variance values have been chosen for all the iterations.

to the result of the particle filter with each radio signal. In order to evaluate the coherence of the application of the EKF algorithm, we analyzed the distribution of the particles resulting from both particle filters.

In order to accomplish this task, the set of particles obtained after the resampling step at a particular time point during the displacement of the robot is saved for both signals. The median (μ) and standard deviation (σ) from the particles set are obtained and a random normal distribution is generated based on the values of μ and σ . The distribution of the particles versus the normal distribution is represented in Fig. 2.26.

Fig. 2.26a shows the percentage of the particles provided by the particle filter using the signal of one of the RF receivers. The similarities of the distribution with the normal distribution (Gaussian) are clearly evident. The same result is obtained in the case of the distribution of the particles using the second RF signal with the 180 degree phase delay (Fig. 2.26b).

From the aforementioned analysis, we can conclude that the assumption of a Gaussian distribution is tenable and therefore the feasibility of the EKF is demonstrated.

2.6 Concluding remarks

There are a number of important aspects that must be taken into account when applying the solution presented along this chapter, summarized in the following:

- The method presented in this chapter is proposed to solve the localization in pipes that are straight and metallic, these having electrical continuity, and that have a

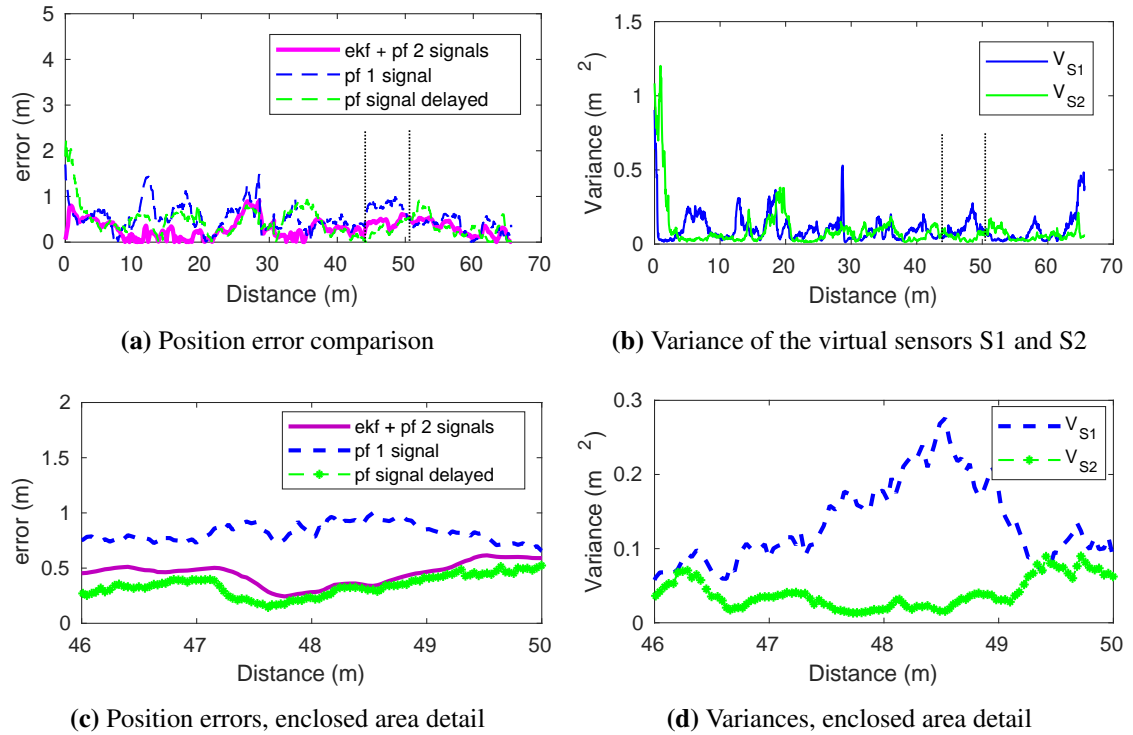
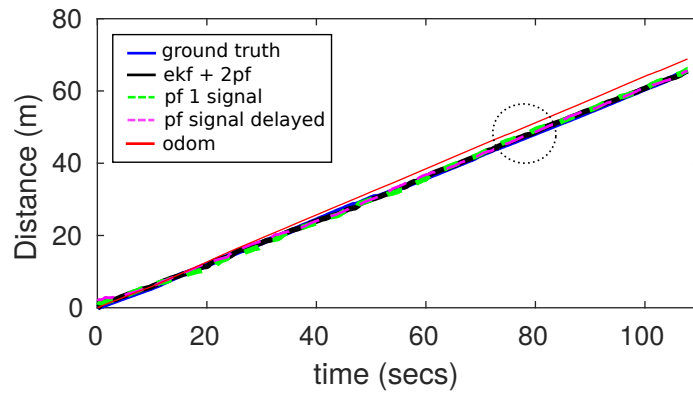
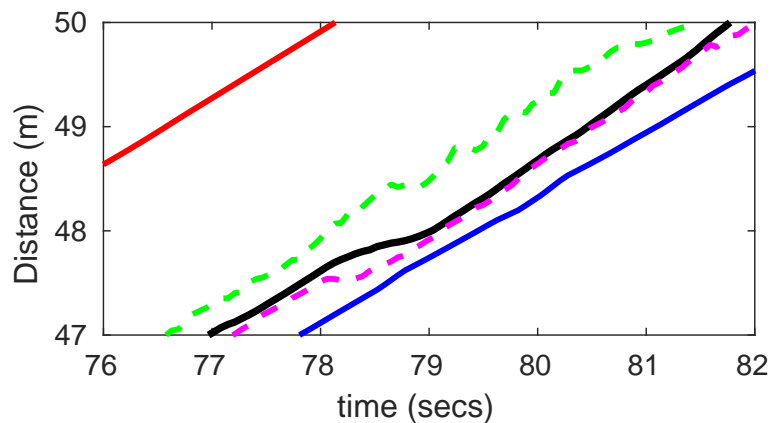


Figure 2.24: EKF localization method results using two RF signals during the displacement of the robot along the pipe: (a) Position error comparison using the proposed method and the particle filter-based method using one single RF signal. (b) Variance representing the uncertainty in the measurement for each virtual sensor. (c) and (d) Detail of both position errors and variances corresponding to the dotted enclosed area. The final position error is influenced by the best of both virtual sensors in terms of uncertainty.



(a) Estimated position comparison using different methods



(b) Position detail of the area enclosed by the dotted circle

Figure 2.25: Estimated position of the vehicle during its displacement along the pipe: (a) Comparison between the EKF method using both RF signals (black), particle filter using one signal (green and purple dashed line), odometry method (red) and ground truth (blue). (b) Detail of changes in the vehicle position over time corresponding to the enclosed area. The position provided by the EKF (black) is adapted to the best estimation of the two virtual sensors.

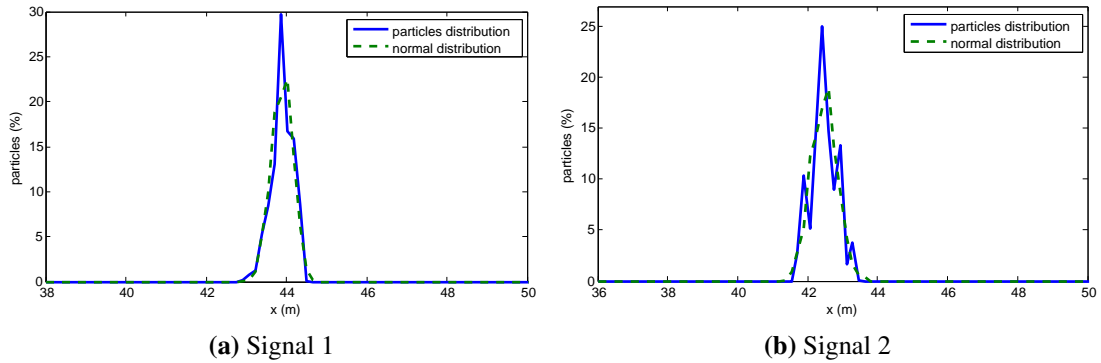


Figure 2.26: Particles distribution vs normal distribution after the resampling step. (a) Result using Signal 1. (b) Result using Signal 2 (180 degree phase difference). The two distributions are similar enough to conclude that the assumption of a Gaussian distribution is tenable.

uniform cross-section. Although this seems a substantial limitation, it was one of the most common situations found in numerous use-cases.

- Previous studies demonstrate that the fadings are periodic, repeatable and predictable, and hence, they are suitable for localization. The fading period is given by the pipe diameter and the interacting modes. It is important to remember that in order to propagate n modes, the operating frequency must be greater than the n^{th} mode cutoff frequency but below the $n^{\text{th}} + 1$ mode cutoff frequency, and that the fading period depends on the frequency chosen. Thus, trimodal propagation, i.e interaction between the first and third modes, has been selected because it produces shorter period fadings compared to the bimodal case, being more useful for localization purposes.
- Inside the pipe, the Faraday cage effect avoids interference from external RF sources, and therefore, the received signal is low in noise.
- The maximum possible length that could be covered is determined by the pipe diameter, material and equipment sensitivity. Metallic pipes have low attenuation rates. In our case study, the Santa Ana dam pipe was carbon steel with an attenuation rate of less than 9 dB per km, and our low cost receiver has a sensitivity of -105 dBm. This gives us a maximum possible coverage length of several kilometers.
- The RF signal model along the pipe is similar enough to the measurements provided by the RF sensor in the real scenario to be considered a position reference.

- The proposed RF-odometry approach are feasible not only for terrain robots but also for flying robots such as drones.
- The use of two antennas and its correct positioning in the cross section of the pipe allows to improve the accuracy and reliability of the continuous RF signal based localization methods by means of exploiting the 180 degree phase difference.
- The position error obtained in this experiment (for 70 m) does not depend on the distance travelled, but on the fidelity of the RF signal with the RF propagation model acting as a RF map. The error will remain bounded under acceptable values over the entire length of the pipe in which the effect of periodic fadings appears, i.e, the coverage area which, as mentioned above, extends to several kilometres.

2.7 Summary

In this chapter, we have presented an alternative RF localization method to those existing in the literature (e.g., fingerprint or UWB), which does not require substantial infrastructure deployment or a previously built RF map. Our method, a type of RF odometry, is able to localize a robot along a pipe by means of generating and detecting a periodic signal fadings pattern, using just one RF transmitter and one receiver for the simplest setup.

Some strategies have been implemented to obtain a continuous localization of the robot during its displacement along the pipe, using the theoretical fadings model as an RF map. The first of them is based on particle filters and the validation with some experimental tests demonstrate its suitability for estimating the position along the pipe even when the actual RF signal slightly differs from the RF map. Building on that work, the feasibility of using different types of robotic platforms has been confirmed by using the IMU during the prediction step of the particle filter-based method. Apart from that, the applicability of the EKF algorithm using the fadings signal and an RF map has been studied and compared to the particle filter solution. Both methods achieve continuous localization along the pipe providing good results. However, the PF algorithm is more appropriate due to the high non linearity of the RF sensor.

Finally, a new strategy for continuous localization taking advantage of using two RF receivers in order to obtain the 180 phase difference has been developed. This approach consists of fusing the information that comes from two particle filters working with their RF signal and RF map, with an EKF algorithm. The result of a coherence analysis demonstrates the validity of the proposed solution.

All the aforementioned methods have been tested and validated with experiments in a real pipe scenario. The reliability of the localization methods has been proven for in-pipe longitudinal localization. Moreover, the continuous localization using two signals yields better results in terms of error, improving the accuracy and the robustness with

regards to the one signal solution. The ability to localize the robot at all times during its displacement along the pipe using the proposed approaches has been demonstrated.

The alternative RF approach presented in this chapter overcomes the lack of features that is one of the main difficulties in robot localization in this type of environment. The singular characteristics of the RF propagation signal inside the pipe enables the robot localization without placing landmarks along the pipe. In addition, there is no need for a previously known map and required modifications of infrastructure are minimal, only an RF transceiver placed at the beginning of the pipe being needed to cover several kilometers.

Chapter 3

Localization based on RF Fadings inside Tunnels

Robot localization inside tunnels is a challenging task due to the hostile conditions of the environment. The difficulties of this type of scenario are similar to those described in the case of pipes: GPS-denied nature in confined environments, low visibility, slippery surfaces, and even lack of distinguishable features. As consequence, methods based on scan-matching techniques using LIDAR sensors or those based on visual SLAM techniques using cameras may not perform adequately. In this chapter, following the same strategy presented in the previous chapter, we develop a discrete localization system which takes advantage of the periodicity nature of the RF signal fadings that also appears inside tunnels under certain configurations. Along this chapter we show the feasibility of the proposed method in order to periodically correct the robot position during its displacement along the tunnel with experimental results. This contribution was presented in [Seco et al., 2018].

3.1 Introduction

There are several labors that need to be carried out inside tunnel-like environments such as inspections, rescue missions and even construction. The hard conditions, as well as the implicit risk for people, make robots the most adequate devices to perform these tasks. Furthermore, the use of autonomous machinery is on the increase [Tardioli et al., 2018].

Similarly to the pipe environments, localization of the robot along the tunnel represents a challenge. Due to the absence of satellite signal in underground scenarios, outdoor methods based on GPS sensors can not be considered. Additionally, the darkness and lack of distinguishable features make the most common techniques for indoor localization – based on cameras or laser sensors – to perform erratically.

[Bakambu, 2006] presents an autonomous platform for exploration and navigation in mines where the localization is based on the detection and matching of natural landmarks over a 2D survey map using a laser sensor. However, these methods are inefficient in monotonic-geometry scenarios with absence of landmarks as shown in [Tardioli and Villarroel, 2014]. Recent alternatives based on visual SLAM techniques ([Jacobson et al., 2018, Marangi et al., 2019]) rely on the extraction of visual features using cameras to provide accurate localization. These methods are highly dependant on a proper illumination, usually poor in these types of environments. Moreover, they do not perform well in low-textured scenarios where the feature extraction process tends to be unstable.

The above mentioned issues have been stated in several works as [Ozaslan et al., 2015] or in [Tardioli et al., 2019] using LiDAR-based systems. The problem has been also studied and formalized in [Zhen and Scherer, 2019] where a tunnel is considered as a geometrically degenerated case. The authors propose fusing the LiDAR sensor information with an Ultra Wide-Band (UWB) ranging system to eliminate the degeneration. Nevertheless, as already mentioned in Section 2.1, this solution involves a previous commissioning step to install in the tunnel a set of UWB anchors that act as a kind of RF landmarks. That is, the tunnel is modified introducing artificial features only for location.

Other localization methods rely on wheel odometers, but besides suffering cumulative errors, they are more unreliable than usual due to uneven surfaces and presence of fluids very common in tunnel environments. Taking into account the aforementioned difficulties, other alternatives must be explored.

Regarding the RF signal propagation in tunnels, a similar phenomena to the pipes case is demonstrated in several intensive studies presented in [Rizzo et al., 2013b, Rizzo et al., 2013a, Rizzo et al., 2019]. If the wavelength of the operating frequency is much smaller than the tunnel cross-section, on the one hand the tunnel behaves as an oversize waveguide extending the communication range but on the other hand, the RF signal suffers from strong attenuation. Along those works the authors developed an extensive analysis about the most adequate transceiver-receiver configurations (i.e. position in the tunnel cross section and operating frequency) to obtain periodic fadings.

Although the RF field structure does not become periodic and clean along all the tunnel as will be seen later, we again take advantage of the useful periodic nature of the fadings to propose an RF-based discrete localization method. Our approach consists of identifying the minimums of the RF signal during the displacement of the robot along the tunnel, and subsequently match these features with an RF map generated from the known signal propagation model. The robot position is periodically adjusted with the position reference provided by the map during the matching process. In order to accomplish these tasks, the combination of two strategies has been proposed as a first approach: Recursive Least Square (RLS) algorithm for the features identifica-

tion [Nelles, 2001], and the Mahalanobis Distance for the matching step. The work presented in this chapter extends the methodology presented in [Rizzo et al., 2014b].

3.2 Fundamentals of electromagnetic propagation in tunnels

In this chapter, we present the basis of the electromagnetic propagation in tunnels relevant for the development of the localization methods presented in this chapter and in Chapter 5.

As in pipes, wireless propagation in tunnels differs from regular indoor and outdoor scenarios. For operating frequencies high enough with free space wavelength much smaller than the tunnel cross-section dimensions, tunnels behave as hollow dielectric waveguides. If an emitting antenna is placed inside a long tunnel, the spherical radiated wavefronts will be multiply scattered by the surrounding walls. The superposition of all these scattered waves is itself a wave that propagates in one dimension – along the tunnel length – with a quasi-standing wave pattern in the transversal dimensions. This allows extending the communication range, but affects the signal with the appearance of strong fadings.

There are many different possible transversal standing wave patterns for a given tunnel shape. Each one is called a *mode* and has its own wavelength, close to – but different from – the free space one, and with its own decay rate (see [Orfanidis, 2014] for a detailed explanation).

The electromagnetic field radiated from the antenna starts propagating along the tunnel distributed among many of the possible propagating modes supported by this waveguide. In contrast to metallic pipes, there is not a well defined cutoff frequency for each mode and all of them propagate with different attenuation rates. Depending on the distance from the transmitter, two regions can be distinguished in the signal due to the different attenuation rate of the propagation modes. In the *near sector*, all the propagation modes are present provoking fast fluctuation on the signal (*fast-fadings*). After a long-enough travel distance, once the higher order modes (which have higher attenuation rate) are mitigated with the distance, the lowest modes survive, giving rise to the so-called *far sector*, where the *slow-fadings* dominate [Dudley et al., 2007]. These fadings are caused by the pairwise interaction between the propagating modes, and therefore, the higher the number of modes, the more complex the fading structure. On the transmitter side, the position of the antenna allows to maximize or minimize the power coupled to a given mode, favoring the interaction between certain modes, and allowing to produce a specific fading structure.

In [Rizzo et al., 2013a, Rizzo et al., 2019] the authors present an extensive analysis of the fadings structure in straight tunnels. These studies demonstrate that, given the

tunnel dimensions and selecting a proper transmitter-receiver setup, the dominant modes are the first three modes (the ones that survive in the far sector as their attenuation constant is low enough to ensure coverage along several kilometers inside the tunnel). By placing the transmitter antenna close to a tunnel wall, the power coupled to the first and second modes is maximized while minimizing the excitation of the third one. In the receiving side, this produces a strictly periodic fading structure. The superposition of the first and second propagation modes (called EH_{11}^z and EH_{21}^z respectively) creates a periodic fading structure (Fig. 3.1a). In the very center of the tunnel there is no contribution from the second mode, and the third mode (EH_{31}^z), with lower energy, becomes observable, creating another fading structure with a different period. However, the received power associated to the fadings maxima is lower compared to the previous fading structure. The situation is illustrated in Fig. 3.1b, which shows the data collected by having one antenna in each half of the tunnel, and another located in the center. It can be seen that there is a spatial phase difference of 180 degrees between both halves of the tunnel (i.e. a maximum of one fading matches a minimum of the other) caused by the transversal structure of the second mode.

During the presented studies, the authors adopt the Modal Theory approach, modeling the tunnel as a rectangular dielectric waveguide of dimensions $a \times b$, using the expressions for the electromagnetic field modes and the corresponding propagation constants obtained by [Laakmann and Steier, 1976] for rectangular hollow dielectric waveguides. As we mentioned before, each mode propagates with its own wavelength λ_{mn} (close but not equal to the free space one) that can be written as:

$$\lambda_{mn} = \frac{\lambda}{1 - \frac{1}{2} \left(\frac{m\lambda}{2a} \right)^2 - \frac{1}{2} \left(\frac{n\lambda}{2b} \right)^2} \quad (3.1)$$

where m represents the number of half-waves along the y axis, n the number of half-waves along the z axis and λ is the free space wavelength which depends on the free space velocity of the electromagnetic waves c and on the operating frequency f :

$$\lambda = \frac{c}{f} \quad (3.2)$$

If two modes with different wavelengths (λ_1 and λ_2) are present, the phase delay accumulated by each one will be different for a given travel distance x . The superposition of the modes will take place with different relative phases in different positions inside the guide, producing constructive interference if both modes are in phase and destructive interference if the relative phase differs by an odd π multiple. This gives rise to a periodic fading structure of the RF power inside the waveguide. As in pipes, the period of this fading structure D is the distance that creates a relative phase of 2π between the two considered modes (see Eq. 2.6). For the case of tunnels, using Eq. 3.3, this is:

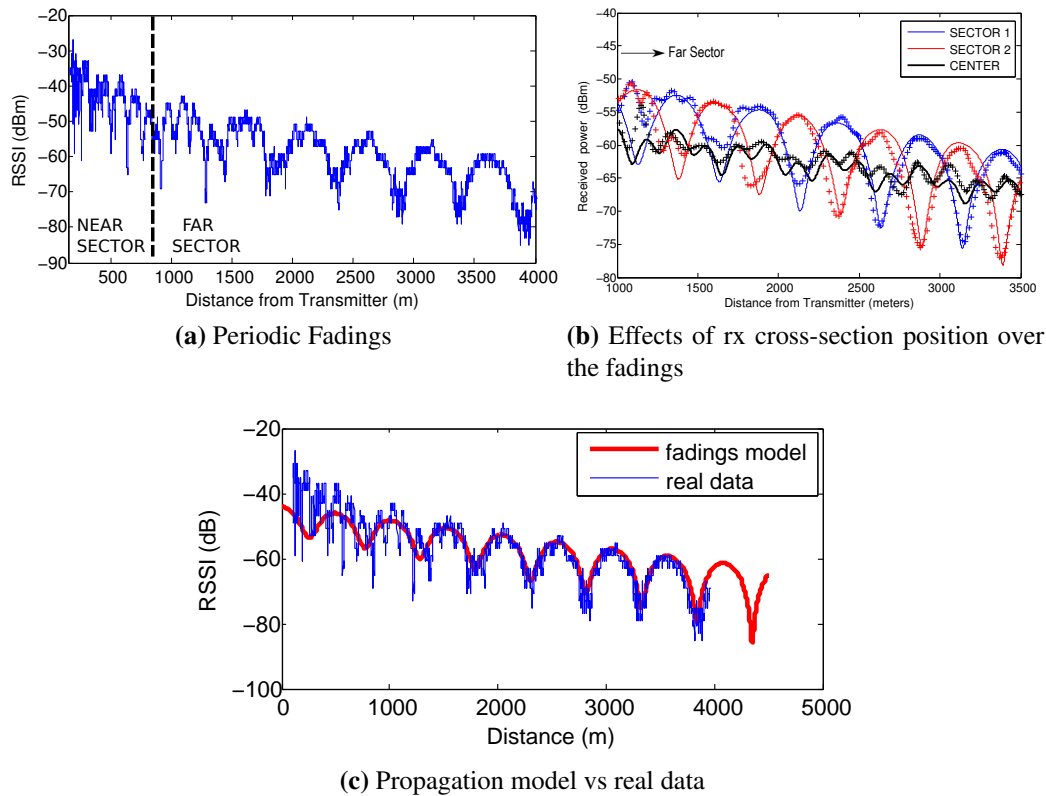


Figure 3.1: (a) Measured Received Power at 2.4 GHz inside the Somport tunnel, from [Rizzo et al., 2013a]. The transmitter was kept fixed and the receiver was displaced along 4 km from the transmitter. In (b), the same experiment was repeated for three different receiver's cross-section positions: left half (sector 1), center and right half (sector 2). The solid lines represent the modal theory simulations, and the dotted lines the experimental results. In (c), the red line represent the modal theory simulations, and the blue the experimental results.

$$D = \frac{8}{\frac{c}{f} \left| \frac{m_2^2 - m_1^2}{a^2} + \frac{n_2^2 - n_1^2}{b^2} \right|} \quad (3.3)$$

As the transmitter-receiver setup used in this work benefits the excitation and detection of the EH_{m1}^z modes (for localization purposes), notice that only the width of the waveguide determines the period of the fadings. Similarly to the metallic pipe case, the total electromagnetic field will be the superposition of all the propagation modes. We encourage the reader to see [Rizzo et al., 2019] for a complete 3-D fadings structure analysis in tunnels.

With this approximation, the obtained theoretical propagation model matches closely the experimental data. The similarity between both signals (Fig. 3.1c) in the *far sector* are enough to make us consider them useful for localization purposes, using the propagation model as a position reference.

3.3 Discrete localization algorithm based on RF minimum detection

The basis of the proposed algorithm is to detect some relevant features of the RF waveform during the displacement of the robot so that it is possible to correct the estimated position with the real distance corresponding to each RF feature provided by the theoretical propagation model.

We consider that the most relevant features of the periodic RF signal are the valleys, where a sharp change in the RSSI value is clearly distinguishable. Using the propagation model, described in detail in [Rizzo et al., 2019] as an RF map, it is possible to know in advance the position of each valley along the tunnel. Thus, the estimated position is corrected with the known positions corresponding to each RF feature detected, removing the odometry cumulative error periodically.

There are two processes involved in the proposed method. The first process consists of getting a theoretical minimums map from the propagation model. Each value of the map corresponds to the position of the RF signal minimum along the tunnel. This position is considered as a global localization reference and will be used as a prior known information. The collection of the minimums map can be executed in an offline process, since the propagation model is known in advance.

The second process consists of identifying the valleys of the actual RSSI signal provided by the RF receivers and then, try to relate them to the minimums map. If the detected minimum corresponds to a minimum of the map, then the estimated position of the robot is corrected with the position reference provided by the minimums map. This process must be carried out during the displacement of the robot so it must be an

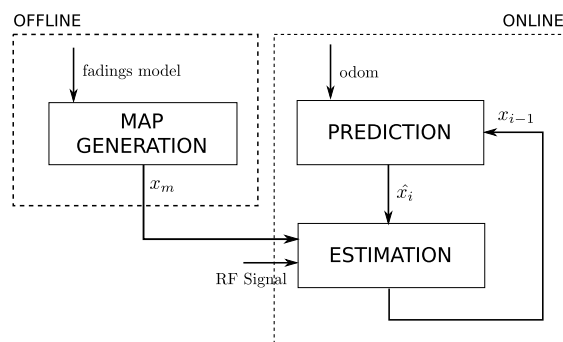


Figure 3.2: General stages of the localization algorithm.

online process. Due to the periodic nature of the RF waveform, the robot position will be corrected periodically.

A general representation of the proposed localization approach is showed in Fig. 3.2 and the main steps of the algorithm are summarized in the following:

1. Obtain a theoretical minimum map. For this purpose, the RLS algorithm is applied to the theoretical model of the fadings. An array with distance values $\mathbf{X}_m = \{x_{m1}, x_{m2}, \dots, x_{mn}\}$ is obtained. Each value corresponds to the position of each minimum of the signal along the tunnel. The result of this offline process will be available in advance and it will be considered as previous information.
2. Obtain the minimum values of the actual signal. For each iteration of the RLS algorithm, the existence of a minimum is checked and the position of the vehicle is estimated.
3. If a potential minimum appears, then the Mahalanobis distance between the estimated position of the vehicle at this timestamp and the position of the minimums in the theoretical map is calculated. If this distance fulfills a defined criteria then the minimum is a real one. If not, the potential minimum is discarded.
4. The position of the robot is corrected with the distance value of the theoretical minimum map.

These steps are described in more detail in the next subsections.

3.3.1 Minimums map generation

The map generation step consists of determining the location of the theoretical minimums from the known fadings model, which relates the RSSI to the distance along the tunnel. Although the map generation is executed in an offline process, the solution applied to this process is the same as the one selected for the online process.

In order to accomplish the online minimums detection, a change in the slope of the signal from negative to positive must be detected. For this purpose, we propose to approximate the signal with a first order function ($\hat{y} = \theta_0 + \theta_1 u$) using the resultant coefficients to check the change in slope. Therefore, a system identification method is needed to obtain the linear approximation at each timestamp. Although Least Squares (LS) method is the most widely applied solution for linear optimization problems, it requires an important quantity of previously recorded data samples for the solution to converge, which means that it is not suitable to solve problems with real time requirements. For this reason, the Recursive Least Square algorithm has been proposed as the solution. The RLS method, which is the recursive formulation of the LS algorithm, is capable of updating the solution online each time new data is available.

The general formulation of the RLS algorithm is based on the following equations:

$$e(k) = y(k) - \hat{y}(k) \quad (3.4)$$

$$\hat{y}_k = u^T(k)\theta(k-1) \quad (3.5)$$

$$\theta(k) = \theta(k-1) + \gamma(k)e(k) \quad (3.6)$$

$$\gamma(k) = \frac{1}{u^T(k)P(k-1)u(k) + \lambda} P(k-1)u(k) \quad (3.7)$$

$$P(k) = \frac{(I - \gamma(k)u^T)P(k-1)}{\lambda} \quad (3.8)$$

being e the error, computed as the difference between the measured data y and the model output \hat{y} , calculated using the input sample u and the previous coefficient estimation θ . P is the inverse correlation matrix and it is proportional to the covariance matrix of the parameter estimates θ . λ is the forgetting factor, a positive scalar taking the form ($0 < \lambda \leq 1$). The smaller the λ , the smaller the contribution of previous samples to the covariance matrix. This makes the filter more sensitive to recent samples, which means more fluctuations in the filter coefficients with noisy signals.

As a result of applying the RLS algorithm to the theoretical fadings model and the slope change detection process, an array of n distance values is obtained ($x_{m1}, x_{m2}, \dots, x_{mn}$). These positions are considered as global localization references and will be use as a prior known information (Fig. 3.3(a)).

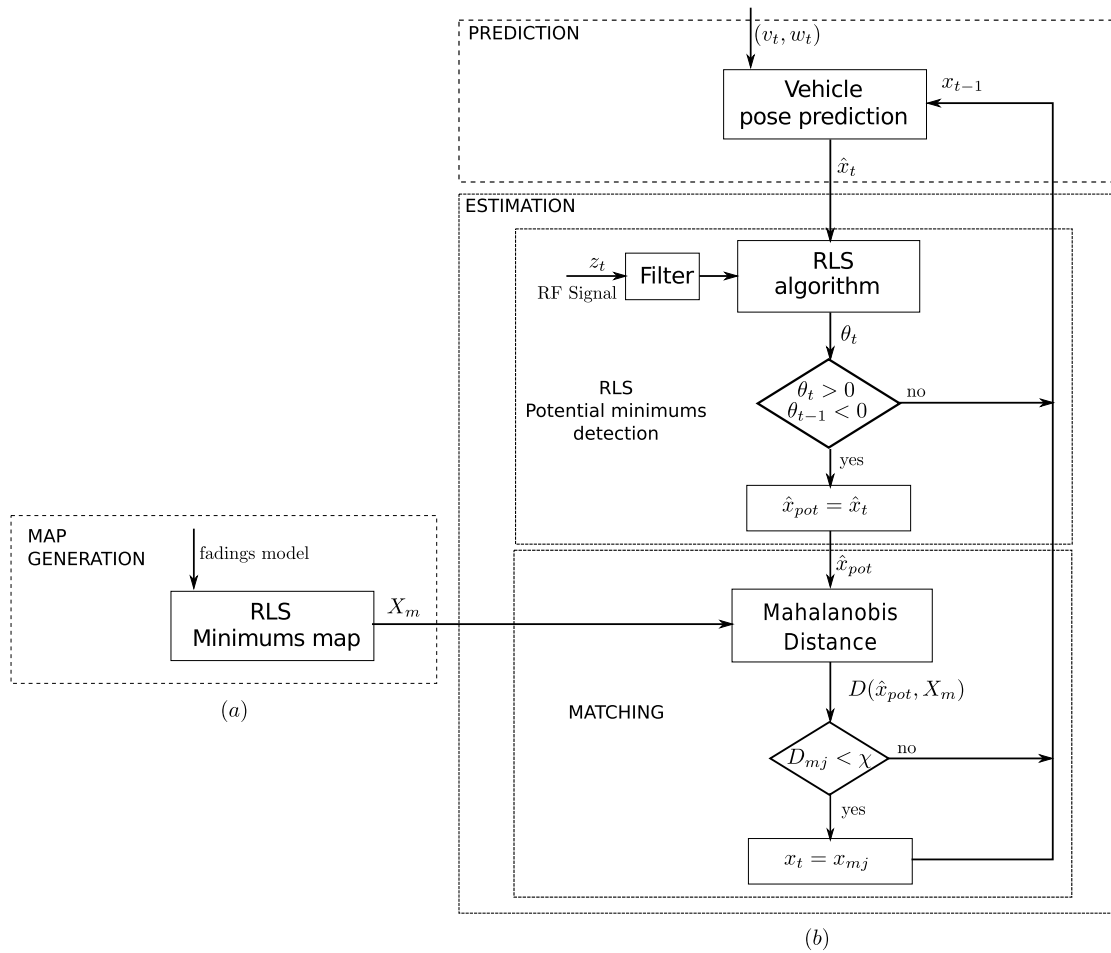


Figure 3.3: Algorithm flow chart: (a) Map generation, (b) Prediction and Estimation steps.

3.3.2 Prediction and estimation using RLS and Mahalanobis Distance

The position of the vehicle \hat{x}_t is predicted using the information provided by the odometry sensors (v_t, w_t) and the position computed in the previous iteration x_{t-1} :

$$\hat{x}_t = x_{t-1} + v * dt + \varepsilon_t, \varepsilon_t \sim \mathcal{N}(0, V_{odom}) \quad (3.9)$$

being ε_t a random variable that models the uncertainty of the vehicle odometry by means of the variance V_{odom} . In our specific case the vehicle travels in a straight line along the center of the tunnel, and therefore slightly heading variations are observed during its displacement.

In the estimation step, the existence of a minimum of the actual RSSI signal (z_i) is checked using the previously described RLS algorithm. If a potential minimum \hat{x}_{pot} appears, a data association technique in order to match the potential minimum with the minimums of the map X_m is required. In this work, the use of the Mahalanobis distance in combination with the individual compatibility test (IC) is proposed. These techniques are the basis for some of the most popular data association algorithm used in SLAM in order to determine the subset of map features that are compatible with a measurement [J.A. Castellanos, 2006].

The Mahalanobis distance is computed between the position of the potential minimum \hat{x}_{pot} and each of the positions of the minimum map (X_m):

$$D_M(\hat{x}_{pot}, x_{mj}) = \sqrt{(\hat{x}_{pot} - x_{mj})^T S^{-1} (\hat{x}_{pot} - x_{mj})} \quad \forall x_{mj} \in X_m, \quad j = 1..n \quad (3.10)$$

It is important to notice that the variance (S) must take into account not only the variances of the vehicle odometry and the minimum map, but also the variance of the sensor which in this case is a *minimums* detector. Being considered a unidimensional problem, the total variance can be obtained by the following expression:

$$S = V_{odom} + V_{map} + V_{minSensor} \quad (3.11)$$

In order to obtain $V_{minSensor}$, a calibration process is required. The data provided by this sensor are the minimum values obtained through the application of the RLS algorithm to the actual RSSI data (including the false positives). A first approach of the calibration procedure consists of measuring the distance between two minimums of the actual data ($dmin$), that would correspond to a known minimum. Fig. 3.4 shows the results of the calibration procedure.

The variance is then obtained through the following expression:

$$V_{minSensor} = \left(\frac{dmin}{2} \right)^2 \quad (3.12)$$

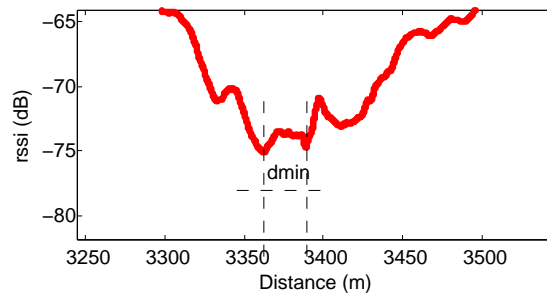


Figure 3.4: Distance calculation between minimums of the actual signal.

The estimated position can be considered corresponding to an actual minimum if the Mahalanobis distance satisfies the individual compatibility test (IC):

$$D^2(\hat{x}_{pot}, x_{mj}) < \chi_{d,1-\alpha}^2, \quad \forall x_{mj} \in X_m, \quad j = 1..n \quad (3.13)$$

where d is the dimension, and $1 - \alpha$ is the desired confidence level (usually more than 95%). The value for χ is obtained from the Student's t Distribution table.

It is important to remark the noisy nature of RF signal in tunnels, which results in false positives during the minimum detection process, even though a digital filter is used. The proposed technique is capable of reducing or even removing the false positives during the matching process.

Finally, if the potential minimum passes the IC test, the estimated position of the vehicle along its displacement x_t is corrected with the position that comes from the corresponding minimum of the theoretical map x_{mj} . Therefore, the accumulated odometry error is reset after identifying a minimum. Also, the prediction and estimation steps (Fig. 3.3(b)) are carried out iteratively.

3.4 Test scenario and Experimental setup

3.4.1 Real scenario: the Somport Tunnel

The validation of the alternative approaches presented along this thesis to solve the localization in tunnels was carried out with real data collected during different experimental campaigns developed along the time in a real scenario, the Somport railway tunnel. It is 7.7 km long old out-of-service tunnel connecting Spain with France through the central Pyrenees. The tunnel is straight but with a change in slope at approximately 4 kilometers from the Spanish entrance. It has a horseshoe-shaped cross section, around 5 m high and 4,65 m wide (Fig. 3.5a).

To be compliant with European directives, tunnels must integrate a set of structural elements to improve the safety. The Somport tunnel is not an exception and it has small

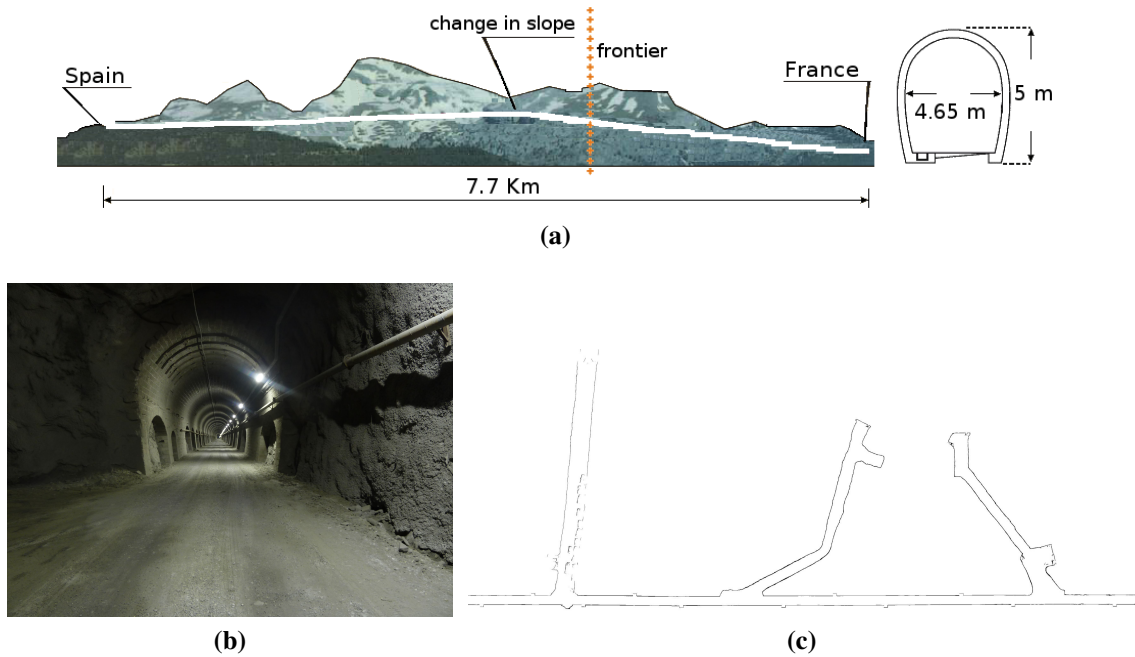


Figure 3.5: The Somport tunnel. (a) general dimensions and shape (b) the interior of the tunnel (c) emergency shelters and galleries map.

emergency shelters every 25 m as well as 17 lateral galleries, each more than 100 m long and of the same height as the tunnel (Fig. 3.5c).

3.4.2 Experimental setup

An all-terrain vehicle was utilized as the mobile platform simulating a service routine. It was equipped with two SICK DSF60 0.036 deg resolution encoders and a SICK LMS200 LIDAR (Fig.3.6).

The real localization of the platform, that will be used as ground truth, is obtained fusing all the data sensor using the algorithm described in [Lazaro and Castellanos, 2010] with a previously built map. It is only feasible to apply this approach due to a very specific characteristic of the Somport testbed, which is emergency shelters every 25 m, acting as landmarks. It is worth noticing that the ground truth is only used for comparison purposes. The existence of these shelters is omitted by the proposed localization system in order to generalize the applicability of the method to other types of tunnels that do not include these structural characteristics.

The platform was also equipped with an array of twelve TPLINK wireless receivers. The antennas were spaced 0.125 m apart and the working frequency was 2.412 GHz. All of them were vertically polarized with a 4 dBi gain. The receiver array was placed at a height of 2.17 m on the moving platform. The radio signal was generated with a

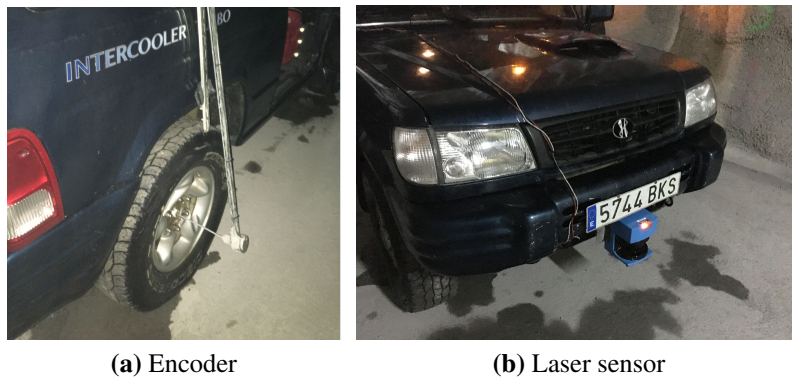


Figure 3.6: Instrumented platform.

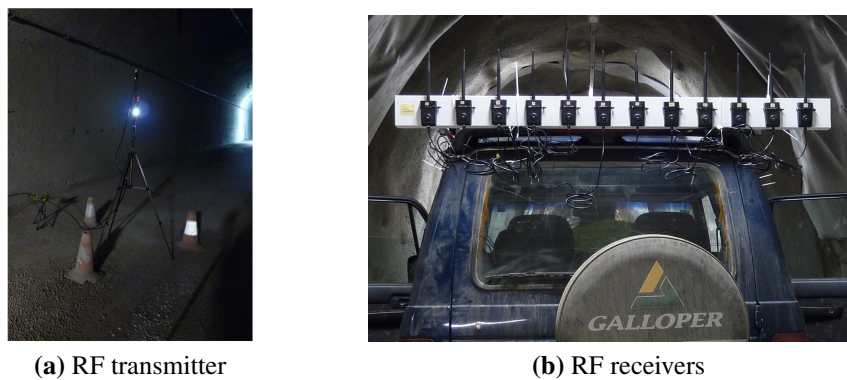


Figure 3.7: Experimental transmitter-receiver setup.

TPLINK tl-wn7200nd wireless adapter with Ralink chipset. It was placed 100 m from the entrance of the tunnel, 0.25 m from the right wall and 2 m above the ground. With these transmitter-receiver settings, the period expected for the fadings is around 512 m. The experimental transmitter-receiver setup can be seen in Fig.3.7.

The mobile platform moved up to 4000 m from the transmitter position along the center of the tunnel in straight line with almost negligible heading variations. This behaviour allows us to simplify the general formulation to a one dimension problem where x represents the longitudinal distance to the tunnel entrance.

During the displacement of the robot, the data provided by the sensors were streaming and logging with a laptop running ROS over Ubuntu 12-04.

The real data used to validate the proposed algorithm are the RSSI values provided by the rightmost antenna. This method is intended to solve the localization problem in the far sector where the periodic fadings are observable. Therefore, the values corres-

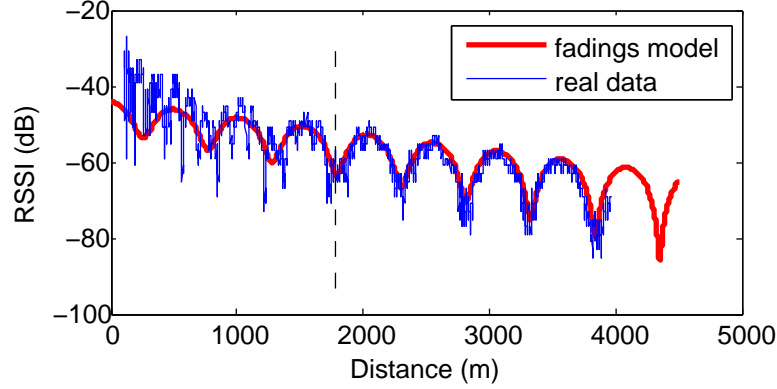


Figure 3.8: Received signal strength from antenna 12. The vertical dashed line denotes the limit between the fast fadings and the selected work zone.

ponding to the near sector have been removed from the data set in order to avoid the fast-fadings effect (Fig. 3.8).

It should be noted that, although the tunnel scenario and the mobile platform are the same for the real validation of all the solutions proposed in this thesis, different RF equipment and configuration were used for each of them. Similarly, the experiments carried out differ from each other in terms of distance covered and tunnel area traverse.

3.5 Results

In order to test the proposed discrete localization method, the algorithm was implemented in Matlab. The main goal was to validate the solution using real data, and for this purpose the dataset logged in the Somport tunnel was used and processed offline.

3.5.1 Localization algorithm implementation

The RLS algorithm needs to be implemented in order to get the minimums of the RF signal (fadings) along the tunnel. For this particular case, the variables involved in RLS method are defined as follows:

- Measured process output: $y = RSSI\ values$
- Inputs: $u = (1 \ \tau)^T$, where τ is the time between two consecutive RSSI received values
- Coefficients: $\theta = (\theta_0 \ \theta_1)^T$
- Model output: $\hat{y} = u^T \theta = \theta_0 + \theta_1 \tau$, first order polynomial

- Initialization: $\theta(0) = 0$ and $P(0) = \delta I$, being δ a constant value to initialize P . Since the knowledge of θ at $t = 0$ is very vague, a very high covariance matrix of the coefficients is to be expected, and thus a high value to δ must be assigned.

A signal minimum is identified when a change in the slope is detected, i.e. when the slope of previous iteration is negative ($\theta_1(k-1) < 0$) and the slope of the current iteration is positive ($\theta_1(k) > 0$).

Minimums map generation:

In this case, the RSSI values of the fadings model are used as the process output. The forgetting factor λ is selected as 0.5 because of the lack of noise in the theoretical model. For the initialization of P a value of 1000 is assigned to δ . The positions corresponding to each minimum are stored $(x_{m1}, x_{m2}, \dots, x_{mn})$.

Minimums detection of the actual RF signal values:

The RLS algorithm is applied using the RSSI value provided by the RF receivers as the process output. Due to the noisy nature of the signal, a major contribution of previous samples in the parameter estimation is needed. For this reason, a 0.95 value is assigned to λ . The value selected for δ is 1000 as in the previous case.

Mahalanobis distance and IC test:

The variance of the minimum sensor obtained during the calibration process is $(20/2)^2(m^2)$. For the IC test (Eq. 3.13) it is necessary to select a value for χ . In this case, for a 95% confidence level with $d = 1$ and $\alpha = 0.05$, the χ value provided by the the Student's Distribution table is 6.314 m.

3.5.2 Experimental results

The result of the minimums detection of the fadings model is shown in Fig. 3.9a. The vector of reference positions (green circles) is used as a prior information in the online process. Due to the noisy nature of the RF signal, a first order butterworth filter has been applied to the real signal (Fig. 3.9b).

The result of the RLS algorithm application to the actual RF signal is shown in Fig. 3.9c. The potential minimums provided by the algorithm are represented as blue asterisks. The green circles are the minimums provided by the map. As it can be observed, only the use of the RLS method is not enough because several false positives are returned as signal valleys. Fig. 3.9d shows the result of the combination of the RLS algorithm with the individual compatibility test based on Mahalanobis distance. It is clearly shown how most of the false positives are discarded using the proposed method.

When a minimum of the RF signal is identified, the estimated position of the robot is set to the reference position of the minimums map. A detail of the position correction corresponding to detected minimum denoted by **A** is shown in Fig. 3.9e. As expected, the position error of the odometry estimation increases reaching a value of 30 m whereas the error of the proposed method (around 8 m) is reduced each time a valley is identified (Fig 3.9f).

3.6 Concluding remarks

When implementing the proposed solution in tunnels, the following practical aspects should be taken into account:

- For a given cross-section, the choice of RF frequency and the selection of appropriate emitter/receiver positions can be used to tailor the RF power distribution inside the tunnel (periodic fadings).
- Unlike pipes, there is no well defined cutoff frequency, all the modes are propagated with different attenuation.
- Higher frequencies attenuate less but creates a more complex fading distribution. Lower operating frequencies provokes shorter fadings period and near sector length. Thus, a compromise choice is mandatory.
- For tunnels with cross-section ranging from 3 to 6 meters, the near sector has around 1 km length.
- The agreement between the RF signal model provided by the modal theory and the experimental results allow us to use the first as a position reference.
- The RF minima detection method provides good performance under the odometry uncertainty corresponding to the Somport tunnel. However, if the error accumulated by the odometry were higher due to a more critical condition of the scenario, false positives could not be discarded using the Mahalanobis distance as the RF real signal would be too much delayed in terms of distance with respect to the RF theoretical model.
- The presented approach is valid in the sector where the periodic signal is observable, i.e. along the far sector. The RF signal complexity in the near sector leads us to look for alternative solutions that will be presented in the following chapters.

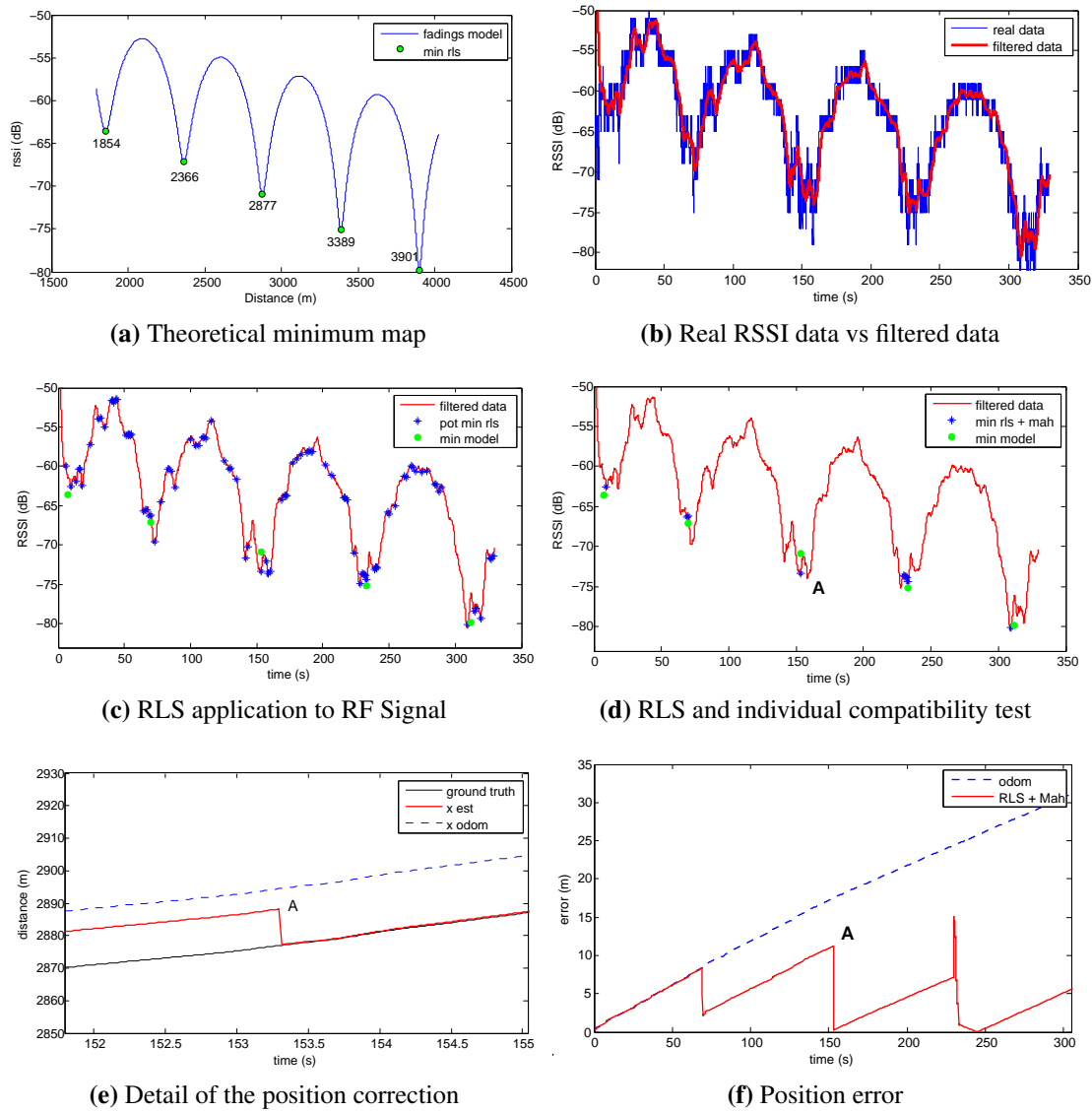


Figure 3.9: Results of the propose algorithm based on RLS and Mahalanobis distance: (a) minimums map from fadings model used as known information, (b) filtered signal obtained by a first order filter, (c) results of the application of the RLS method to actual data, (d) final minimums detection result after the IC Test , (e) position correction during the displacement of the vehicle, (e) position error comparison between odometry method and the presented approach.

3.7 Summary

In this chapter, a discrete localization system based on RF fadings for tunnel environments has been presented. The proposed method is based on the periodic nature of the RF fadings in this environment. It takes advantage of the RF propagation model to generate a minimums map used as position references. The online identification of singular characteristics of the RF signal along the tunnel (minima) and their matching with the known RF minimums map, allows the robot position to be corrected.

The algorithm has been validated with real data collected during an experimental test in a real scenario. The empirical preliminary results show that it is possible to periodically reset the error accumulated by the odometry with a frequency corresponding to the fadings signal period.

The implemented discrete localization algorithm overcomes the lack of distinctive features in tunnels needed by other algorithms based on laser or cameras. Moreover, the only equipment required are the odometers and the RF transmitter and receiver.

Although this approach is a discrete method, it provides enough localization corrections for some applications where a continuous precise localization is not critical.

As seen throughout this chapter, localization inside tunnels fusing the information provided by the odometry and the RF periodic signal is even more challenging than in the case of pipes. On the one hand, the proposed method is very sensitive to the odometry uncertainty. On the other hand, the presented approach cannot solve the localization where the periodicity of the signal is not observable (near sector) where all the modes propagates until being attenuated. As mentioned before in the concluding remarks section, the fast fadings area can be decreased by using lower frequencies, although this also causes a reduction in coverage.

In order to overcome the near sector issues, the use of two different RF signals simultaneously, one at low frequency and other at high frequency, is proposed in Chapter 5 of [Rizzo, 2015]. With this configuration, the localization method could work with the observable periodic fadings in both areas. Nevertheless, this solution increases the complexity of the RF setup and equipment as well as the need of previous experiments in order to overlap the near sectors provoked by the two signals (forcing the appearance of periodic fadings corresponding to the low frequency signal in the near sector with fast fadings resulting from the higher frequency signal). Moreover, the RF signal inside tunnels is much more noisy than in metallic pipes, making unfeasible the continuous localization approach using particle filters to match the real signal with the RF map.

Due to these reasons, the next natural step consists of trying to solve the localization along the tunnel taking advantage of the valuable information provided by the periodic structure of the fadings where available and adding other sources of information to the localization process coming from the different characteristics that we can find along the tunnel.

The next part of the thesis includes a new localization approach based on graphs that entails a series of advantages over filtering solutions as will be seen later.

Part II

Graph-based Robot Localization in Tunnel-like environments

Chapter 4

Tunnel Features detection for Localization purposes

In the previous chapter we have seen how the periodic structure of the RF signal together with the RF signal model provides useful information involved during the localization process. Additionally, tunnels present structural characteristics in order to be in compliance with safety regulations, such as emergency exits and shelters. These relevant features constitute also a very valuable source of information that can be used for localization purposes. Our proposal consists of addressing the robot localization problem as an online pose-graph localization problem, adding to the graph both sources of information coming from the RF signal and the structural characteristics. The first step is to obtain the data to be incorporated to the graph by detecting the relevant features, not only the structural ones from the scenario but also from the RF periodic signal. In this chapter we describe two detection methods: a scan-pattern based method to detect the galleries of the tunnel and an alternative method to detect the minima of the RF signal. The information provided by both methods will be introduced into the pose graph, as will be described in the next chapter.

4.1 Introduction

Accidents can be very serious when they occur in tunnels. Because of the confined environment, accidents in tunnels, particularly those involving fires, can have dramatic consequences. In the European Union, as a result of the tragic tunnel accidents in 1999 to 2001, the European Commission developed a Directive [Union, 2004] aimed at ensuring a minimum level of safety in road tunnels on the trans-European network. A total of 515 road tunnels of more than 500 m long were identified. The total length of these tunnels is more than 800 km.

To be compliant with these kind of directives, tunnels must integrate a set of struc-

tural elements to improve safety. Some examples from the European Directive are:

- Emergency exits as direct exits from the tunnel to the outside, cross-connections between tunnel tubes, exits to an emergency gallery, shelters with an escape route separate from the tunnel tube. The distance between two emergency exits shall not exceed 500 m.
- In twin-tube tunnels where the tubes are at the same level or nearly, cross-connections suitable for the use of emergency services shall be provided at least every 1500 m.
- Emergency stations shall be provided near the portals and inside at intervals which for new tunnels shall not exceed 150 m.

Thus, due to the obligation to comply with safety regulations, tunnels present a set of relevant structural characteristics that can be used as a source of information to improve the localization inside tunnels. Many of them are pseudo-periodic along the longitudinal dimension.

The use of relevant structural characteristics for localization purposes was explored in [Alejo et al., 2019]. The authors present a global localization system for inspection ground robots in sewer networks. The system takes advantage of the mandatory existence of manholes every certain distance at known positions and with a particular shape, to identify them (by using machine learning techniques) during the robot traveling along the sewer. The global position of the robot is corrected with each manhole identification resetting the position error.

Apart from these structural features present in tunnels at known positions, the periodic nature of the RF signal and its RF signal model used as RF map in these scenarios, can also provide position references in those areas where the fadings are distinguishable along the tunnel as we have seen in Chapter 3.

It has also been proven that working only with the radio signal might be insufficient to achieve a continuous location along the tunnel due to all the potential problems previously described, mainly the fast fadings in the near sector and the noisy nature of the RF signal.

For all these reasons, it is necessary to explore a new solution to solve the localization, with a twofold objective: on the one hand, to take advantage of the specific characteristics (structural features, periodic fading) offered by the tunnel. On the other hand, to overcome the problems found in different areas of the tunnel, such as the lack of lighting and the monotonous and smooth surfaces without distinctive features.

Recent advances in the field of graph-SLAM result in new localization approaches that model the localization problem as a pose-graph optimization. The pose graph encodes the poses of the robot during data acquisition as well as spatial constraints between them. The former are modeled as nodes in a graph and the latter as edges between

nodes. These constraints arise from sensor measurements. One of the main advantages of these approaches is the ease of incorporating measurements from different sources of information to the graph, not only local (wheel odometry, scan-matching results) but also global measurements (GPS, IMU).

Following this strategy, in this second part of the thesis we address the robot localization problem in tunnels as an online pose-graph localization problem, where we originally introduce the results of two detection processes into the graph optimization: a RF signal minima detection method taking advantage of the periodic nature of the RF signal inside tunnels, and an alternative galleries detection method. The resultant absolute positions provided by the detection methods are introduced as constraints into the pose-graph, that is being generated with the information that comes from the odometry. Each time new information is incorporated into the graph, it is optimized and the position of the robot is corrected, allowing to locate the main characteristics to be inspected more accurately.

In this chapter, we describe the design and implementation of both detection methods. On the one hand, an alternative method to identify the minimums of the RF signal minimums and match them with the RF map is presented. This method exploits the capability provided by the graph to add delayed measurements to improve the robustness of the method presented in Chapter 3. On the other hand, a scan-matching method based on patterns to identify tunnel galleries is developed. Both methods are validated experimentally with real data. The outputs of the described methods are subsequently added to the localization process as will be explained in Chapter 5.

4.2 Reference systems definition

Before the description of the detection methods, the reference systems involved in the proposed procedures need to be defined (see Fig. 4.1):

ABS_REF (A): Global or absolute reference frame of the tunnel. It is located at the middle of the tunnel entrance, that is over the tunnel axis.

ROB_REF (R): Local reference frame of the mobile robot. It is located in a point on the robot chassis.

MOB_REF (M): Sliding reference over the tunnel axis. It has the same orientation as the tunnel axis and the same absolute x position as the *ROB_REF*.

FEA_REF_i (F): The relevant i-th feature (gallery, fading or others) is expressed in this reference. It is located at tunnel axis in the feature location.

In order not to overload the nomenclature, the reference system will only be indicated in the case that the magnitude is referred to a system other than *ABS_REF*. The

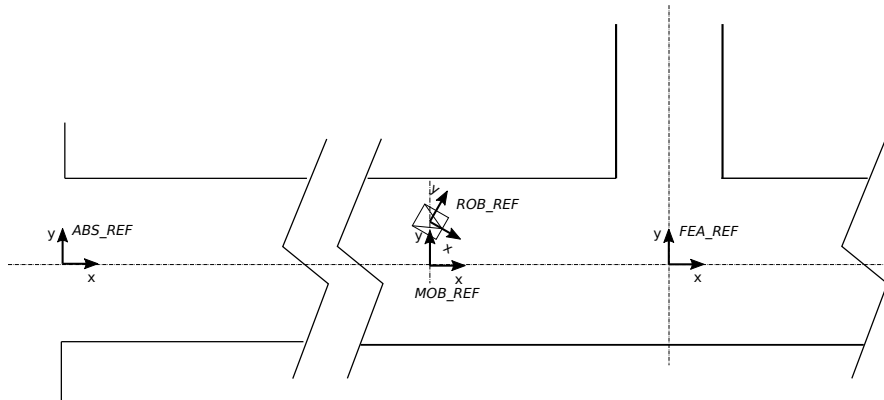


Figure 4.1: Involved reference frames in the robot localization problem.

only exception will be when talking about reference positions provided by maps. e.g. the minimum position provided by the RF map, x_m^A , or the gallery position provided by the geometrical map, x_g^A .

4.3 RF Minima Detection

As stated before, the agreement between the signal propagation model and the real RF signal let us consider the first one as an RF map, which relates the RSSI values to the distance along the tunnel. As already mentioned, due to the noisy nature of the RF signal, the most distinguishable features of the RF waveform are the valleys (fadings). The main objective of this alternative method remains the same, i.e., to identify the minima of the real signal during the robot displacement and to extract the reference position associated to each valley from the RF map. The information provided by the virtual minima detector will be added to the pose-graph as it will be explained in the next chapter.

The main difference between this proposal and the one presented in Section 3.3 of Chapter 3 lies in that the identification of the minimum is based on the matching of two geometric models, one representing the minimum of the real signal and the other representing a minimum in the theoretical model of the RF signal (RF map). Using this strategy we aim to improve the response of the detector to greater odometry uncertainty values with respect to the previously proposed detection method.

The first step of the method consists of extracting a discrete model representing the theoretical minimum model from the RF map. Using the propagation model, it is possible to know the position of each valley along the tunnel and then, the theoretical minimum model can be obtained in advance. During the displacement of the vehicle, the algorithm tries to match the discrete real model, generated during the movement, with

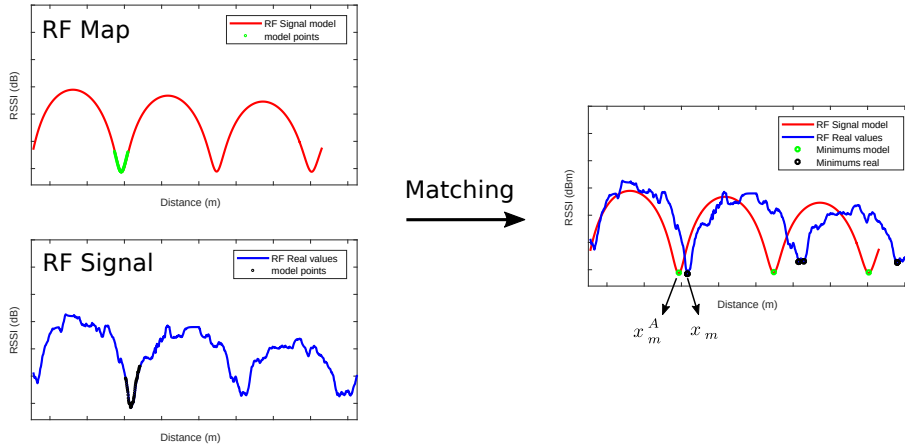


Figure 4.2: RF minimum detection process. The green points represent the theoretical minimum model and the black points the real minimum model.

the theoretical model. When the two models match, a minimum is found and the information about the estimated position of the minimum x_m together with its corresponding position in the map x_m^A is available (Fig. 4.2).

Fig. 4.3 shows the steps of the proposed strategy. The discrete theoretical model is extracted from the RF signal model in advance (Fig. 4.3a). The theoretical model consists of a set of points (x, y) where x is the position corresponding to each theoretical RSSI value y . Both values are provided by the RF map. The real model is obtained by accumulating points (x_t, y_t) during a certain period of time corresponding to a fixed distance D (Fig. 4.3b) where x_t is the position estimated by the odometry and y_t corresponds to the actual RSSI value provided by an RF sensor. Once the real model is available, the matching process starts using the previously recorded theoretical model. The points enclosed in the B blue area, which contains a potential minimum x_m , represent the real model used to describe the matching procedure that involves the following steps:

- Relate the theoretical model to the reference system of the real model (Fig. 4.3c). Both models have in common the minimum value.

Before starting this referencing step, a condition must be complied: the value of the RSSI minimum of the real model y_m^{real} does not have to differ a specific quantity Δ^{RSSI} from the RSSI minimum value of the theoretical model y_m^{theo} to consider the current real model as a potential set of points to start the matching process:

$$y_m^{real} - y_m^{theo} \leq \Delta^{RSSI} \quad (4.1)$$

being Δ^{RSSI} the amplitude of the theoretical minimum model $\Delta^{RSSI} = y_{max}^{theo} - y_m^{theo}$.

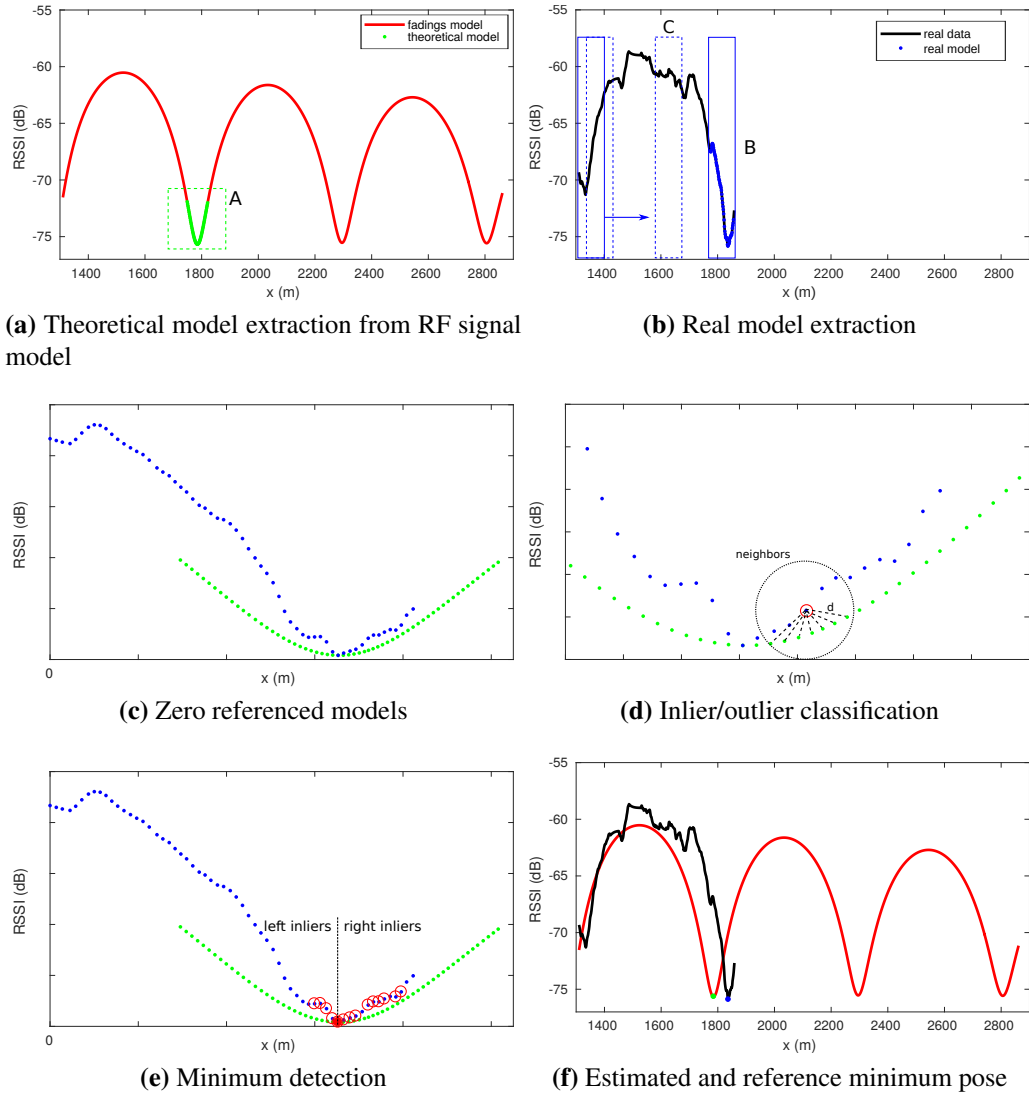


Figure 4.3: RF signal minima detection steps: (a) Theoretical model (green points inside the dashed green square A) extracted from the RF signal model (red). (b) Real model generation during the displacement of the vehicle from the real RF signal. (c) Both models referenced to the same system coordinates. (d) Point classification depending on the Mahalanobis distance between the real data and the closest neighbors from the theoretical model (e) Minimum detection if the number and proportion of inliers satisfy the threshold. (f) Estimated position by the odometry x_m (blue point) and position reference from the RF map $x_{m_i}^A$ (green point) of the detected minimum.

For example, the real model enclosed in C area does not comply this condition and therefore it is discarded from the matching process. The benefits are twofold: false positives are avoided and the execution time of the detection process is improved.

- For each real point $p_i^{real} = (x_i, y_i)^{real}$, calculate the Mahalanobis distance d_M between the real point and the N closest neighbors from the theoretical model $P_{neig} = \{p_1^{theo}, \dots, p_N^{theo}\}$ (Fig.4.3d).

$$d_M^2(p_j^{theo}, p_i^{real}) = (p_j^{theo} - p_i^{real})^T S^{-1} (p_j^{theo} - p_i^{real}), \forall p_j^{theo} \in P_{neig} \quad (4.2)$$

being $p_j^{theo} = (x_j, y_j)^{theo}$ the theoretical point j that belongs to the N closest neighbors set (selected using an euclidean distance). S is the covariance matrix obtained using Eq. 4.3:

$$S = \begin{pmatrix} \sigma_x^2 & \sigma_{xRSSI}^2 \\ \sigma_{RSSIx}^2 & \sigma_{RSSI}^2 \end{pmatrix} \quad (4.3)$$

- Classify each point as inlier or outlier based on the Mahalanobis distance using the χ^2 test. A point p_i^{real} is considered an inlier if the following condition is met with any of its neighbors:

$$d_M^2(p_j^{theo}, p_i^{real}) < \chi_{d,1-\alpha}^2 \quad (4.4)$$

where $\chi_{d,1-\alpha}^2$ is the threshold obtained from the χ^2 distribution table being d the dimension, 2 in our case, and $1 - \alpha$ the desired confidence level (usually 95%).

- If the number of inliers is greater than a certain threshold and the ratio r between left and right inliers is balanced, we can conclude that a minimum has been found (Fig. 4.3e). With only the first condition, there would be false positives in those areas around the minimum just before reaching it or after it has occurred. The ratio condition is formulated as follows:

$$1 - \delta_r < r \leq 1 + \delta_r, \delta_r \in (0, 1) \quad (4.5)$$

where δ_r is a real number ranging from 0 to 1 which allows us to play with non exact 50% balanced value between left and right. The ratio is calculated using Eq. 4.6:

$$r = \frac{n_{left}^{in}}{n_{right}^{in}} \quad (4.6)$$

being n_{left}^{in} and n_{right}^{in} the number of left and right inliers.

- The Mahalanobis distance is again calculated between the real minimum detected (x_m) and the minimums of the theoretical model, selecting the theoretical one with the least distance (Fig. 4.3f). The identification of the minimum position in the RF map $x_{m_i}^A$ is obtained with this last step.
- This process is repeated iteratively using a sliding window to generate the discrete real model (dashed blue area in Fig. 4.3b).

The resulting data are the estimated robot position provided by the odometry ($x_r = x_m$) and the position reference of the RF map ($x_{m_i}^A$), both corresponding to a minimum of the RF signal. The uncertainty of the position reference (σ_m) is a measure of the RF signal model fidelity with respect to the ground truth. This value is initially estimated offline knowing the absolute position of the transmitter in the tunnel, being adjusted online in a practical approach after each trip, comparing the positions of the real minimums provided by the localization approach with the absolute minimums position from the RF signal model.

It is worthy to notice that the information provided by the virtual sensor corresponds to delayed measurements, i.e., the position of the minimum is detected at a timestamp (T) after its appearance ($T - k$). This implies incorporating in the estimation process information referred to a past position. This can be handled thanks to the use of a graph representation, having an impact on the current pose estimation after the optimization process. The strategy followed to add these measurements to the pose-graph is explained in the next chapter.

4.4 Emergency galleries detection

As stated before, in this work we face the detection of relevant and mandatory structural characteristics present in the tunnel for safety reasons (galleries) to improve the location inside the tunnels using the known absolute position of each of them.

For this purpose, starting from [Ruiz and Villarroel, 2019], we propose a scan-pattern matching technique to establish the robot localization in the longitudinal dimension when the gallery is detected. Our method matches a pattern composed by small set of relevant points extracted from a geometrical map of the tunnel, with a scan reading. The patterns, different for each gallery, allow to unequivocally identify the gallery that is being passed through. The proposed technique assumes that the robot heading and transverse position are calculated with enough precision from sensor readings and being both known, the problem is addressed as 1D.

The following points summarize the steps of the gallery detection approach:

1. Extract from the whole scanned tunnel a unique pattern that represents each of the galleries. The pattern is composed by a set of relevant points (keypoints) extracted from the geometrical map of the tunnel.

2. All the information regarding the galleries is saved in a database that contains the gallery pattern ($[p_x, p_y]_{g_i}^F$), the global localization of the gallery ($x_{g_i}^A$) and an incremental unique identification along the tunnel (id_{g_i}). This information is available in advance.
3. A scan-pattern matching process takes place in order to identify in real time the gallery that has been traversed by the robot.
4. The gallery is detected from several robot positions as it passes by (before and after the reference position of the gallery defined by the pattern). The relative distance between each of the robot positions and the gallery and the uncertainty of the detection are provided during the matching process.
5. Once a gallery is detected and knowing the robot's current location and direction of movement, the next pattern is extracted from the database and the scan-pattern process starts again.

Gallery pattern extraction

As stated before, the pattern must identify unequivocally each gallery. It consists of a set of m relevant points $[p_x, p_y]_m^F$ extracted from the geometrical map, which represents the contour of the gallery.

The global localization of a gallery ($x_{g_i}^A$) usually corresponds to a relevant feature of the gallery such as the right or left corner or the axis. This question must be determined during the topographic work of the tunnel. In the present work, the localization of a gallery corresponds (without loss of generality) to the intersection of the gallery axis and the tunnel axis. The origin of the *FEA_REF* refers to this point and therefore, to this known gallery position ($x_{g_i}^A$). The (p_x, p_y) values for each point of the pattern are calculated with respect to this reference system (Fig. 4.4).

Scan-pattern matching process

In order for the scan-pattern matching to work properly, the laser data referenced with respect to the *ROB_REF* frame must be aligned with the pattern which is defined with respect to the *FEA_REF* frame. This condition is only met when the robot travels through the center of the tunnel parallel to the tunnel walls. In other cases, when the robot moves at a distance y_r from the tunnel axis and the angle of the robot to the wall (θ_r) differs from zero, a translation and rotation of the laser data are needed in order to align it to the pattern reference system. This converts the laser points to the *MOB_REF* frame. The mechanism proposed to calculate the angle and distance between the robot and the center axis consists of the identification of the straight line corresponding to the tunnel right wall using the laser data. We propose the use of the Hough Transform for this

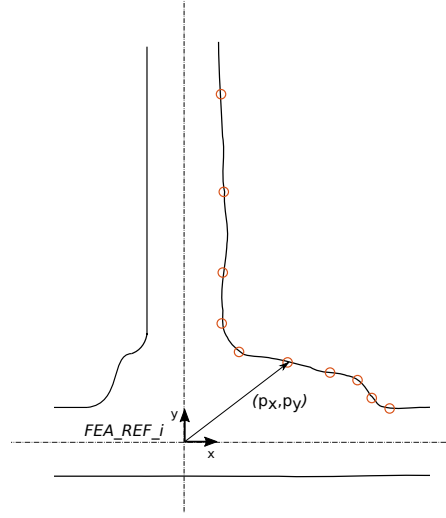


Figure 4.4: Pattern extraction (gallery 17 of the Somport tunnel). The origin of the pattern reference system FEA_REF_i corresponds to the intersection of two lines: the axis of the tunnel and the axis of the gallery (in the present example).

purpose. The Hough Transform, a well-known features extraction method, was initially introduced as a technique for extracting straight lines in images [Duda and Hart, 1972].

Let us consider the line L corresponding to the tunnel right wall in Fig. 4.5, being parametrized by the normal distance to the origin ρ and the normal angle α . These parameters ρ and α define the Hough space. Each laser scan point represented in Cartesian form $(l_x, l_y)^R$ with respect the ROB_REF frame is transformed into a discretized curve in the Hough space. The transformation is based on the parametrization of the line in polar coordinates using Eq. 4.7.

$$\rho = l_x * \cos \alpha + l_y * \sin \alpha \quad (4.7)$$

Values of α and ρ are discretized with $\alpha \in [-\pi, 0]$ and $\rho \in [-30, 30]$ for a typical commercial laser sensor ranges of 180 degrees and 30 m reading distance. Applying the Hough transform algorithm with these values, we can obtain the parameters (ρ, α) corresponding to the tunnel right wall, being ρ the distance to the wall and α the incidence angle. Both values are directly related to y_r and θ_r , being the transform matrix between ROB_REF and MOB_REF calculated as:

$${}^M T_R = \begin{bmatrix} \cos \theta_r & -\sin \theta_r & 0 \\ \sin \theta_r & \cos \theta_r & y_r \\ 0 & 0 & 1 \end{bmatrix} \quad (4.8)$$

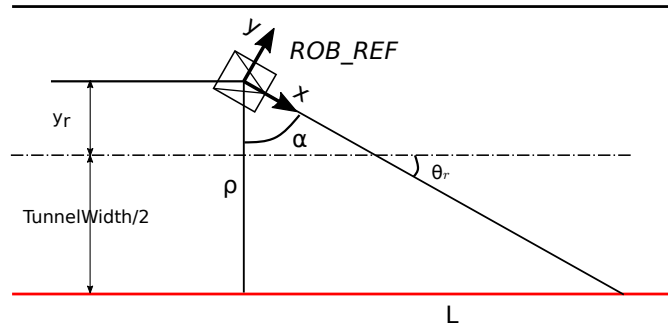


Figure 4.5: Hough transform to obtain the line in polar coordinates which represents the tunnel right wall. The resultant parameters ρ and α are used to transform the laser points from ROB_REF to MOB_REF .

The laser points lp^R are converted to the MOB_REF frame using the previously defined transform matrix with:

$$lp^M = {}^M T_R * lp^R \quad (4.9)$$

Once the laser points and the pattern are aligned, the matching process takes place. It should be noticed that in the environment where the experiments were carried out, the galleries are present only in the left wall of the tunnel. For this reason, previously to the scan-pattern process, the readings corresponding to the right wall of the tunnel are removed from the laser data resulting in a set of n laser points only corresponding to the left wall: $[l_x, l_y]_n^M$.

Metrics definition

The first step in a scan-pattern matching is the definition of a metric to measure the distance between the pattern and the scan reading. For this work we have selected the Nearest point-to-point metric although it is possible to easily use any other type of metric such as point-to-line metrics.

The Nearest Neighbor Search (NNS) method is widely used for pattern recognition applications. The NNS problem in multiple dimensions is stated as follows: given a set S of n points and a novel query point q in a d -dimensional space, find the closest point in the set S to q . Particularly in this case, it consists of finding the nearest point from the laser data $[l_x, l_y]_n^M$ to each point of the pattern $[p_x, p_y]_m^F$ computing the corresponding distances. The method provides a distance vector (d_1, d_2, \dots, d_m) of size m , being m the number of points which conforms the pattern. The position error between the pattern and the scan reading is calculated as the mean quadratic error of the distance vector using Eq. 4.10.

$$err_x = \sqrt{\frac{1}{m} \sum_{i=1}^m d_i^2} \quad (4.10)$$

For each iteration, the matching process between the laser data and the gallery pattern using the NNS algorithm is applied for a range of $[-r, +r]$ meters around the reference position of the pattern (*FEA_REF*). The distance in that range for which the matching process provides the least position error is obtained. That distance will correspond to the relative position between the *MOB_REF* and the reference position from where the pattern is captured, i.e., the relative distance between the longitudinal robot position and the gallery (d_{rg}). A gallery is considered as detected if the corresponding position error is lower than a defined threshold (*th*). The variance of the gallery detection system is directly related to the position error by means of: $\sigma_{rg}^2 = err_x^2$.

Data association process

Once the gallery is considered detected using the position error criteria, the next step is to unequivocally identify the gallery the robot is passing by, avoiding false positives. For this purpose, knowing the estimated position of the robot x_r and the absolute position of the gallery provided by the geometrical map $x_{g_i}^A$, both values should be close enough to consider that gallery i has been identified:

$$x_r \in [(x_{g_i}^A - m), (x_{g_i}^A + m)] \quad (4.11)$$

where m is a safety margin distance and it is related to the accumulated error by the localization system.

It should be noted that the starting position of the robot is known and therefore, the data corresponding to the first gallery to identify (pattern, global position and identification) can be extracted from the database. Once the gallery is detected, and knowing the direction of movement, the next gallery information is loaded into the matching process to be subsequently identified. This strategy avoids trying to match the current laser readings with all the available patterns, improving the efficiency of the detection process.

To sum up, the resultant of the emergency gallery detection algorithm at each time stamp is on the one hand, the relative distance (d_{rg}) between the current position of the robot (x_r) and the gallery position (defined by the pattern reference system) and on the other hand, the gallery detection uncertainty (σ_{rg}). A gallery is considered detected from the robot if the uncertainty value is below a certain threshold (*th*). The absolute real position of each gallery is also known from the geometrical map of the tunnel ($x_{g_i}^A$). This information will be added to the graph following the strategy explained in the next chapter. It is worth noting that each gallery will be detected from different robot positions in the defined search area around the pattern reference position $[-r, +r]$.

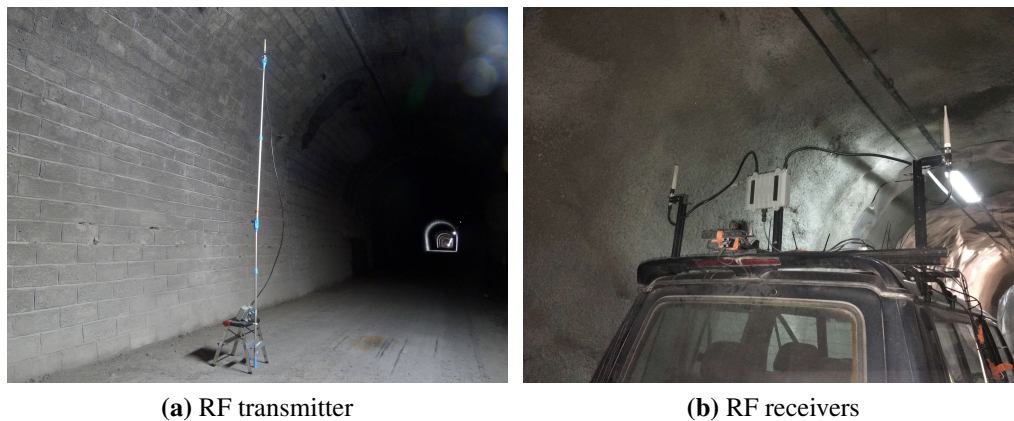


Figure 4.6: RF transmitter-receivers setup during the experiments in the Somport tunnel.

4.5 Experimental results

4.5.1 Scenario and Experimental setup

In order to validate the features detection methods, the proposed algorithms were implemented in *MATLABTM* and tested with real data collected during another experiment campaign conducted in the Somport tunnel. The main characteristics of this real scenario have been described previously in section 3.4. The tunnel has 17 lateral galleries, connecting the out-of-service railway tunnel with the operating road Somport tunnel. The galleries are numbered 17 to 1, from Spain to France. The same instrumented all-terrain vehicle, equipped with two encoders and a horizontal placed 2D LIDAR sensor, was used as the mobile platform simulating a service routine. The laser data is used during the galleries detection as has been described in Section 4.4.

For this set of experiments, the platform was equipped with two RF Alpha receivers placed at 2.25 m in height from the ground and with the antennas spaced 1.40 m apart. The transmitter, a TPLINK tl-wn7200md wireless adapter with Ralink chipset, was placed at approximately 850 m from the entrance of the tunnel, 3.50 m above the ground and 1.50 m from the right wall. Using a 2.412 GHz working frequency and under this receiver-transmitter setup, the expected fadings period is around 512 m. The RF data used to validate the proposed method are the RSSI values provided by the rightmost antenna. Fig. 4.6 shows the RF experimental setup.

The mobile platform started from gallery number 17 (50 m from the tunnel entrance) and moved up to gallery 6 traveling around 5000 m along the center of the tunnel in straight line with almost negligible heading variations. This behavior during the experiment makes feasible the simplification of the general formulation of our approach, where \mathbf{x} refers to (x, y, θ) , to a one dimension problem where \mathbf{x} corresponds to the lon-

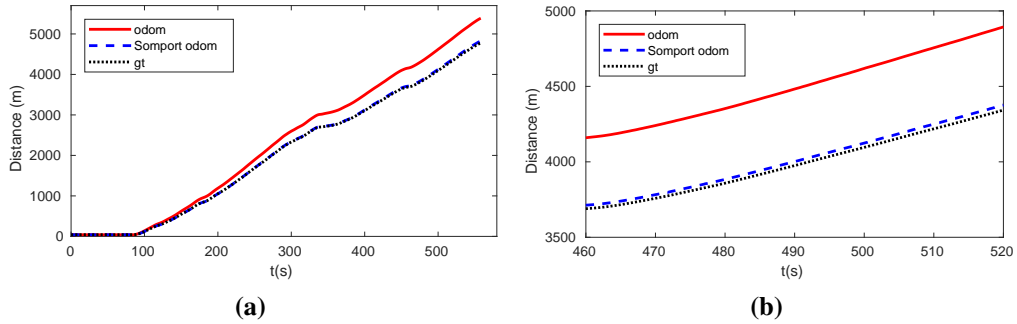


Figure 4.7: Odometry conditions. (a) Comparison between the ground-truth, the odometry position in the Somport tunnel and the degraded odometry for the validation. (c) Detail of the positions.

itudinal distance from the entrance of the tunnel. As in previous experiments, during the displacement of the vehicle, the data provided by the sensors were streaming and logging with a laptop running ROS. The ground truth, obtained as explained in Section 3.4.2, is also available and it is used only for comparison purposes.

To simulate worse conditions of the environment than those found in the Somport tunnel, the value returned by the odometry has been degraded increasing its uncertainty with respect to its real odometry value. Fig. 4.7 shows a comparison of the vehicle position provided by the odometry and the modified odometry with respect to the ground truth.

4.5.2 Minima detection results

Fig. 4.8 shows the results of the minima detection method. The number of points accumulated to create the real model corresponds to an estimated distance D of 80 m. This value is selected based on the distance corresponding to the theoretical minimum model. The RSSI data provided by the RF receiver is represented related to the position estimated by the odometry and the RF signal model related to the ground truth (Fig. 4.8a). The periodicity of the RF signal fadings under the transmitter-receiver setup of the Somport experiments is observed from 2.1 to 3.8 kilometer points approximately. When the vehicle reaches that area, some odometry error is accumulated and therefore, the real signal waveform does not exactly match with the RF signal model. However, the detection method is able to identify the real minimums and associate them to the RF map minimums providing the data needed to be incorporated to the graph. As can be seen in Fig. 4.8b, two different values have been identified corresponding to the same RF map minimum (second and third). This situation is handled by the mechanism explained in Section 5.3.

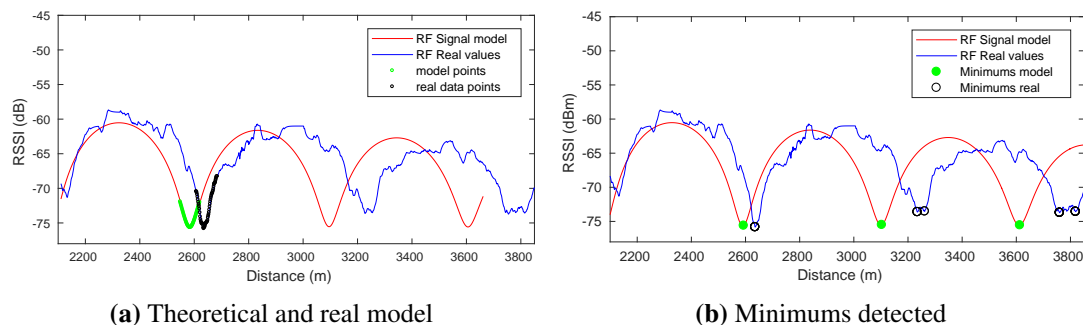


Figure 4.8: Results of the minima detection process. The RF signal model is represented with respect to the ground truth whereas the RF real values are represented with respect to the position estimated by the odometry.

4.5.3 Gallery detection results

The results of the gallery detector process for gallery number 17 of the Somport tunnel are shown in Fig. 4.9. The first row represents the laser scan reading together with the gallery 17 pattern at three different timestamps. The second and the third rows show the evolution of the uncertainty and the evolution of relative distance between the vehicle and the gallery respectively. Fig. 4.9a shows the first steps of the gallery observation from the vehicle. When the uncertainty σ_{rg} falls below a threshold (Fig. 4.9d), the gallery is considered detected and the relative distance d_{rg17} between the current position of the robot and the gallery is calculated (Fig. 4.9g). The relative position of the gallery is provided by the detector as long as the uncertainty remains below the threshold (0.5 m). Figs. 4.9b, 4.9e and 4.9h show the timestamp when the error in the scan-pattern matching process is close to 0. This situation corresponds to the vehicle passing by at the reference position of the gallery in the tunnel (*FEA_REF*). Lastly, when the uncertainty increases above the threshold, the detection process of the current gallery is considered finished. Fig. 4.9i shows the relative distance from the different vehicle positions to gallery 17 during all the detection process. As stated before, knowing the current estimated position of the vehicle and the movement direction, the pattern of the next expected gallery is loaded and the detection process starts again. The results of the matching process for other galleries can be observed in Fig. 4.10.

The evolution of the gallery detection uncertainty during the displacement of the vehicle along the tunnel can be observed in Fig. 4.11. It clearly shows a sharp drop in uncertainty indicating the detection of each gallery.

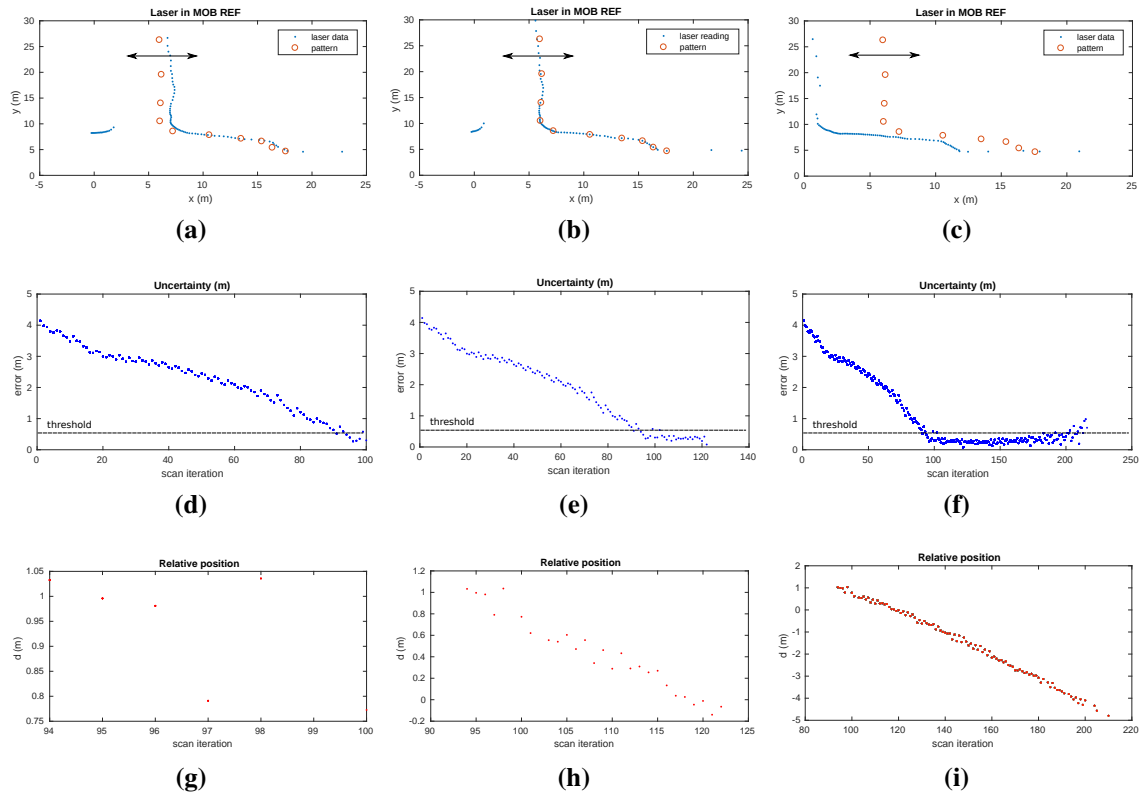


Figure 4.9: Gallery detection process. (a) First gallery detection timestamp. The detection uncertainty falls below the threshold (around the 90th iteration) (d) and the relative distance between the vehicle position and the gallery is provided by the detection algorithm (g). (b) The vehicle passes through the gallery position corresponding to the pattern reference. The uncertainty remains under the threshold (e) and the relative distance is provided during this time (h). (c) The vehicle (laser data) moves away from the gallery (pattern) and the uncertainty increases above the threshold (f). The condition of gallery detection is unsatisfied. (i) Relative distances between the vehicle position and the gallery during all the detection process.

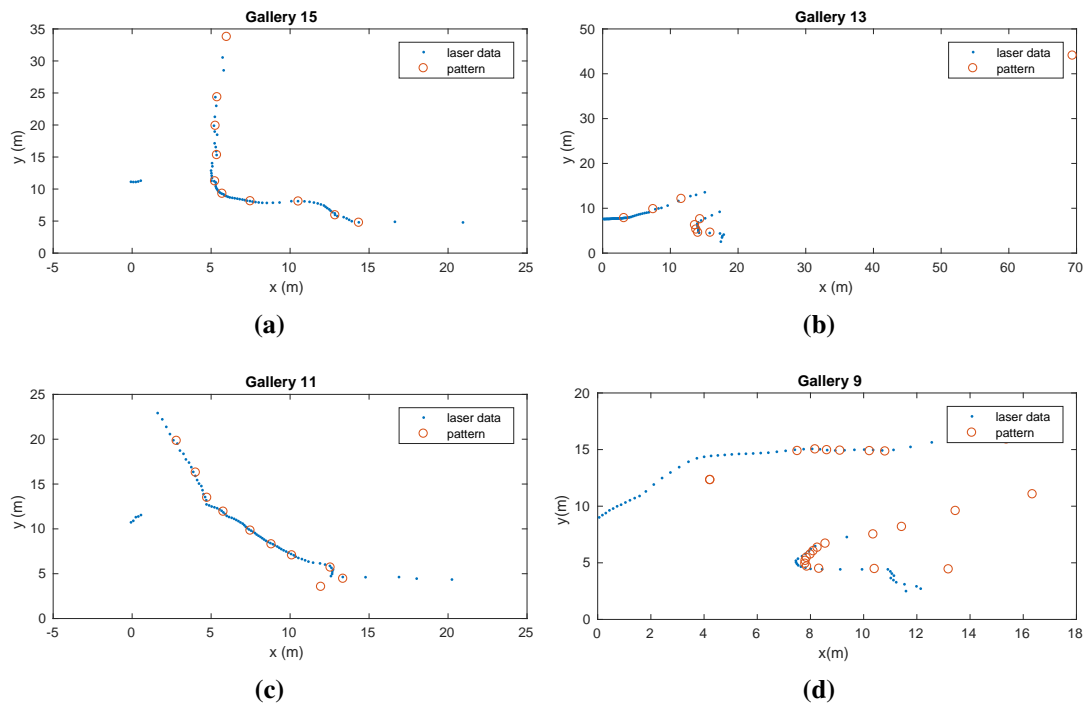


Figure 4.10: Matching process results for several galleries represented by different patterns during the displacement of the vehicle.

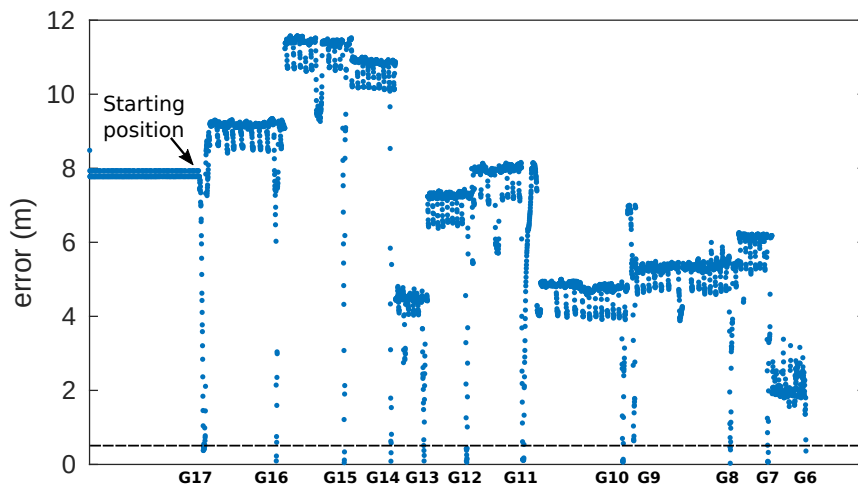


Figure 4.11: Evolution of the gallery detection uncertainty during the displacement of the vehicle from gallery 17 to gallery 6. The starting position of the vehicle corresponds to gallery 17.

4.6 Summary

With the objective of adopting the graph-based approach to solve the localization in tunnels, along this chapter we have developed two methods to detect relevant characteristics present in tunnels that provide valuable information to be introduced in the graph.

The first method described aims to detect the minima of the RF periodic signal by means of matching the geometrical model that represents the minimum in the RF signal model (RF map) with the model extracted from the real signal during the displacement of the robot. When both models match, the available information consists of, on the one hand, the robot position at which the minimum occurred and, on the other hand, the reference position of the minimum provided by the RF map. It is worth noticing that, as the method is based on a geometric matching between signals, it needs to accumulate RF values and the minimum is not detected until some time after it has actually occurred. Therefore, the results correspond to information from the past.

Secondly, a scan-pattern based method has been developed to detect structural features of the tunnel, specifically the galleries mandatory present in this type of scenario by regulations. Matching the laser data and the pattern which represents each gallery, this method is able to provide the relative distance between the robot position, from which the gallery is detected, and the gallery position, as well as the uncertainty of the gallery detection.

The feasibility of both detection methods has been validated with the data collected during an experimental campaign developed in a real tunnel scenario. On the one hand, the validity of the proposed minima detection method has been proven even when the RF actual signal and the RF signal model differs due mainly to odometry uncertainty and amplitude differences in the RSSI signal values. This method provides more robustness than the method presented in Section 3.3 against scale differences in the RF signal. Moreover, it is less sensitive to greater uncertainties in the odometry. This improved method could be implemented, as we will see in the next chapter, thanks to the great advantage provided by the graph approach to incorporate measurements from the past.

On the other hand, the results also show that it is possible to correctly detect all the galleries present in the tunnel. Each gallery is detected from different robot positions being the detector able to provide, not only the gallery position but also the relative distance to the gallery from all these robot positions. This information will be integrated with the one obtained from the RF minima detector to improve the absolute localization.

The data provided by both detectors is originally introduced in the graph as absolute measurements as we will see in the next chapter.

Chapter 5

Multi sensor graph-based robot localization in Tunnels

Recent advances in the field of graph-SLAM result in new localization approaches that model the localization problem as a pose-graph optimization with the advantage of easily incorporating measurements from different sources of information to the graph, not only relative but also global measurements. Building on this approach, in this chapter we present a graph-based solution to solve the localization in tunnels which makes use of the information provided by the detection methods described in the previous chapter. Along this chapter, the strategies developed to incorporate to the graph the global information coming from the RF minima and gallery detectors are detailed. The results of the experiments carried out in a real scenario together with the performance evaluation, demonstrate the potential of the proposed solution to overcome the identified difficulties in tunnel scenarios. The contributions of this and the previous chapter were reflected initially in [Seco et al., 2020] and finally in [Seco et al., 2021].

5.1 Introduction

The SLAM problem is one of the fundamental challenges of robotics, dealing with the necessity of building a map of an unknown environment while simultaneously determining the localization of the robot within this map. Robot mapping is characterized by uncertainty and sensor noise and therefore the SLAM problem must be handled using probabilistic techniques. These algorithms tackle the problem by explicitly modeling different sources of noise and their effects on the measurements.

In the literature, a large variety of solutions to this problem is available, being classified in filtering and optimization (graph) approaches. Filtering approaches ([Thrun et al., 2005, Aulinas et al., 2008]), have become dominant in SLAM. This group includes probabilistic formulations based on Kalman (KF) and its variations

[Nieto et al., 2007], particle filters (PF) [Grisetti et al., 2007] and Expectation Maximization (EM) [Rogers et al., 2010].

Optimization approaches address the SLAM problem via the so-called graph-based formulation [Grisetti et al., 2010a]. These techniques estimate the full trajectory of the robot from the full set of the measurements. The trajectory is represented by a graph which consists of nodes corresponding to robot poses, and edges between two nodes encoding sensor measurements that constrains the connected poses. Once the graph is constructed, the optimization process takes place to find a configuration of the nodes that best satisfies the constraints. Therefore, the graph-SLAM problem needs to address two tasks: the graph construction (front-end) in charge of constructing the graph from the raw sensor measurements, and the graph optimization (back-end) focused on determining the most likely configuration of the poses given the edges of the graph, solving an error minimization problem.

Although the graph-based formulation of the SLAM problem was introduced by [Lu and Milios, 1997], its use was not extended because the optimization of the graph was too time-consuming for real-time performance due to the complexity of solving the error minimization problem with standard techniques. It was not until recently that it has re-gained popularity, thanks to the advances in linear algebra that allow to solve the optimization problem in an efficient way. Georgia Tech Smoothing and Mapping (GTSAM) [Dellaert and Kaess, 2006], Hierarchical Optimization on Manifolds (HOG-Man) [Grisetti et al., 2010b] and General (Hyper) Graph Optimization (g2o) [Kümmerle et al., 2011] are some of the most popular global optimizers (back-ends).

The graph-based approaches offer improved performance and the capability of incorporating information from the past being memorized all the data. The main disadvantage of filtering techniques is that the data is processed and then discarded, making it impossible to revisit the past data. All these advantages in addition to being able to easily incorporate relative and absolute measurements coming from different sources of information, led to the emergence of new localization approaches that model the localization problem as a pose-graph optimization.

In [Imperoli et al., 2018], the authors provide a positioning framework targeted for agricultural applications. They integrate several heterogeneous sensors into a pose graph where the relative constraints between nodes are provided by wheel odometry and visual odometry, and the global (so-called prior) information is provided by a low-cost GPS and an IMU. The proposed system also introduces further constraints exploiting domain-specific patterns present in these environments. The effectiveness of incorporating prior information is also demonstrated in [Kümmerle et al., 2009a]. The presented solution relies on a graph-based formulation of the SLAM problem based on 3D range information and using aerial images as prior information. The latter is introduced to the graph as global constraints that contain absolute locations obtained by

Monte Carlo localization on a map computed from the aerial images. In a similar way, [Boniardi et al., 2019] also proposes the use of prior constraints to improve the localization in industrial scenarios. The prior information is provided by a CAD drawing allowing the robot to estimate its current pose with respect to the global reference frame of a floor plan.

Taking into account the aforementioned works, our approach consists of addressing the localization in tunnels as a pose-graph optimization problem, incorporating the data provided by the RF minima detector and the gallery detector. The main advantages of adopting a graph-based representation are twofold: it allows to easily incorporate delayed measurements into the estimation process, and to recover (undo) from wrong decisions such as the inclusion of incorrect measurements. Moreover, and for the particular case of tunnel localization, the use of different sources of information allows to reset the localization cumulative error not only in the area of appearance of periodic fadings but also each time a gallery is detected.

In this chapter, we first describe the formulation involved in the proposed solution based on graphs. Secondly, we present the strategies to originally introduce the discrete data provided by the previously described detection methods as absolute measurements in the graph, that it is being constructed with the odometry data. Finally, the experimental validation and the performance evaluation demonstrate the adequacy of our method as a novel alternative to solve the localization in these types of environments.

5.2 Pose Graph formulation

Inspired by the graph-SLAM paradigm, our approach models the robot localization problem as a graph-based pose optimization problem. Such an approach represents the trajectory of the robot $\mathbf{x}_{0:T} = \{\mathbf{x}_0, \dots, \mathbf{x}_T\}$ by a graph where nodes symbolize discrete robot positions \mathbf{x}_t at time step t while the edges impose position constraints on one or multiple nodes ([Grisetti et al., 2010a]). Hence, some nodes in the graph are related by *binary* edges encoding relative position constraints between two nodes $(\mathbf{x}_i, \mathbf{x}_j)$, characterized by a mean \mathbf{z}_{ij} and information matrix $\mathbf{\Omega}_{ij}$. These relative measurements are typically obtained through odometry or scan matching. Furthermore, it is possible to incorporate into the graph global or prior information associated only to one robot position \mathbf{x}_i by means of *unary* edges characterized by the measurement \mathbf{z}_i with information matrix $\mathbf{\Omega}_i$. These measurements typically come from sensors providing direct absolute information about the robot pose such as GPS or IMU.

Let $\hat{\mathbf{z}}_i(\mathbf{x}_i)$ and $\hat{\mathbf{z}}_{ij}(\mathbf{x}_i, \mathbf{x}_j)$ be the functions that compute the expected global and relative observations given the current estimation of the nodes. Following [Grisetti et al., 2010a], we formulate for each unary and binary edge an error function

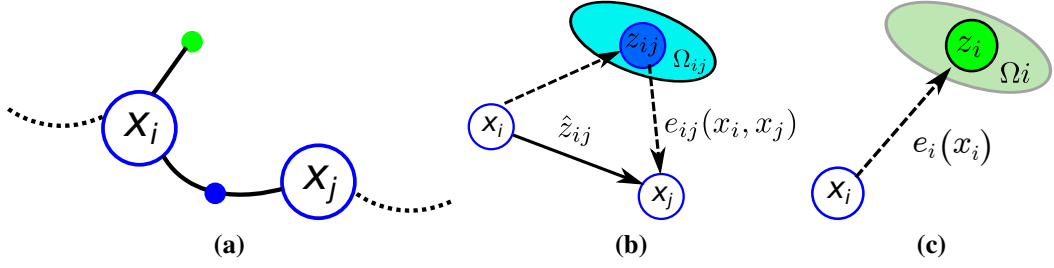


Figure 5.1: (a) Graphical representation of a portion of a pose graph where two nodes \mathbf{x}_i and \mathbf{x}_j are related by a binary edge (blue point) and where a unary edge is associated to node \mathbf{x}_i (green point). (b) Binary edge representing the relative position between \mathbf{x}_i and \mathbf{x}_j nodes. (c) Unary edge corresponding to an absolute position associated to \mathbf{x}_i node.

that computes the difference between the real and the expected observation:

$$\begin{aligned} \mathbf{e}(\mathbf{x}_i, \mathbf{z}_i) &= \mathbf{e}_i(\mathbf{x}_i) = \mathbf{z}_i - \hat{\mathbf{z}}_i(\mathbf{x}_i) \\ \mathbf{e}(\mathbf{x}_i, \mathbf{x}_j, \mathbf{z}_{ij}) &= \mathbf{e}_{ij}(\mathbf{x}_i, \mathbf{x}_j) = \mathbf{z}_{ij} - \hat{\mathbf{z}}_{ij}(\mathbf{x}_i, \mathbf{x}_j) \end{aligned} \quad (5.1)$$

Fig. 5.1 depicts a detail of the graphical representation used along this paper for the pose graph and the binary and unary edges.

The goal of a graph-based approach is to find the configuration of nodes that minimizes the sum of the errors introduced by the measurements, formulated as:

$$\mathbf{x}^* = \underset{\mathbf{x}}{\operatorname{argmin}} \left(\sum_{i,j} \mathbf{e}_{ij}^T \boldsymbol{\Omega}_{ij} \mathbf{e}_{ij} + \sum_i \mathbf{e}_i^T \boldsymbol{\Omega}_i \mathbf{e}_i \right) \quad (5.2)$$

The above Eq. 5.2 poses a non-linear least-squares problem that can be solved iteratively using the Gauss-Newton algorithm.

Our approach for localization inside tunnels considers measurements coming from three sources of information: odometry data, RF signal minima detection and gallery detection using the procedures described in Chapter 4. Odometry measurements are straightforwardly introduced into the graph as binary constraints encoding relative displacement between consecutive nodes ($\mathbf{x}_{t-1}, \mathbf{x}_t$). The output provided by the minima detection mechanism can be considered as an absolute positioning system inside the tunnel which can be used as a unary constraint during the graph optimization process. Additionally, the absolute gallery location provided by the gallery detector algorithm is also introduced as an unary edge into the graph. Once the constraints derived from the measurements are incorporated to the graph the error minimization process takes place, where the optimization time depends directly on the number of nodes.

Graph-based localization and mapping systems usually perform a rich discretization of the robot trajectory, where the separation between nodes ranges from few centimeters

to few meters. This type of dense discretization would be intractable in a tunnel-like environment with few distinguishable features where the length of the robot trajectory is measured in the order of magnitude of kilometers. It is therefore necessary to maintain a greater distance between nodes to manage a sparser and more efficient graph.

This general criteria to introduce spread nodes in the graph is modified when a minimum or a gallery is detected as will be described in the next section.

5.3 Graph-based robot localization using fadings and galleries

During the displacement of the robot along the tunnel, the pose-graph is constructed by adding nodes each time a certain distance is traveled (in the order of meters to maintain a sparse graph). The relative position between them is encoded with the information provided by the odometry using binary edges. In addition, new information is incorporated into the graph with any RF minimum or gallery detection event. The proposed strategies to introduce the nodes and restrictions coming from these events occurrence are explained in the following sections.

5.3.1 Management of RF fadings minima detection in the pose-graph

As described in Section 4.3, the detection of the RF signal minima is obtained on a posterior time T in which it actually occurred. This involves incorporating to the graph measurements from a past timestamp.

Under an RF signal minimum detection event, we need to associate a unary constraint to the past robot position where the minimum occurred. In view of the need to maintain a sparse graph, it can happen that the referred robot position is not represented in the graph as a node, having to modify the current graph structure to include it.

The procedure to include the global measurement corresponding to a past robot position \mathbf{x}_{T-k} , is illustrated in Fig. 5.2 and described in the following:

- At timestamp T , a RF signal minimum corresponding to timestamp $T - k$ is identified. Since robot position \mathbf{x}_{T-k} is not present in the graph, we determine between which two nodes \mathbf{x}_i and \mathbf{x}_j it should be included, based on the timestamps stored in each node. We also maintain a buffer containing the odometry information associated to each timestamp (Fig. 5.2a).
- Once the two nodes are identified, the new node \mathbf{x}_{T-k} is inserted into the graph connected to nodes \mathbf{x}_i and \mathbf{x}_j by using binary edges labeled with relative odometry

information, and the unary edge is associated to the node \mathbf{x}_{T-k} . Previous odometry measurement connecting \mathbf{x}_i and \mathbf{x}_j is removed to prevent double-counting of information (Fig. 5.2b).

- In the event of detecting another minimum corresponding to the same minimum in the RF map, the unary constraint of the previous minimum is deactivated and same procedure is followed (Fig. 5.2c). This can be the case of false positives or improved detections after the accumulation of more data.

Fig. 5.2d shows an example of a final graph after detecting three RF minimums at different timestamps T_1 , T_2 and T_3 . As can be clearly seen, the nodes with their unary edges are introduced into the graph representing their real positions corresponding to the minimums occurrences, showing the ease of the pose-graph approach to incorporate information from the past. The optimization process takes place after each graph modification, so the estimation position is corrected taking into account the new incorporated restrictions.

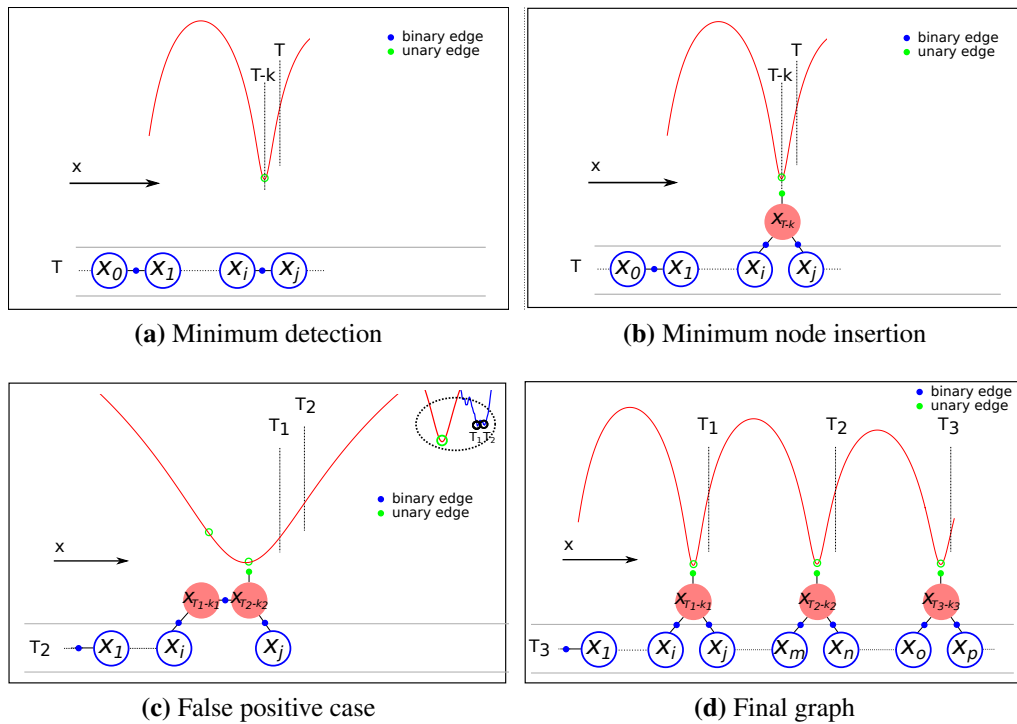


Figure 5.2: Pose-graph creation steps: (a) Minimum identification at time T . (b) Insertion of the node and the unary constraint corresponding to the detected minimum. (c) False positive case detail, deactivation (removal) of the previous unary edge. (d) Resulting pose-graph after three minimums.

5.3.2 Management of the galleries detection in the pose-graph

In addition to the information introduced to the graph each time an RF minimum is detected, the graph is also enriched with the gallery data, causing an improvement in the localization in the whole tunnel. Although both data corresponds to absolute measurements, the mechanism to introduce this information in the case of the galleries differs from the one proposed for the minima detection.

The gallery detector provides the relative position of the gallery and its associated error with respect to the robot positions from which the gallery is observed. Thus, the position of the gallery is obtained from an indirect measurement. For this reason, instead of adding the unary representing the known absolute position of the gallery directly to each node, we associate the unary constraint only to a gallery node and encode the relative position between the trajectory nodes and the gallery by using binary edges.

The procedure to introduce the gallery information to the graph starts once a particular gallery is detected for the first time. Fig. 5.3 illustrates the process that consists of the following steps:

- The discrete robot poses are represented by trajectory nodes in the graph that are related between them by means of the constraints encoded as binary edges. Fig. 5.3a shows an example of initial situation.
- At timestamp T , the uncertainty provided by the gallery detector complies the criteria to consider that a gallery is detected. A new node (\mathbf{x}_{k_1}) corresponding to the robot position from which the gallery has been observed is added to the graph using the relative odometry information with respect to the previous node \mathbf{x}_j .
- The first time the gallery is detected, the node corresponding to the gallery position (\mathbf{x}_g) is also added to the graph using a binary edge which represents the relative position between the gallery and the current position of the robot (d_{k_1g}). A unary edge encoding the absolute position of the gallery (\mathbf{z}_g) is also attached to the gallery node. This gallery position is provided by the geometrical map (\mathbf{x}_g^A) (Fig. 5.3b).
- Each time the gallery is detected, a new node (\mathbf{x}_{k_i}) is inserted into the graph connected to the previous node using the relative odometry position, and connected to the gallery node through a binary edge using the information provided by the gallery detection (relative position $d_{k_i g}$ and uncertainty of the measurement $\sigma_{k_i g}$). Both edges are encoded as binary edges. (Fig. 5.3c)
- When the gallery is no longer detected, i.e. the uncertainty raises above the threshold, the nodes are again introduced to the graph following the regular criteria (sparse graph). (Fig. 5.3d)

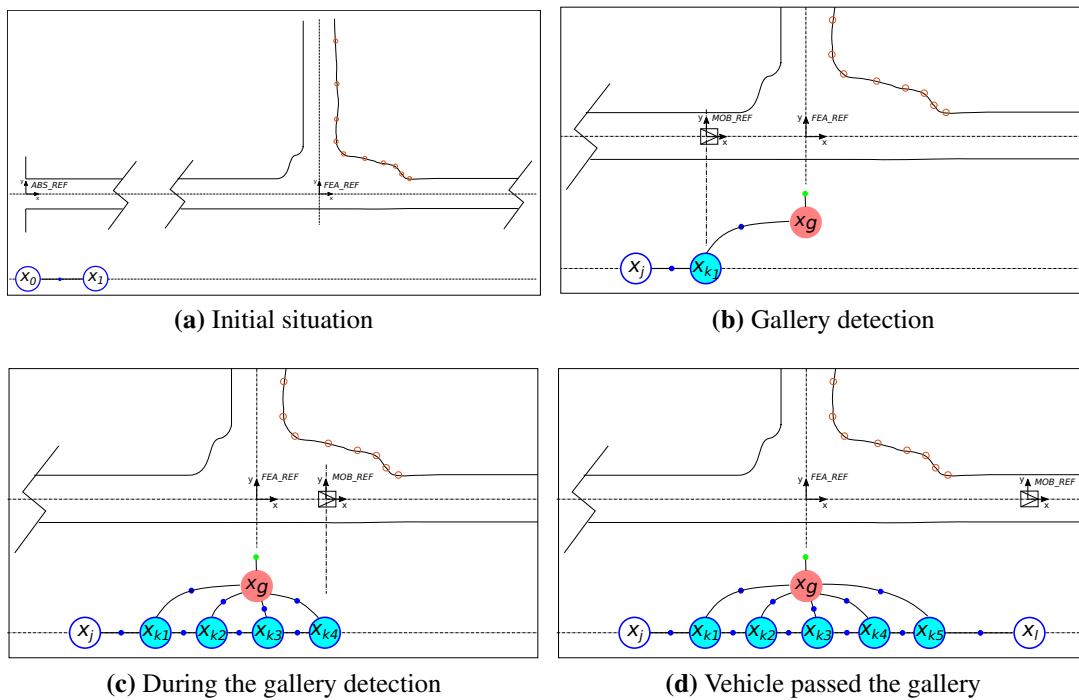


Figure 5.3: Gallery pose-graph creation steps: (a) Initial situation. The vehicle starts moving (b) The gallery is detected for the first time and the gallery node is introduced. (c) Nodes addition each time the gallery is detected. (d) Graph nodes once the vehicle has traversed the gallery. Blue dots denote binary edges and green dots unary edges.

To sum up, the pose-graph is updated with the positions from which the gallery is observed, adding the constraints as binary edges between nodes and as unary edge associated to the gallery node. As a result of this process, the localization resolution increases during the gallery detection. Again, the estimated position is corrected after executing the optimization process with each new node incorporation.

5.4 Experimental results

5.4.1 Scenario and Experimental setup

The validation of the proposed graph-based localization approach was performed using the real data collected during the experiments conducted in the Somport tunnel already described in Section 4.5.1.

As previously mentioned, the instrumented all-terrain vehicle traveled around 5000 m along the center of the tunnel, from gallery 17 to gallery 6. The platform moved in a straight line without significant heading variations, simplifying the location to a one-dimensional problem where x represents the longitudinal distance to the tunnel entrance. The data provided by the sensors, i.e. odometry, laser data and RSSI values, were collected using the onboard laptop.

Table 5.1a shows the absolute position of each gallery x_g^A provided by the geometrical map. These absolute positions, considered as ground truth, correspond to reference points from which the gallery patterns have been generated.

Table 5.1: Features absolute positions

(a) Galleries					
Gallery #	x_g^A (m)	Gallery #	x_g^A (m)	Gallery #	x_g^A (m)
17	51	13	1813.9	9	3365.2
16	489.5	12	2260	8	4091.5
15	1026.9	11	2702.4	7	4475.8
14	1469.2	10	3275.1	6	4841

(b) RF Minimums	
MIN #	x_m^A (m)
1	2593.4
2	3103.6
3	3613.5

It should be noted that the periodicity of the RF signal under the defined transmitter-receiver setup is observable once the near sector is crossed, i.e., from 2.1 km point. The

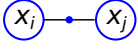
graph	node	binary edge	error
	$x_j = x_i + d_{ij}^{odom}$ $d_{ij}^{odom} = x_j^{odom} - x_i^{odom}$	$z_{ij} = d_{ij}^{odom}$ $\mathbf{\Omega}_{ij} = [\sigma_{odom_{ij}}^2]^{-1}$ $\sigma_{odom_{ij}} = f(d_{ij}^{odom})$	$e_{ij} = d_{ij}^{odom} - (x_j - x_i)$

Table 5.2: First time a new node is introduced into the graph using the odometry information.

position references of the minima x_m^A extracted from the RF map are shown in Table 5.1b. These values are obtained by applying the same strategy followed in Section 3.3.1 to the theoretical model of the RF signal.

During the route of the vehicle there will be areas where the graph-based approach will only incorporate information from the galleries, while there will be other areas where both the galleries and the RF signal minima coexist and thus the data provided by the detection of both features will be introduced into the graph.

5.4.2 Algorithm implementation

As previously mentioned, the nodes are added to the graph at regular intervals corresponding to the distance traveled by the platform. The selected interval is 40 m which is adequate to fulfill a twofold purpose: on the one hand, it provides enough discretization of the total distance traveled (in the range of km) avoiding the complexity of a more dense graph. On the other hand, sufficient resolution is ensured between tunnel features detection. The constraints between two consecutive nodes ($\mathbf{x}_i, \mathbf{x}_j$) are modeled with *binary* edges $\langle \mathbf{z}_{ij}, \mathbf{\Omega}_{ij} \rangle$ using the relative position between them provided by the odometry as the measurement, $\mathbf{z}_{ij} = (x_j^{odom} - x_i^{odom})$, and the odometry uncertainty $\sigma_{odom_{ij}}$ for the information matrix $\mathbf{\Omega}_{ij} = [\sigma_{odom_{ij}}^2]^{-1}$. The uncertainty is scaled by the traveled distance from node i to node j . Table 5.2 shows the equations involved the first time a new regular node \mathbf{x}_j is introduced into the graph with the labeling of the binary edge. The formulation used to compute the error at each iteration is also detailed.

The two detection processes run concurrently in real time, waiting for an occurrence of a minimum or gallery event. If a minimum is detected at time T , a new node \mathbf{x}_m is introduced into the graph using the mechanism described in Section 5.3.1. First, the odometry robot position corresponding to the minimum occurrence (x_m^{odom}) is used to create *binary* edges with \mathbf{x}_i and \mathbf{x}_j as previously described. The position reference of the minimum (x_m^A) provided by the RF map is considered as the measurement \mathbf{z}_m and it is included as a global information with a *unary* edge associated to this new minimum node, being $\mathbf{\Omega}_m = [\sigma_m^2]^{-1}$ the information matrix. σ_m corresponds to the uncertainty of the measurement provided by the RF map. Table 5.3 summarizes the process when a new minimum node is introduced into the graph for the first time with the unary edge and the error computation.

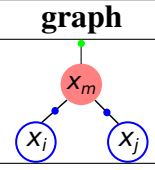
graph	node	unary edge	error
	$x_m = x_i + d_{im}^{odom}$ $d_{im}^{odom} = x_m^{odom} - x_i^{odom}$	$z_m = x_m^A$ $\Omega_m = [\sigma_m^2]^{-1}$	$e_m = x_m^A - x_m$

Table 5.3: First time a new minimum node is introduced into the graph.

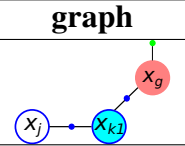
graph	node	binary edge	unary edge	error
	$x_g = x_{k_1} + d_{k_1g}$	$z_{k_1g} = d_{k_1g}$ $\Omega_{k_1g} = [\sigma_{k_1g}^2]^{-1}$	$z_g = x_g^A$ $\Omega_g = [\sigma_g^2]^{-1}$	$e_{k_1g} = d_{k_1g} - (x_g - x_{k_1})$ $e_g = x_g^A - x_g$

Table 5.4: First time a new gallery node is introduced into the graph.

Similarly, when a gallery is detected for the first time, a new node \mathbf{x}_{k_1} corresponding to the estimated robot position from which the gallery is observed is added to the graph using the odometry position ($x_{k_1}^{odom}$). A *binary* edge $\langle \mathbf{z}_{jk_1}, \Omega_{jk_1} \rangle$ is created between the previous node j and the new one using the same mechanism previously described in Table 5.2. At the same timestamp, a node representing the position of the gallery \mathbf{x}_g is also incorporated to the graph. The constraint between the \mathbf{x}_{k_1} and the gallery node \mathbf{x}_g is modeled by a *binary* edge $\langle \mathbf{z}_{k_1g}, \Omega_{k_1g} \rangle$ using the information provided by the gallery detector: the relative distance d_{k_1g} between them as the measurement \mathbf{z}_{k_1g} , and the detection uncertainty (σ_{k_1g}) for the information matrix Ω_{k_1g} . Lastly, the absolute position of the gallery in the tunnel (x_g^A) is introduced to the graph as a global measurement \mathbf{z}_g by means of a *unary* edge $\langle \mathbf{z}_g, \Omega_g \rangle$ associated to the gallery node. Since the gallery global position is obtained from the geometrical map of the tunnel, it is considered as ground truth being selected a very low value for the uncertainty of the unary edge ($\sigma_g = 10^{-4}$). Each time the gallery is detected from a new position, a new node \mathbf{x}_{k_i} is incorporated to the graph by encoding the constraints with the previous node ($\mathbf{x}_{k_{i-1}}$) and the gallery node (\mathbf{x}_g) by means of two binary edges as just described. Once the gallery is no longer detected because the vehicle has passed through the gallery area, the next gallery pattern is loaded waiting for the next detection. Table 5.4 shows the equations of the nodes and edges involved when a gallery is detected for the first time, along with the corresponding formulation to compute the errors.

Each time a new node or measurement is added to the graph, the optimization process takes place. The goal of this process is to find the assignment of poses to the nodes of the graph which minimizes the sum of the errors introduced by the measurements. The bigger the information matrix (Ω_{ij}, Ω_i) the more the edge matters in the optimization. In our case, the measurements associated to the minimum and gallery nodes have the less uncertainty as they are observations from the maps. Therefore, they play the

role of "anchors" in the pose-graph. The least square optimization process has been implemented in Matlab following the formulation of [Kümmerle et al., 2011].

Our approach guarantees continuous robot localization by accumulating the odometry data to the last estimated robot position in the graph even in those areas where the nodes separation is large in the graph (when nor gallery neither RF minimum is detected).

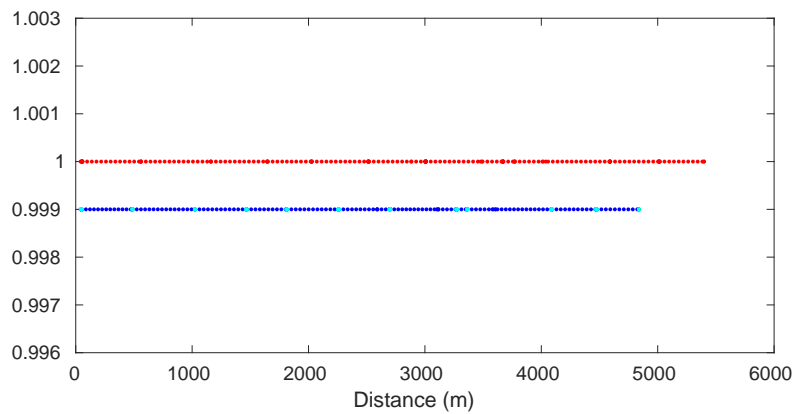
5.4.3 Graph-based localization results

The pose-graph is continuously generated during the displacement of the vehicle along the Somport tunnel, incorporating the information provided by the odometry, the RF minima detection and the gallery detection. Fig. 5.4a shows the resulting graph with all the sources of information before (red) and after the optimization (blue). It is clearly seen how the positions of the vehicle represented by the nodes, which have an evident forward odometry drift, are corrected after the optimization. As previously mentioned, the criteria to add the trajectory nodes at regular intervals in order to maintain a sparse graph, changes in case of a gallery detection, being a node added from each vehicle position from which the gallery is observed. This situation is represented in Figs. 5.4b and 5.4c for gallery 17 where it is observed how the graph density increases in those areas providing bigger discretization. In a similar way, when a RF minimum is detected, a node is incorporated at the position where the minimum occurred.

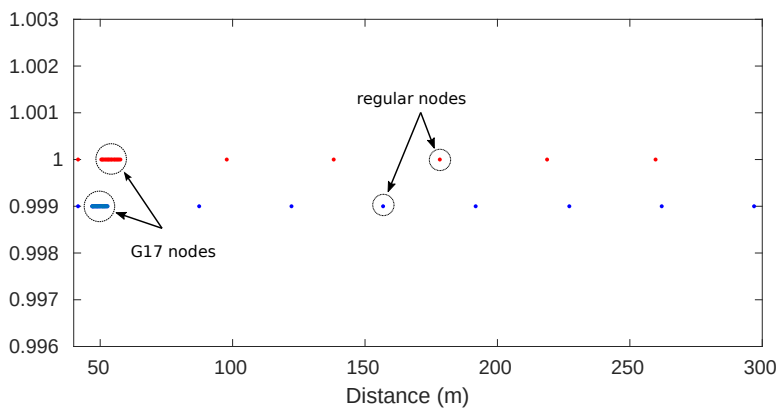
The resulting pose graph corresponding to the entire displacement of the vehicle consists of 223 nodes and 306 edges. The total number of nodes includes 3 nodes which represent the positions of the vehicle corresponding to RF minimum occurrences, 12 nodes which represent the position of the galleries present in the Somport tunnel, 81 nodes from which any of the galleries are detected and 127 regular nodes. Table 5.5 summarize these figures. The total quantity of edges includes unary edges encoding absolute positions related to minimums and gallery nodes (3 and 12) and binary edges, which represents relative constraints between nodes and gallery nodes (81) and between regular nodes (210). Table 5.6 shows the edges classification.

Table 5.5: Resulting pose-graph nodes

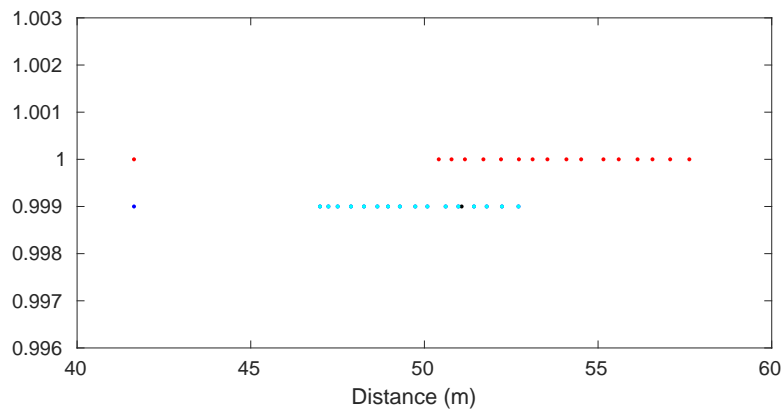
Nodes	Qty.
Minimum nodes	3
Gallery nodes	12
Nodes with gallery detection	81
Sparse regular nodes	127
Total	223



(a) Graph before and after optimization



(b) Gallery 17 detection



(c) Nodes corresponding to gallery 17

Figure 5.4: Node graph with RF minimums and galleries detection. (a) Complete node graph before (red) and after (blue) optimization. The y axis values have been set only for visualization purposes to avoid the overlapping of both graphs. (b) Area of the node graph showing the nodes incorporated during the gallery 17 detection join together with regular nodes before and after the gallery detection. (c) Detail corresponding to the nodes representing the vehicle position from which gallery 17 is detected (cyan). The node corresponding to the gallery position is represented in black.

Table 5.6: Resulting pose-graph edges

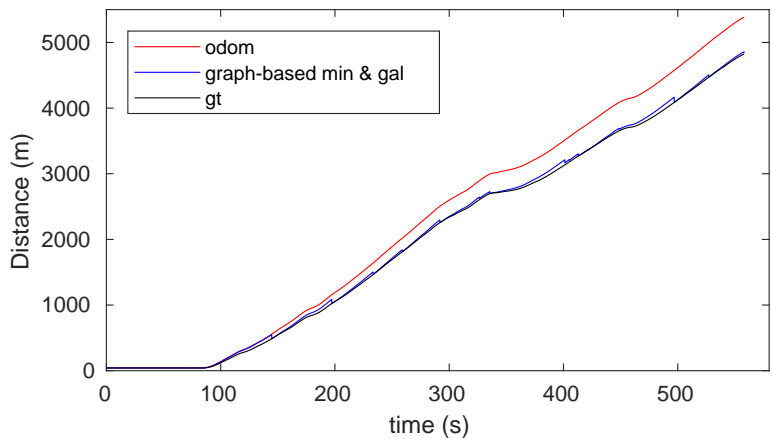
Edges	Qty.
<i>Unary</i> edges associated to minimum nodes	3
<i>Unary</i> edges associated to gallery nodes	12
<i>Binary</i> edges from nodes to galleries	81
<i>Binary</i> edges between sparse regular nodes	210
Total	306

The results of our pose-graph localization approach are represented in Fig. 5.5. Fig. 5.5a shows the pose estimation of the vehicle during the continuous localization process in comparison with the pose estimation using only the odometry information. The position is corrected with each RF minimum or gallery detection, as can be clearly seen in detail in Fig. 5.5b. As a consequence of the optimization process, the localization error accumulated during the movement of the vehicle is reset each time a discrete feature providing absolute position is detected, as shown in Fig. 5.5c.

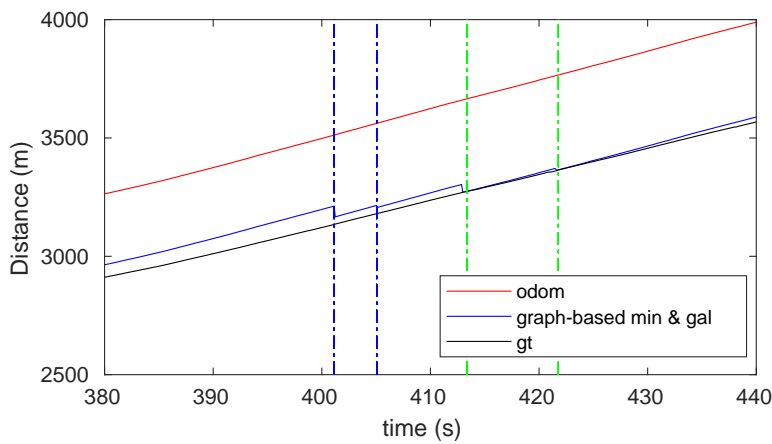
One of the main benefits of the proposed approach is the ability, not only to online correct the error position during the displacement of the vehicle, but also to modify the location of some specific features observed during the vehicle trajectory once the service routine is complete. Fig. 5.6 shows the results when the position and the error are calculated once the tunnel has been traversed, i.e. when the optimization process takes place with all the information included in the graph at the end of the travel. Fig. 5.6a shows how the estimated position obtained through our proposed method follows closely the real position of the vehicle whereas the purely odometry-based estimation moves away. The position error along the tunnel remains bounded under very acceptable values in comparison with the resulting error using only the odometry information which increases along the time as shown in Fig. 5.6b. It is worthy to notice that the error graph is greatly flattened with respect to the online case, showing the strengths of the method for inspection applications.

5.4.4 Graph-based localization performance evaluation

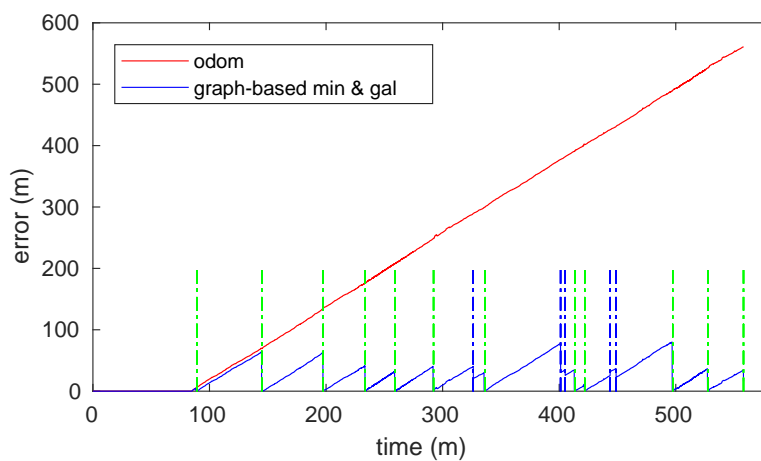
In order to compare the performance of the graph-based localization approach using different sources of information, we use the metric proposed in [Kümmerle et al., 2009b]. The graph accuracy is not based in the calculation of the absolute error among poses but in the creation of a graph consisting of virtual edges created by using the ground-truth measurements evaluated in the estimated pose of the nodes. This well-known technique is commonly used to compare SLAM approaches that use different estimation techniques or different sensor modalities since all computations are made based on the corrected trajectory of the robot.



(a) Pose estimation

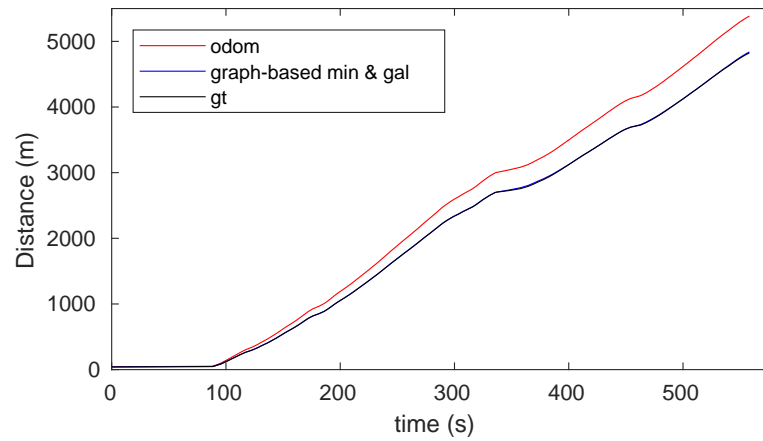


(b) Minima and galleries detection

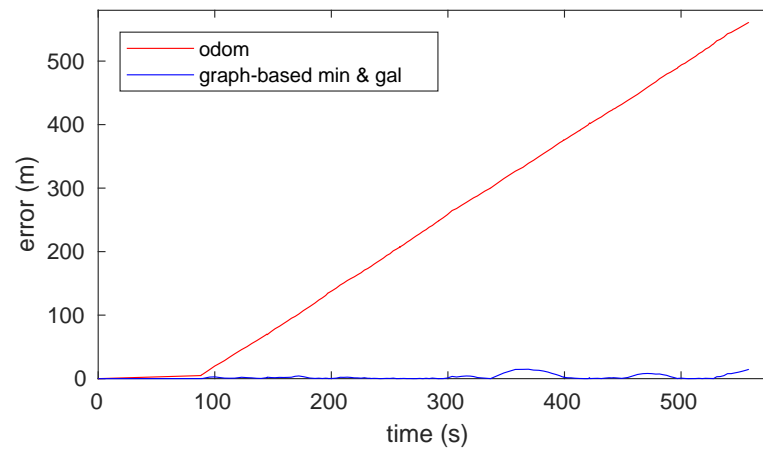


(c) Error pose

Figure 5.5: Results of the online pose-graph localization approach. (a) Estimated position along the tunnel provided by the odometry (red) and our proposed approach (blue) in comparison with the ground truth (black). (b) Detail of the estimated positions corresponding to the time slot when a RF minimum (dashed blue lines) and two galleries (dashed green lines) are detected. The position is corrected with each detection. (c) Position error during the displacement of the vehicle.



(a) Pose estimation



(b) Error pose

Figure 5.6: Results of the pose-graph approach after the service routine of the vehicle.

Table 5.7 shows a comparison of the overall mean χ^2 error per edge during the localization process using different sources of information.

Table 5.7: Graph accuracy analysis

Source of data	χ^2
Only odom	12.87
Minima and odom	4.20
Galleries and odom	1.23
Minima, galleries and odom	1.15

As expected, using the most information sources during the localization process, i.e, minima and galleries position as absolute measurements and odometry data as relative measurements, yields the best result in terms of accuracy. When using only the galleries and the odometry, the result is also good and better than using only the minima and odometry, mainly because the galleries are distributed all along the tunnel, whereas the minimums are detected only in a certain area. The biggest mean error is obtained when only the odometry data is introduced to the graph.

5.5 Concluding remarks

In addition to the considerations already mentioned in Section 3.6 there are other aspects resulting from the proposed graph-based approach that are worth highlighting, such as the following:

- Each of the detected features provided by the tunnel are involved in the localization algorithm during the displacement of the vehicle. Along the tunnel three different scenarios can be found depending on the coexisting measurements : only with odometry data, odometry and absolute gallery position during the first kilometers and with all the measurements including the galleries position when the far sector is reached.
- The accuracy and resolution of the method depends on the sources of information available for the localization.
- In order to check the performance of the method, the resultant graphs from a batch of tests using different sources of information were recorded and subsequently modified replacing the edges involved with the ground-truth measurements. The resulting graph were exported to a g2o compatible format. Lastly, the g2o¹ library was used for the graph optimization and the χ^2 calculations.

¹g2o-General Graph Optimization <https://github.com/RainerKuemmerle/g2o>

- The proposed method does not require infrastructure modifications, being only needed to place an RF transmitter in the tunnel as the simplest configuration.

5.6 Summary

Along the second part of the thesis, we have presented a graph-based localization approach for tunnel-like environments using different sources of information: the odometry data, the absolute positions provided by an RF signal minima detector based on a theoretical fadings model that acts as an RF map, and the absolute position provided by a gallery detector.

Different strategies have been developed to incorporate the data provided by the detectors to the graph. On the one hand, the information from the past corresponding to the RF minimums is introduced by revisiting the nodes stored in the graph and modifying the existing edges. On the other hand, the discretization of the graph is increased adding the data of all the robot positions from which the galleries are detected. In both cases, unary constraints are associated to the detected feature – RF minima and galleries – using the position references obtained from the RF map and the geometric map.

The feasibility of the proposed approach has been validated with the data collected during an experimental campaign developed in a real tunnel scenario. The empirical results demonstrate the validity of all the processes involved in the localization during the displacement of the vehicle.

Besides the good performance of the detection methods already demonstrated in the previous chapter, the results shows that the implemented approach allows the online correction of the localization error each time a new absolute measurement is added. This error is further reduced if the optimization process is executed once the tunnel has been traversed and hence with all the information incorporated to the graph. As a consequence, it is possible to accurately locate features of interest observed during an inspection task in a service routine for example.

A performance evaluation of the graph has also been developed which provides the expected results in terms of localization accuracy depending on the sources information used during the process.

In view of the above, we can say that our approach has a number of advantages over other methods addressed in the literature, usually probabilistic methods based on filters, to solve the localization in tunnels:

- It allows to easily incorporate different sources of information. In the tunnel case, the method takes advantage of the features present in this type of environment: structural as in the case of the galleries and the RF periodic signal fadings.
- It allows to keep track of the history of the robot positions and revert from wrong decisions produced during the estimation process such as the integration of wrong

measurements. Because of this, it is also possible to incorporate information from the past that has influence on the present.

- This solution can be extrapolated to other types of environments of this type, pipes, sewers and even mines, selecting the most appropriate sources in each case (e.g. results of a scan-matching process in case of more texturized environment).

To the best of our knowledge, the application of the graph-based solution has not been previously explored to solve the localization in this type of environment, constituting therefore a novel work in the context of localization in tunnel-like environment.

Chapter 6

Conclusions

6.1 Conclusions

In this thesis, we have presented several contributions to the field of robot localization in tunnel-like environments. Our goal was to overcome the main difficulties present in these type of scenarios that make obtaining an accurate localization a challenge. We addressed the problem by means of an alternative RF approach that benefits from the periodic nature of the radio signal in two of the most common tunnel-like environments: pipes and tunnels. Going one step further, we have also presented a graph-based global solution that tries to take advantage of different sources of information present in tunnels.

First of all, we faced the problem of robot localization in metallic pipes. In **Chapter 2**, we developed a robot localization method using a particle filter which takes advantage of the periodicity nature of spatial RF signals fadings that appears inside pipes under certain settings. The fadings waveform and its period can be calculated in advance using the modal theory, playing the theoretical model the role of an RF map. The actual RF signal provided by the sensor and the RF map are used during the weighting step of the particle filter. The algorithm was validated using the data collected during some experiments conducted in the Santa Ana dam pipe with a ground robot. The proposed localization method was able to provide accurate continuous localization during the displacement of the robot along the pipe. Building on these promising results, we implemented an EKF-based solution following the same strategy and we compared both results. The applicability of the solution to other types of robotic platforms was also demonstrated by using the IMU sensor during the prediction step. Finally, in this chapter, an evolved version of the previous method was presented, exploiting the transversal structure of the fadings. The use of two RF receivers placed at defined positions on the robot, provides a 180 phase difference between the RF signals. The proposed approach consists of fusing with an EKF algorithm the information provided by two particle filters, working each

of them with an RF signal and its corresponding RF map. This method using two radio frequency signals, also validated in the real scenario, yielded improvements in terms of error, robustness and accuracy over the single-signal solution.

The periodic fading phenomena, with some peculiar characteristics, is also evident in tunnels, so, we addressed the localization in these scenarios following a similar technique through **Chapter 3**. In this case, an RF-based discrete localization method was designed and implemented. This approach consists in identifying the minimums of the RF signal during the displacement of the robot and subsequently matching these features with the minimums of the theoretical propagation model acting as an RF map. Two strategies are combined to accomplish both tasks: the RLS algorithm for the identification process, and the Mahalanobis distance with the individual compatibility test for the matching. The algorithm was validated with data from a campaign of experiments carried out in the Somport tunnel using an all-terrain equipped vehicle. The results showed how the robot position is periodically adjusted with the position reference provided by the map, resetting the error accumulated by the odometry.

Up to this point, we saw how the periodic structure of the RF signal, together with the RF signal model, provides useful information that can be fused with the odometry data to improve the localization in pipes and tunnels. However, the complexity of the fading structure in the tunnel case, makes even more challenging to obtain a continuous localization in these environments. This motivated us to take a step beyond and propose a new approach based on graphs, taking advantage not only of the periodic signal of the fadings, but also of the structural characteristics mandatory present in tunnels. The alternative method models the localization problem as a pose-graph optimization problem, where we introduce relevant discrete features detected during the displacement of the robot. The methods for the discrete features detection have been presented in **Chapter 4**. First, a geometrical-based matching technique was developed to identify the RF minimums of the signal, obtaining their absolute position from the RF map. Secondly, a scan-pattern method was implemented to detect and identify structural features of the tunnel. The experimental scenario was again the Somport tunnel which contains emergency galleries at known positions. Both detection methods provide the absolute measurements to be introduced in the pose-graph.

The alternative pose-graph approach have been thoroughly explained in **Chapter 5**. The robot trajectory is modeled by a graph, where the nodes represent the estimated position of the robot and the edges encode the constraints among them, using the relative measurements provided by the odometry (*binary*) and the absolute measurements coming from the discrete features detection (*unary*). All the formulation regarding the graph construction and the mechanisms implemented to introduce the position of the discrete features as prior information were described. Again, the terrain-vehicle was used for the experiments in the Somport tunnel. The results showed the efficiency and robustness of the RF minima and galleries detection methods, being identified all of

them during the displacement of the vehicle. In addition, the graph was able to deal with information from the past and cope with false positives. It was also demonstrated that the localization error is corrected after the optimization process each time a discrete feature is detected. The error is highly reduced when the graph is optimized once completed after the service routine, being able to accurately locate points of interest during inspection tasks. A performance evaluation was developed to analyze the accuracy of the graph depending on the sources involved during the process. As expected, the more incorporated sources, the better localization accuracy. As a summary, the applicability and adequacy of the graph-based approach to solve the localization in tunnel-like environments have been proven, providing some advantages with respect to classical solutions, such as easily involve different sources of information, introduce information from the past and even correct from wrong decisions.

6.2 Future Work

This thesis presents promising approaches focused on obtaining accurate localization in tunnel-like environments. However, there is still work to be done. On the one hand, to improve the accuracy and robustness provided by the proposed methods, and on the other hand, to address other tasks taking as a starting point the results obtained with these approaches. In this context, this section points out some possible future developments.

All the methods have been experimentally tested with ground robots. The use of flying robots would provide flexibility to cover difficult access areas as the tilted parts of pipes. To implement in a drone the continuous solution based on particle filters, presented in **Chapter 2**, using the information from the IMU and the RF sensors, would be a task to work on.

Another area of improvement would be to exploit the transversal structure of the fadings in tunnel scenarios. Similarly to pipes, it is possible to obtain a 180 degree phase difference between two RF receivers placed at specific locations in the platform. Taking advantage of this, both the discrete (**Chapter 3**) and the graph-based (**Chapter 5**) solution for tunnels would be improved in terms of accuracy.

The alternative RF-based localization approaches require a minimum setup to obtain the periodic fadings. The RF transmitter has to be placed with precision at a known position in the tunnel in order to estimate in advance the position of the fadings and then be able to match the real signal with the RF map. In order to relax this requirement, a SLAM strategy applied to RF could be implemented being the RF minima detected incorporated to the graph each time it is observed from different positions. In this case, the constraints would be modeled as binary edges instead of using unary edges with the position reference provided by the RF map. In this way, the RF minimums would be detected and "mapped" online and then it would be enough to place the transmitter at

any longitudinal position in the tunnel, fulfilling the requirements of orientation, height and distance to the wall of the transmitting antenna to obtain the periodic fadings.

One of the major challenges in tunnels is the noisy nature of the RF signal which makes unfeasible the continuous localization solution based on particle filters presented in **Chapter 2**, due to the disparities between the real signal and the theoretical model. One potential solution could be to refine the RF map with each trip of the platform in the tunnel. The idea to be implemented would be to use the real signal of the first trip as an RF map for the next trip and so on, in a kind of RF-learning process.

The pose-graph localization method presented in this thesis tries to maintain a sparse graph to handle it in an efficient way. However, even with distances between nodes in order of tens of meters, the optimization of the whole graph each time a node is added, could not guarantee a real-time performance in the case of long-distance tunnels. One enhancement aspect of the algorithm would be to prune the graph, working only with a sub-graph that includes a sequence of recent nodes. The optimization process would be applied only to the sub-graph, improving the efficiency of the solution.

Chapter 7

Conclusiones

7.1 Conclusiones

En esta tesis hemos presentado varias contribuciones en el campo de la localización de robots en entornos tipo túnel. Nuestro objetivo era superar las principales dificultades que aparecen en estos escenarios que hacen que obtener una localización precisa suponga todo un reto. Hemos abordado el problema de la localización mediante un enfoque alternativo que se beneficia de la naturaleza periódica de la señal radio en dos de los entornos más comunes tipo túnel: tuberías y túneles. Yendo un paso más allá, también hemos presentado una solución global basada en grafos que intenta aprovechar todas las fuentes de información presentes en los túneles.

En primer lugar, afrontamos el problema de la localización en tuberías metálicas. En el **Capítulo 2**, desarrollamos un sistema de localización para el robot usando un filtro de partículas. El método se beneficia de la naturaleza periódica de los desvanecimientos (o fadings) que aparecen en este tipo de tuberías bajo ciertas configuraciones. Aplicando la teoría modal, es posible calcular con antelación la forma de onda y el periodo de los fadings, obteniéndose un modelo teórico que juega el papel de un mapa de RF. La señal RF real proporcionada por el sensor radio y el mapa de RF se utilizan durante la etapa de pesado (weighting) del filtro de partículas. El algoritmo fué validado utilizando los datos recogidos durante una serie de experimentos llevados a cabo en la tubería de Santa Ana utilizando un robot terrestre. El método propuesto de localización fue capaz de proporcionar localización continua precisa durante el desplazamiento del robot a lo largo de la tubería. Partiendo de estos prometedores resultados, implementamos un solución basada en EKF siguiendo la misma estrategia y llevamos a cabo una comparativa de los resultados proporcionados por ambos métodos. La aplicabilidad de esta solución a otro tipo de plataformas robóticas fue también demostrada por medio de la utilización de la IMU durante la etapa de predicción. Finalmente, en este capítulo, se presentó una versión evolucionada del método anterior que explotaba la estructura

transversal de los fadings. El uso de dos sensores radio ubicados en determinadas posiciones del robot, proporciona una diferencia de fase de 180 grados entre las dos señales. La aproximación propuesta consiste en fusionar mediante un algoritmo EKF, la información proporcionada por dos filtros de partículas, cada uno trabajando con una señal radio y su correspondiente mapa RF. Este método utilizando dos señales radio fue igualmente validado en el escenario real, proporcionando mejoras en términos de error, robustez y precisión con respecto a la solución basada en una sola señal.

El fenómeno de los fadings periódicos, con alguna característica peculiar, es también evidente en túneles, así que, a lo largo del **Capítulo 3**, abordamos la localización en este tipo de escenario siguiendo una estrategia similar. En este caso se diseñó e implementó un sistema de localización discreto basado en la señal RF. Esta aproximación consiste en identificar los mínimos de la señal radio durante el desplazamiento del robot y emparejar estas características con los mínimos del modelo teórico de propagación radio que actúa como un mapa RF. Para llevar a cabo ambas tareas se combinan dos estrategias: el algoritmo RLS para el proceso de identificación, y la distancia de Mahalanobis con el test de compatibilidad individual para el emparejamiento. El algoritmo fue validado con los datos obtenidos durante una campaña de experimentos realizados en el túnel de Somport, utilizando un vehículo todo terreno equipado con los diferentes sensores. Los resultados mostraron cómo la posición del robot se ajusta periódicamente con la referencia de posición proporcionada por el mapa RF, reseteando el error acumulado por la odometría.

Hasta ese punto, vimos como la estructura periódica de la señal radio, junto con el modelo teórico, proporcionan información útil que puede ser fusionada con los datos de odometría para mejorar la localización en túneles y tuberías. Sin embargo, la complejidad de la estructura de los fadings en el caso del túnel, hace que sea aún más difícil obtener una localización continua en estos entornos. Esto nos motivó a dar un paso más y proponer un nuevo enfoque basado en grafos aprovechando no sólo la señal periódica de los fadings, sino también las características estructurales obligatoriamente presentes en los túneles. El método alternativo modela el problema de la localización como un problema de optimización de grafos (pose-graph), donde introducimos las características discretas relevantes detectadas durante el desplazamiento del robot. En el **Capítulo 4** se han presentado los métodos para la detección de características discretas. En primer lugar, se desarrolló una técnica basada en emparejamiento geométrico entre la señal real y el modelo teórico para identificar los mínimos de la señal y obtener su posición absoluta a partir del mapa RF. En segundo lugar, se implementó un método basado en patrones para detectar e identificar las características estructurales del túnel, en este caso las galerías. El escenario experimental fue de nuevo el túnel de Somport, que dispone de galerías de emergencia cuyas posiciones son conocidas. Ambos métodos de detección proporcionan las medidas absolutas que se introducirán en el grafo.

El enfoque alternativo basado en grafos se ha explicado detalladamente en el **Capí-**

tulo 5. La trayectoria del robot es modelada mediante un grafo donde los nodos representan la posición estimada del robot y las aristas codifican las restricciones entre ellos, usando las medidas relativas proporcionadas por la odometría (*bynary*) y las medidas absolutas provenientes de la detección de características discretas (*unary*). Se describió toda la formulación relativa a la construcción del grafo y los mecanismos implementados para incorporar la posición de las características discretas como información previamente conocida. Nuevamente se utilizó el vehículo todo terreno para los experimentos en el túnel de Somport. Los resultados mostraron la eficiencia y la robustez de los métodos de detección de los mínimos de la señal radio y de las galerías, siendo identificados todos ellos durante el desplazamiento del vehículo. Además, el grafo fue capaz de manejar información del pasado y hacer frente a los falsos positivos. También se demostró que el error de localización se corrige después del proceso de optimización cada vez que se detecta una característica discreta. El error se reduce en gran medida cuando el grafo se optimiza una vez construido en su totalidad, por ejemplo después de una rutina de servicio, pudiéndose localizar con precisión los puntos de interés durante las tareas de inspección. Se ha desarrollado una evaluación del rendimiento para analizar la precisión del grafo en función de las fuentes de información involucradas durante el proceso. Como era de esperar, cuantas más fuentes se incorporan, mayor precisión de localización. En resumen, se ha demostrado la aplicabilidad y adecuación del enfoque basado en grafos para resolver la localización en entornos tipo túnel, lo que ofrece algunas ventajas con respecto a las soluciones clásicas, tales como añadir fácilmente diferentes fuentes de información, introducir información del pasado e incluso recuperarse de decisiones erróneas.

7.2 Trabajo futuro

Esta tesis presenta una serie de prometedoras aproximaciones enfocadas a obtener una localización precisa en entornos tipo túnel. Sin embargo, todavía hay trabajo por hacer. Por un lado, mejorar la precisión y robustez proporcionada por los métodos propuestos y por otro, abordar otra serie de tareas tomando como punto de partida los resultados obtenidos con las soluciones presentadas. En relación a esto, esta sección nombra algunas de los posibles desarrollos futuros.

Todos los métodos han sido validados experimentalmente utilizando robots terrestres. El uso de robots aéreos (drones) proporcionaría mayor flexibilidad a la hora de poder acceder a las partes inclinadas de la tubería. Se propone como acción futura por tanto, la implementación sobre un dron de la solución basada en filtro de partículas, presentada en el **Capítulo 2**, utilizando la IMU y los receptores radio.

Otra área de mejora sería el explotar la estructura transversal de los fadings en el túnel. De la misma forma que ocurre en las tuberías, es posible obtener una diferencia de fase de 180 grados entre la señales proporcionadas por dos receptores radio ubicados

en posiciones concretas de la plataforma. Aprovechando esto, tanto la solución discreta (**Capítulo 3**) como la solución basada en grafos (**Capítulo 5**) para la localización en túneles se vería mejorada en términos de precisión.

Los métodos de localización basados en la señal radio requieren una cierta configuración inicial para obtener los fadings periódicos. El transmisor de la señal radio se tiene que colocar con precisión en una posición conocida del túnel para poder estimar con anterioridad la posición de los fadings. Con el fin de relajar este requisito, se podría llevar a cabo un proceso de SLAM aplicado a la señal RF, de forma que el mínimo que se detecta se incorpore al grafo desde las diferentes posiciones desde las cuales es observado. En este caso, las restricciones se modelarían mediante enlaces binarios en vez de utilizar enlaces unarios con la posición de referencia proporcionada por el mapa. De esta forma, los mínimos de la señal serían detectados y "mapeados" sobre la marcha. Esto nos permitiría colocar el transmisor radio en cualquier posición longitudinal del túnel, respetando los requisitos de orientación, altura y distancia a la pared de la antena emisora para obtener los fadings periódicos.

Una de las principales dificultades que aparecen en los túneles es la naturaleza ruidosa de la señal radio. Debido a la disparidad existente entre la señal real y el modelo teórico, es inviable aplicar la localización continua basada en filtro de partículas presentada en el **Capítulo 2**. Una posible solución sería la de refinar el mapa RF con cada uno de los viajes de la plataforma a lo largo del túnel. La idea a implementar sería usar la señal real del primer viaje como mapa RF para el siguiente viaje, y así sucesivamente en una especie de proceso de aprendizaje RF.

El método de localización basado en grafos presentado en esta tesis intenta mantener un grafo disperso con el fin de poder manejarlo de una forma eficiente. Sin embargo, incluso con distancias entre nodos del orden de decenas de metros, el tiempo de proceso que consume la optimización de todo el grafo podría no garantizar tiempo real en caso de túneles muy largos. Un aspecto de mejora del algoritmo sería podar el grafo y trabajar únicamente con un sub-grafo que incluyese los nodos más recientes. El proceso de optimización se aplicaría únicamente al sub-grafo, mejorándose así la eficiencia de la solución.

Appendix A

Experiments

The experiments conducted to validate the proposed approaches were performed in different real scenarios using the robotic platforms from University of Zaragoza and ITAINNOVA. This appendix describes the main actors involved during the experimental stage.

A.1 Robotic Platforms

A.1.1 Pioneer 3-AT

The Pioneer 3-AT robot ([Pioneer,]) was used during the experiments in the Santa Ana dam pipe as the mobile platform. Pioneer 3-AT is a small four-wheel, four-motor skid-steer robot. In addition to the built-in two wheel encoders that provides the odometry data, it was equipped with a Xsens MTi 100 IMU, a SICK LMS200 long-range laser sensor and two portable spectrum analyzers, RF Explorer model 3G ([RFExplorer,]), as RF receivers. The data provided by the sensors is collected by a Dell D360 laptop using ROS (Fig. A.1).

A.1.2 All-terrain Vehicle

Once of the vehicles used as mobile robotic platform for the tunnel experiments was a Galloper 4x4 all-terrain vehicle. It allows to travel the long distances corresponding to the Somport tunnel at major speeds, making it feasible to perform multiple experiments. The vehicle was driven by a human operator collecting the data provided by the sensors placed in the vehicle.

For all the experiments, the platform was equipped with two SICK DSF60 encoders of 0.036 resolution degrees assembled to the axis of the rear wheels (Fig. A.2a). A SICK LMS200 LIDAR was placed in the front part of the vehicle (Fig. A.2b).



(a)



(b)

(c)

Figure A.1: Pioneer 3-AT Robot: (a) Santa Ana pipe experiment. (b) Detail of the instrumented robot. (c) RF Explorer receiver.



(a)

(b)

Figure A.2: All-terrain vehicle: (a) wheel-encoders. (b) SICK laser sensor.



Figure A.3: All-terrain vehicle: RF sensors layouts.

Different transmitter-receivers setups were configured throughout the experimental campaigns that were developed during the thesis period. Fig. A.3 shows the RF layouts in the vehicle which correspond to the following RF receivers:

- 12 TPLINK TL-WN7200ND 2.4 GHz wireless receivers [TP-LINK,] (see Fig. A.3a).
- 3 RF Explorer model 3G (see Fig. A.3b).
- 2 ALFA AWUS036NH receivers [ALPHA-NETWORK,] (see Fig. A.3c).

A.1.3 Robucar TT

The Robucar TT robot is a four-wheel robot with individual driving motors attached to each wheel. The front and rear axles can be steered allowing the robot to move in dual drive. It is equipped with two frontal and two rear lidar SICK sensors, two in a horizontal orientation and two tilted (Fig. A.4a). The odometry data is provided by the wheel encoders and a Xsens IMU.

The platform also provides enough flexibility to assemble different RF receivers configurations as shown in Fig. A.4b.

A.1.4 Robotized Dumper

A robotized dumper (Fig. A.5c) was also used during the experimental stage in the Somport Tunnel and also in the tunnel under construction in Durango. This mobile platform consist of a conventional dumper where its original traction and steering system can be also activated using additional electrical and mechanical elements attached to the original components. This robot was the main platform used during the Autodump project.

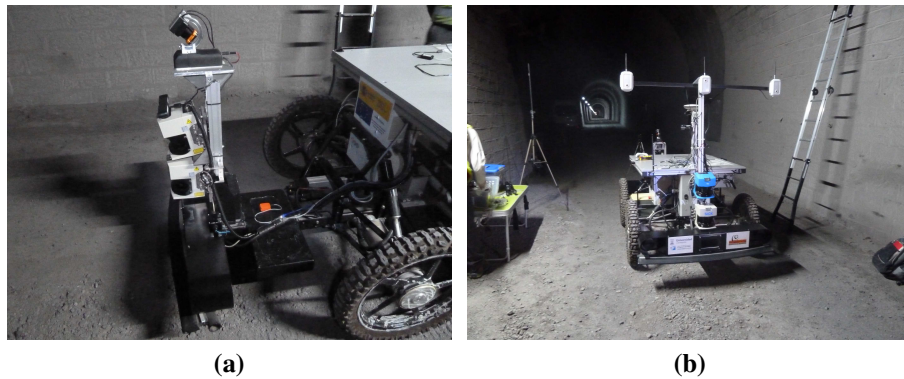


Figure A.4: Robucar TT robotic platform.

Several sensors were installed for autonomous navigation. Four rangefinder SICK sensors, two in the frontal part (Fig. A.5a) and two in the rear part which allowed forward and backward navigation. The two rangefinders on the roof of the vehicle were installed tilted, heading the floor, to scan the imperfections and irregularities of the ground. Furthermore, an Inertial Measurement Unit (IMU) was installed on the chassis of the vehicle to fulfill two tasks. On the one hand, the 3D orientation provided by this sensor was used to compensate the rangefinders information, that can be misleading when the vehicle goes through irregular terrain. On the other hand, the data generated by the IMU was fused with other sources to improve the pose estimation of the prototype. The odometry data is provided by two encoders assembled to the front wheel, and the steering angle is measured by means of two potentiometer sensors placed at the rear wheels. Regarding the RF equipment, two Alpha receivers were used, placing their antennas at the dumper roof (Fig. A.5d). An industrial computer with ROS was in charge of collecting all the sensors information needed for the localization and navigation algorithms (Fig. A.5b).

A.2 Scenarios

A.2.1 The Santa Ana Dam pipe

The Santa Ana dam pipe is located in the surroundings of Castillonroy, a region in the province of Huesca (Spain). The drainpipe is intended to provide water to the agricultural fields, transporting it from the dam over the highway (Fig. A.6). It is a 300 m long carbon steel pipe and has a diameter of 4 m. It consists of three sectors, two of them open to air and tilted 23 and 30 degrees respectively, and a 120 m straight sector where the experiments took place.

This pipe is a representative scenario since it shows most of the challenging condi-

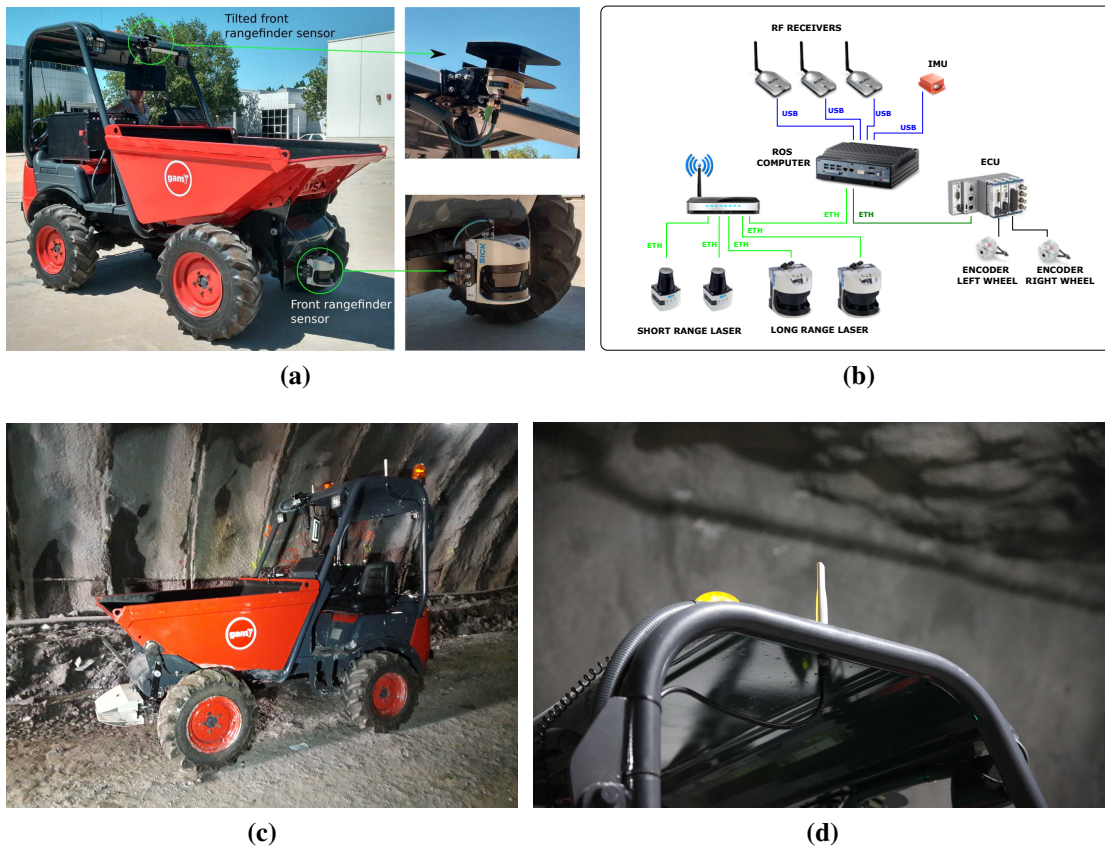


Figure A.5: The robotized dumper. Front part of the vehicle (a). Dumper hardware and communications architecture (b).

tions presented in **Chapter 2**: monotonic inner surface, lack of distinguishable features and lighting and presence of fluids on the ground. In addition, the periodic fading phenomena was previously demonstrated in this scenario making this environment very appropriate to validate the localization approaches proposed in this thesis.

The experiments were conducted during maintenance periods when the pipeline is emptied. In order to access to the straight sector, special climbing material was needed to go down to the horizontal part with the equipment (Fig. A.7). Each experimental session lasted around 12-13 hours invested in the travel, assembling of the equipment and transmitter-receiver setup, and the experiments themselves collecting the data along multiple trips (Fig. A.8).



Figure A.6: Santa Ana dam pipe.

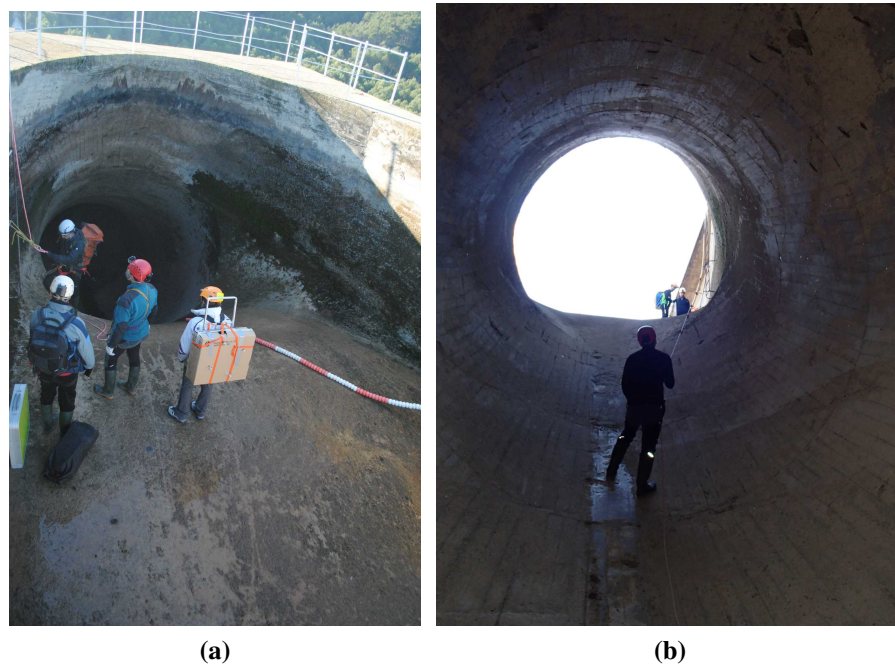


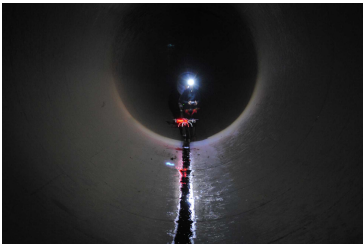
Figure A.7: Access to the Santa Ana dam pipe.



(a)



(b)



(c)

Figure A.8: Experiments in the Santa Ana dam pipe.

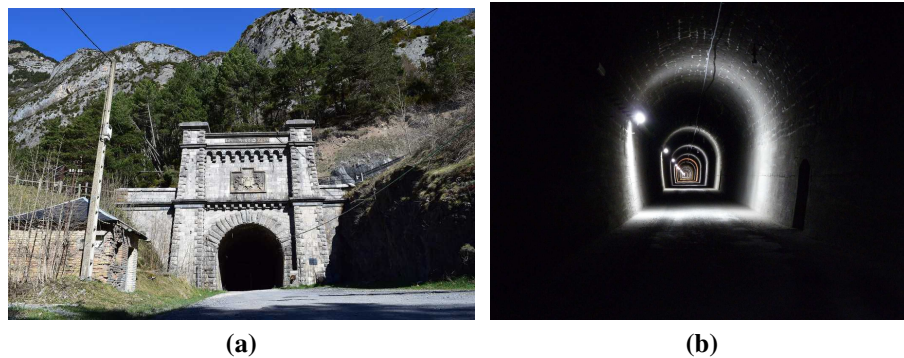


Figure A.9: Somport railway tunnel.

A.2.2 The Somport Railway Tunnel

The Somport road Tunnel located in Canfranc (Huesca) is a cross-border mono-tube tunnel between Spain and France through the central Pyrenees, situated at an altitude of 1.100 metres and with a length of 8.608 metres (two thirds on Spanish territory, and one third on French territory). The tunnel runs parallel to the out of service Somport railway tunnel (Fig. A.9a). It was previously used in the Pau - Canfranc railway line. Both tunnels are connected by 17 lateral galleries that have the function of emergency exits for the road tunnel. The railway tunnel was the scenario selected to perform the experiments.

The railway tunnel has a length of 7.7 kilometers. The tunnel is straight but suffers a change in slope at approximately 4 km from the Spanish entrance. It has a horseshoe-shape cross section (Fig. A.9b), around 5 m high and 4.65 m wide. The tunnel has small emergency shelters every 25 m. The lateral galleries are more than 100 meters long and of the same height as the tunnel. The galleries are numbered 17 to 1, from Spain to France. This tunnel is a good representative model of a common long straight tunnel and it shows the hostile conditions that makes the localization inside these environments a challenge. The periodicity of the RF signal was also demonstrated in this scenario under different transmitter-receiver configurations.

During the thesis, several measurement campaigns were carried out using different mobile platforms. Each experimental session involved the trip to the tunnel location from Zaragoza and the platform transport, which in some cases required the use of a special vehicle (Fig. A.10a).

Once arriving to the tunnel, a initial step was needed to place the RF transmitters at different locations along the tunnel (Fig. A.10b) and to finish the instrumentation of the platform assembling the sensors and the RF receivers (Figs. A.10c and A.10d). Usually, this initial setup stage lasted between two and thee hours. After that, the mobile platform travelled the planned distance multiple times collecting the information provided

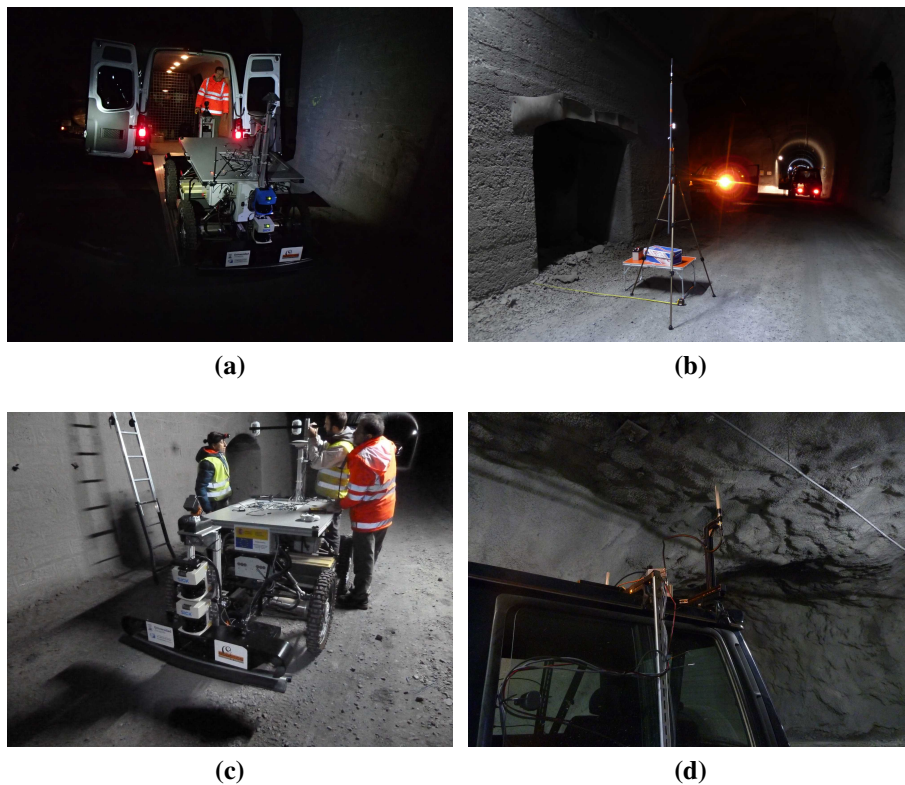


Figure A.10: Experiments preparation and setup.

by the sensors. Figs. A.11 and A.12 show the all-terrain and dumper on going experiments respectively. The total time spent inside the tunnel was approximately 7 hours. Therefore, the mean duration of an experimental day in the Somport tunnel was around 13 hours.

The data collected during the experiments in this scenario was used for the validation of the localization approaches presented in **Chapters 3, 4 and 5**.



Figure A.11: Experiments with the all-terrain vehicle.

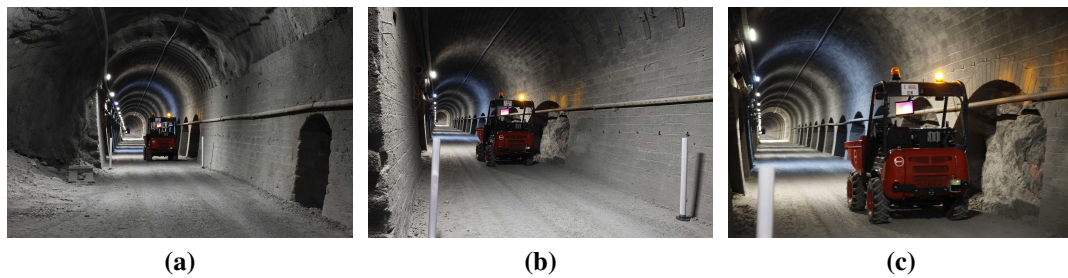


Figure A.12: Experiments with the robotized dumper.



Figure A.13: Tunnel under construction Durango-Amorebieta.

A.2.3 The under construction Tunnel Durango-Amorebieta

The last experiments were performed in the tunnel section under construction Durango-Amorebieta, belonging to the High Speed Railway Line Vitoria-Bilbao-San Sebastian located in the region of Pais Vasco (Spain). This tunnel has a total length of 1102 meters, using only the first 500 meters for the tests.

As can be seen in A.13, this environment is extremely challenging, with mud, water and potholes making the terrain extraordinarily uneven. These added difficulties increase the complexity of the localization problem.

The experiments lasted two days. The first day was mainly invested in travelling to the area and transporting the robotized dumper up to the tunnel, overcoming the difficulties of the access to the entrance and the bad weather. The setup of the experiments was performed placing the RF transmitter and preparing the dumper for the tests. A first batch of experiments were conducted. During the second day, the tunnel was traversed several times (Fig. A.14).

The approaches presented in these thesis were not validated with the data collected during these experiments due to limited time of stay for access permission issues. However, the promising results of the RF-based localization methods, with the great advan-



Figure A.14: Experiments with the robotized dumper in the tunnel under construction.

tage of reducing the odometry accumulated error in these irregular environments, lead us to consider worthy to go forward with this thesis line in the future.

A.3 Experiments

The next table shows a summary of the experiments perform during the thesis:

Table A.1: Summary of experiments

Date	Place	Mobile Platform
2014-11-07	Santa Ana dam pipe	Pioneer 3-AT
2014-12-02	Santa Ana dam pipe	Hexacopter
2016-06-30	Somport Tunnel	Robucar-TT
2017-03-31	Somport Tunnel	Robucar-TT
2017-06-06	Somport Tunnel	All-terrain vehicle
2017-10-27	Somport Tunnel	All-terrain vehicle
2017-12-01	Somport Tunnel	All-terrain vehicle
2018-02-07	Somport Tunnel	Dumper
2018-02-16	Somport Tunnel	Dumper
2018-03-01	Durango Tunnel	Dumper

A.4 The team



Figure A.15: The team during the experiments.



Figure A.16: Autodump project team.

Bibliography

- [Al-Masri et al., 2018] Al-Masri, W., Abdel-Hafez, M., and Jaradat, M. (2018). Inertial navigation system of pipeline inspection gauge. *IEEE Transactions on Control Systems Technology*, PP:1–8. (Cited on page 12.)
- [Alarifi et al., 2016] Alarifi, A., Al-Salman, A. S., Alsaleh, M., Alnafessah, A., Alhadhrami, S., Al-Ammar, M. A., and Al-Khalifa, H. S. (2016). Ultra wideband indoor positioning technologies: Analysis and recent advances †. In *Sensors*. (Cited on page 14.)
- [Alejo et al., 2017] Alejo, D., Caballero, F., and Merino, L. (2017). RGBD-based robot localization in sewer networks. In *Intelligent Robots and Systems (IROS), 2017 IEEE/RSJ International Conference on*, pages 4070–4076. (Cited on page 12.)
- [Alejo et al., 2019] Alejo, D., Caballero, F., and Merino, L. (2019). A robust localization system for inspection robots in sewer networks. *Sensors*, 19:4946. (Cited on page 74.)
- [ALPHA-NETWORK,] ALPHA-NETWORK. Awus036nh https://www.alfa.com.tw/products_detail/8.htm. (Cited on page 121.)
- [Aulinas et al., 2008] Aulinas, J., Petillot, Y., Salvi, J., and Llado, X. (2008). The slam problem: a survey. volume 184, pages 363–371. (Cited on page 91.)
- [Bakambu, 2006] Bakambu, J. N. (2006). Integrated autonomous system for exploration and navigation in underground mines. In *2006 IEEE/RSJ International Conference on Intelligent Robots and Systems*, pages 2308–2313. (Cited on page 52.)
- [Boniardi et al., 2019] Boniardi, F., Caselitz, T., Kümmerle, R., and Burgard, W. (2019). A pose graph-based localization system for long-term navigation in cad floor plans. *Robotics and Autonomous Systems*, 112:84 – 97. (Cited on page 93.)
- [Chiang et al., 2009] Chiang, Y.-H., Chen, Y.-C., and Huang, P. (2009). Towards practical probabilistic location inference for indoor environment. In *15th ACM Annual International Conference on Mobile Computing and Networking*. (Cited on page 26.)

- [Corke, 2011] Corke, P. I. (2011). *Robotics, Vision & Control: Fundamental Algorithms in Matlab*. Springer. (Cited on page 28.)
- [Cox and Wilfong, 1990] Cox, I. J. and Wilfong, G. T., editors (1990). *Autonomous Robot Vehicles*. Springer-Verlag New York, Inc., New York, NY, USA. (Cited on page 12.)
- [Daixian and Kechu, 2011] Daixian, Z. and Kechu, Y. (2011). Particle filter localization in underground mines using uwb ranging. In *2011 Fourth International Conference on Intelligent Computation Technology and Automation*, volume 2, pages 645–648. (Cited on page 14.)
- [Dellaert et al., 1999] Dellaert, F., Fox, D., Burgard, W., and Thrun, S. (1999). Monte Carlo Localization for mobile robots. In *IEEE International Conference on Robotics and Automation (ICRA99)*. (Cited on page 15.)
- [Dellaert and Kaess, 2006] Dellaert, F. and Kaess, M. (2006). Square root sam: Simultaneous localization and mapping via square root information smoothing. *The International Journal of Robotics Research*, 25(12):1181–1203. (Cited on page 92.)
- [Douc, 2005] Douc, R. (2005). Comparison of resampling schemes for particle filtering. In *In 4th International Symposium on Image and Signal Processing and Analysis (ISPA)*, pages 64–69. (Cited on page 27.)
- [Duda and Hart, 1972] Duda, R. O. and Hart, P. E. (1972). Use of the hough transformation to detect lines and curves in pictures. *Commun. ACM*, 15(1):11–15. (Cited on page 82.)
- [Dudley et al., 2007] Dudley, D., Lienard, M., Mahmoud, S., and Degauque, P. (2007). Wireless propagation in tunnels. *Antennas and Propagation Magazine, IEEE*, 49(2):11–26. (Cited on page 53.)
- [Grisetti et al., 2010a] Grisetti, G., Kümmerle, R., Stachniss, C., and Burgard, W. (2010a). A tutorial on graph-based slam. *IEEE Intelligent Transportation Systems Magazine*, 2(4):31–43. (Cited on pages 92 and 93.)
- [Grisetti et al., 2010b] Grisetti, G., Kümmerle, R., Stachniss, C., Frese, U., and Hertzberg, C. (2010b). Hierarchical optimization on manifolds for online 2d and 3d mapping. In *2010 IEEE International Conference on Robotics and Automation*, pages 273–278. (Cited on page 92.)
- [Grisetti et al., 2005] Grisetti, G., Stachniss, C., and Burgard, W. (2005). Improving grid-based slam with rao-blackwellized particle filters by adaptive proposals and selective resampling. In *Robotics and Automation, 2005. ICRA 2005. Proceedings of the 2005 IEEE International Conference on*, pages 2432–2437. (Cited on page 22.)

- [Grisetti et al., 2007] Grisetti, G., Stachniss, C., and Burgard, W. (2007). Improved techniques for grid mapping with rao-blackwellized particle filters. *Robotics, IEEE Transactions on*, 23(1):34–46. (Cited on pages 22 and 92.)
- [Guan et al., 2017] Guan, L., Cong, X., Sun, Y., Gao, Y., Iqbal, U., and Noureldin, A. (2017). Enhanced mems sensors aided pipeline surveying system by pipeline junction detection in small diameter pipeline. *IFAC-PapersOnLine*, 50:3560–3565. (Cited on page 12.)
- [Guan et al., 2019] Guan, L., Gao, Y., Liu, H., An, W., and Noureldin, A. (2019). A review on small-diameter pipeline inspection gauge localization techniques: Problems, methods and challenges. In *2019 International Conference on Communications, Signal Processing, and their Applications (ICCSPA)*, pages 1–6. (Cited on page 12.)
- [Hansen et al., 2011a] Hansen, P., Alismail, H., Browning, B., and Rander, P. (2011a). Stereo visual odometry for pipe mapping. In *2011 IEEE/RSJ International Conference on Intelligent Robots and Systems*, pages 4020–4025. (Cited on page 12.)
- [Hansen et al., 2011b] Hansen, P., Alismail, H., Rander, P., and Browning, B. (2011b). Monocular visual odometry for robot localization in LNG pipes. In *Robotics and Automation (ICRA), 2011 IEEE International Conference on*, pages 3111–3116. (Cited on page 12.)
- [Hansen et al., 2015] Hansen, P., Alismail, H., Rander, P., and Browning, B. (2015). Visual mapping for natural gas pipe inspection. *The International Journal of Robotics Research*, 34(4-5):532–558. (Cited on page 12.)
- [Hong and Lim, 2018] Hong, E. and Lim, J. (2018). Visual-inertial odometry with robust initialization and online scale estimation. *Sensors*, 18:4287. (Cited on page 37.)
- [Imperoli et al., 2018] Imperoli, M., Potena, C., Nardi, D., Grisetti, G., and Pretto, A. (2018). An effective multi-cue positioning system for agricultural robotics. *IEEE Robotics and Automation Letters*, 3(4):3685–3692. (Cited on page 92.)
- [J.A. Castellanos, 2006] J.A. Castellanos, J. Neira, J. T. (2006). Map building and slam algorithms. In *Autonomous Mobile Robots*, pages 335–371. (Cited on page 60.)
- [Jacobson et al., 2018] Jacobson, A., Zeng, F., Smith, D., Boswell, N., Peynot, T., and Milford, M. (2018). Semi-supervised slam: Leveraging low-cost sensors on underground autonomous vehicles for position tracking. In *2018 IEEE/RSJ International Conference on Intelligent Robots and Systems (IROS)*, pages 3970–3977. (Cited on page 52.)

- [Kümmerle et al., 2011] Kümmerle, R., Grisetti, G., Strasdat, H., Konolige, K., and Burgard, W. (2011). G2o: A general framework for graph optimization. In *2011 IEEE International Conference on Robotics and Automation*, pages 3607–3613. (Cited on pages 92 and 102.)
- [Kümmerle et al., 2009a] Kümmerle, R., Steder, B., Dornhege, C., Kleiner, A., Grisetti, G., and Burgard, W. (2009a). Large scale graph-based slam using aerial images as prior information. *Autonomous Robots*, 30:25–39. (Cited on page 92.)
- [Kümmerle et al., 2009b] Kümmerle, R., Steder, B., Dornhege, C., Ruhnke, M., Grisetti, G., Stachniss, C., and Kleiner, A. (2009b). On measuring the accuracy of slam algorithms. (Cited on page 104.)
- [Laakmann and Steier, 1976] Laakmann, K. D. and Steier, W. H. (1976). Waveguides: characteristic modes of hollow rectangular dielectric waveguides. *Appl. Opt.*, 15(5):1334–1340. (Cited on page 54.)
- [Lazaro and Castellanos, 2010] Lazaro, M. T. and Castellanos, J. A. (2010). Localization of probabilistic robot formations in SLAM. In *Robotics and Automation (ICRA), 2010 IEEE International Conference on*, pages 3179–3184. (Cited on pages 22 and 62.)
- [Li et al., 2015] Li, T., Bolic, M., and Djuric, P. (2015). Resampling methods for particle filtering: Classification, implementation, and strategies. *Signal Processing Magazine, IEEE*, 32(3):70–86. (Cited on page 27.)
- [Lu and Milios, 1997] Lu, F. and Milios, E. (1997). Globally consistent range scan alignment for environment mapping. *Auton. Robots*, 4(4):333–349. (Cited on page 92.)
- [Ma et al., 2017] Ma, K., Schirru, M. M., Zahraee, A. H., Dwyer-Joyce, R., Boxall, J., Dodd, T. J., Collins, R., and Anderson, S. R. (2017). Robot mapping and localisation in metal water pipes using hydrophone induced vibration and map alignment by dynamic time warping. In *2017 IEEE International Conference on Robotics and Automation (ICRA)*, pages 2548–2553. (Cited on page 14.)
- [Marangi et al., 2019] Marangi, A., Olia, K., Daneshgaran, F., Bruno, N., Lizzio, F., and Mondin, M. (2019). Simultaneous localization and mapping with application to monitoring of underground transportation infrastructure. In *2019 International Symposium on Advanced Electrical and Communication Technologies (ISAECT)*, pages 1–4. (Cited on page 52.)

- [Murtra and Tur, 2013] Murtra, A. C. and Tur, J. M. M. (2013). Imu and cable encoder data fusion for in-pipe mobile robot localization. In *2013 IEEE Conference on Technologies for Practical Robot Applications (TePRA)*, pages 1–6. (Cited on page 13.)
- [Nelles, 2001] Nelles, O. (2001). *Nonlinear System Identification: From Classical Approaches to Neural Networks and Fuzzy Models*. Engineering online library. Springer. (Cited on page 53.)
- [Nieto et al., 2007] Nieto, J., Bailey, T., and Nebot, E. (2007). Recursive scan-matching slam. *Robotics and Autonomous Systems*, 55:39–49. (Cited on page 92.)
- [Orfanidis, 2014] Orfanidis, S. J. (2014). *Electromagnetic waves and antennas*. Rutgers University. (Cited on page 53.)
- [Ozaslan et al., 2017] Ozaslan, T., Loianno, G., Keller, J., Taylor, C. J., Kumar, V., Wozencraft, J. M., and Hood, T. (2017). Autonomous navigation and mapping for inspection of penstocks and tunnels with MAVs. *IEEE Robotics and Automation Letters*, 2(3):1740–1747. (Cited on page 13.)
- [Ozaslan et al., 2015] Ozaslan, T., Shen, S., Mulgaonkar, Y., Michael, N., and Kumar, V. (2015). Inspection of penstocks and featureless tunnel-like environments using micro UAVs. In *Field and Service Robotics.*, number 105 in Springer Tracts in Advanced Robotics, pages 123–136. Springer, Cham. (Cited on pages 13 and 52.)
- [Pioneer,] Pioneer. <https://www.generationrobots.com/media/Pioneer3AT-P3AT-RevA-datasheet.pdf>. (Cited on page 119.)
- [Pozar, 2005] Pozar, D. (2005). *Microwave Engineering*. John Wiley & Sons, 3rd edition. (Cited on page 17.)
- [Quigley et al., 2009] Quigley, M., Conley, K., Gerkey, B. P., Faust, J., Foote, T., Leibs, J., Wheeler, R., and Ng, A. Y. (2009). ROS: an open-source robot operating system. In *ICRA Workshop on Open Source Software*. (Cited on page 22.)
- [RFExplorer,] RFExplorer. <http://rfexplorer.com/>. (Cited on page 119.)
- [Rizzo, 2015] Rizzo, C. (2015). *Propagation, Localization and Navigation in Tunnel-like Environments*. PhD thesis, University of Zaragoza. (Cited on pages 3, 4, 5, and 68.)
- [Rizzo et al., 2014a] Rizzo, C., Kumar, V., Lera, F., and Villarroel, J. (2014a). RF odometry for localization in pipes based on periodic signal fadings. In *Intelligent Robots and Systems (IROS), 2014 IEEE/RSJ International Conference on*. (Cited on pages xv, 14, 15, 16, and 17.)

- [Rizzo et al., 2013a] Rizzo, C., Lera, F., and Villarroel, J. (2013a). Transversal fading analysis in straight tunnels at 2.4 GHz. In *13th Int. Conf. on ITS Telecommunications*, pages 313–318. (Cited on pages xvii, 52, 53, and 55.)
- [Rizzo et al., 2014b] Rizzo, C., Lera, F., and Villarroel, J. (2014b). A methodology for localization in tunnels based on periodic RF signal fadings. In *Military Communications Conference (MILCOM), 2014 IEEE*, pages 317–324. (Cited on page 53.)
- [Rizzo et al., 2013b] Rizzo, C., Lera, F., and Villarroel, J. L. (2013b). UHF and SHF fading analysis using wavelets in tunnel environments. In *IEEE 78th Vehicular Technology Conference*, pages 1–6. (Cited on page 52.)
- [Rizzo et al., 2019] Rizzo, C., Lera, F., and Villarroel, J. L. (2019). 3-D fadings structure analysis in straight tunnels toward communication, localization, and navigation. *IEEE Transactions on Antennas and Propagation*, 67(9):6123–6137. (Cited on pages 52, 53, and 56.)
- [Rizzo et al., 2021] Rizzo, C., Seco, T., Espelosín, J., Lera, F., and Villarroel, J. L. (2021). An alternative approach for robot localization inside pipes using RF spatial fadings. *Robotics and Autonomous Systems*, 136:103702. (Cited on pages xv, 6, 11, 14, 15, 18, 19, and 20.)
- [Rogers et al., 2010] Rogers, J. G., Trevor, A. J. B., Nieto-Granda, C., and Christensen, H. I. (2010). Slam with expectation maximization for moveable object tracking. In *2010 IEEE/RSJ International Conference on Intelligent Robots and Systems*, pages 2077–2082. (Cited on page 92.)
- [Ruiz and Villarroel, 2019] Ruiz, I. and Villarroel, J. L. (2019). *Detección de galerías laterales de un túnel basada en mapa previo*. Universidad de Zaragoza. (Cited on page 80.)
- [Sahli and El-Sheimy, 2016] Sahli, H. and El-Sheimy, N. (2016). A novel method to enhance pipeline trajectory determination using pipeline junctions. *Sensors*, 16:567. (Cited on page 12.)
- [Seco et al., 2021] Seco, T., Lázaro, M. T., Espelosín, J., Montano, L., and Villarroel, J. L. (2021). Robot Localization in Tunnels. Combining Discrete Features in a Pose-Graph Framework. *Under review*. (Cited on pages 7 and 91.)
- [Seco et al., 2020] Seco, T., Lázaro, M. T., Rizzo, C., Espelosín, J., and Villarroel, J. L. (2020). Graph-based robot localization in tunnels using RF fadings. In Silva, M. F., Luís Lima, J., Reis, L. P., Sanfeliu, A., and Tardioli, D., editors, *ROBOT 2019: Fourth Iberian Robotics Conference*, pages 580–592, Cham. Springer International Publishing. (Cited on pages 7 and 91.)

- [Seco et al., 2018] Seco, T., Rizzo, C., Espelosín, J., and Villarroel, J. L. (2018). Discrete robot localization in tunnels. In Ollero, A., Sanfeliu, A., Montano, L., Lau, N., and Cardeira, C., editors, *ROBOT 2017: Third Iberian Robotics Conference*, pages 823–834, Cham. Springer International Publishing. (Cited on pages 6 and 51.)
- [Seco et al., 2016] Seco, T., Rizzo, C., Espelosín, J., and Villarroel, J. L. (2016). A Robot Localization System based on RF Fading using Particle Filters inside Pipes. In *2016 International Conference on Autonomous Robot Systems and Competitions (ICARSC)*, pages 28–34. (Cited on pages 6 and 11.)
- [Siqueira et al., 2016] Siqueira, E., Botelho, S., Azzolin, R., and Oliveira, V. (2016). A review about robotic inspection considering the locomotion systems and odometry. In *IECON 2016 - 42nd Annual Conference of the IEEE Industrial Electronics Society*, pages 571–576. (Cited on page 12.)
- [Tardioli et al., 2018] Tardioli, D., Riazuelo, L., Seco, T., Espelosín, J., Lalana, J., Villarroel, J. L., and Montano, L. (2018). A robotized dumper for debris removal in tunnels under construction. In Ollero, A., Sanfeliu, A., Montano, L., Lau, N., and Cardeira, C., editors, *ROBOT 2017: Third Iberian Robotics Conference*, pages 126–139, Cham. Springer International Publishing. (Cited on pages 5 and 51.)
- [Tardioli et al., 2019] Tardioli, D., Riazuelo, L., Sicignano, D., Rizzo, C., Lera, F., Villarroel, J. L., and Montano, L. (2019). Ground robotics in tunnels: Keys and lessons learned after 10 years of research and experiments. *J. Field Robotics*, 36:1074–1101. (Cited on pages 13 and 52.)
- [Tardioli and Villarroel, 2014] Tardioli, D. and Villarroel, J. L. (2014). Odometry-less localization in tunnel-like environments. In *2014 IEEE International Conference on Autonomous Robot Systems and Competitions (ICARSC)*, pages 65–72. (Cited on page 52.)
- [Thrun et al., 2005] Thrun, S., Burgard, W., and Fox, D. (2005). *Probabilistic Robotics (Intelligent Robotics and Autonomous Agents)*. The MIT Press. (Cited on pages 24, 37, and 91.)
- [Thrun et al., 2001] Thrun, S., Fox, D., Burgard, W., and Dellaert, F. (2001). Robust Monte Carlo localization for mobile robots. *Artificial Intelligence*, 128:99–141. (Cited on page 15.)
- [Torres-Solis and Falk, 2017] Torres-Solis, J. and Falk, T. H. (2017). A review of indoor localization technologies : towards navigational assistance for topographical disorientation. In *Ambient Intelligence*. (Cited on page 14.)

- [TP-LINK,] TP-LINK. Tl-wn7200nd <http://rfexplorer.com/>. (Cited on page 121.)
- [Union, 2004] Union, E. (2004). Directive 2004/54/ec of the european parliament and of the council of 29 april 2004 on minimum safety requirements for tunnels in the trans-european road network. *Official Journal of the European Union*, 167:39–91. (Cited on page 73.)
- [Wu et al., 2016] Wu, D., Chatzigeorgiou, D., Youcef-Toumi, K., and Ben-Mansour, R. (2016). Node localization in robotic sensor networks for pipeline inspection. *IEEE Transactions on Industrial Informatics*, 12(2):809–819. (Cited on page 14.)
- [Zhao and Whittaker, 2020] Zhao, D. and Whittaker, W. (2020). High precision in-pipe robot localization with reciprocal sensor fusion. (Cited on page 13.)
- [Zhen and Scherer, 2019] Zhen, W. and Scherer, S. (2019). Estimating the localizability in tunnel-like environments using lidar and uwb. In *2019 International Conference on Robotics and Automation (ICRA)*, pages 4903–4908. (Cited on page 52.)
- [Zàruba et al., 2007] Zàruba, G., Huber, M., Kamangar, F., and Chlamtac, I. (2007). Indoor location tracking using RSSI readings from a single Wi-Fi access point. *Wireless Networks*, 13(2):221–235. (Cited on page 26.)